UNSATURATED SOIL BEHAVIOR UNDER LARGE DEFORMATIONS USING A FULLY SERVO/SUCTION-CONTROLLED RING SHEAR APPARATUS

by

CLAUDIA LILIANA VELOSA GAMBOA

Presented to the Faculty of the Graduate School of

The University of Texas at Arlington in Partial Fulfillment

of the Requirements

for the Degree of

DOCTOR OF PHILOSOPHY

THE UNIVERSITY OF TEXAS AT ARLINGTON

MAY 2011

To my parents and brothers: Sixto, Amparo. Alfonso y Alejandro

for being my motivation and strength.

ACKNOWLEDGEMENTS

This work was made possible thanks to the support and guidance given by my supervisor Dr. Laureano Hoyos. Special thanks are given to Dr. Anand Puppala for his help, guidance and enthusiasm during all the activities of this work. I would also like to give thanks to all the committee members: Dr. Sahadat Hossain, Dr. Siamak Ardekani and Dr. Danny Dyer for their advice and support.

I also would like to thank Dr. Manuel Padilla, Mr. Peter Goguen, and Mr. Tamas Vicsocsean, of Geotechnical Consulting and Testing systems (GCTS), for all their technical assistance during the early stages of this research effort.

Special thanks are given to all my research colleagues for their friendship and support throughout my time at the University of Texas at Arlington. I also would like to give thanks to Mr. Keith Livernois and his family, and all my Colombian friends (Ricardo Ramirez, Carmen Alvarez, Juan Pablo Garzon and Jorge Barrero) for making me feel at home in Texas. Special thanks to my family in Colombia. It is to my parents and brothers that I dedicate this work.

ABSTRACT

UNSATURATED SOIL BEHAVIOR UNDER LARGE DEFORMATIONS USING A FULLY SERVO/SUCTION-CONTROLLED RING SHEAR APPARATUS

Claudia Liliana Velosa Gamboa, PhD.

The University of Texas at Arlington, 2011

Supervising Professor: Laureano R. Hoyos

In recent years, the key hypotheses of most elasto-plastic constitutive frameworks postulated for unsaturated soils have been validated via suction-controlled oedometer, triaxial, and direct shear testing. These techniques, however, allow for the application of loads along limited modes and levels of soil deformation. Today, it is well known that most geotechnical infrastructure resting on unsaturated ground involves a wide range of deformations. Calculation of foundation settlement, for instance, requires a good estimation of soil stiffness at relatively small strains. Analysis of slopes, embankments, and soil bearing capacity, on the other hand, requires an adequate estimation of shear strength, from peak to residual. To date, however, there is very limited experimental evidence of unsaturated soil response under mid-to-large strain levels under controlled-suction states. This paper introduces a novel suction-controlled ring shear apparatus suitable for modeling unsaturated soil response over a whole range of deformations using the axis-translation technique. The apparatus features a 113 N-m torque motor along with a 360-degree-range angular deformation sensor. The lower annular shear platen accommodates a 15.24-cm OD x 9.65-cm ID x 1.5-cm thickness specimen and also

features custom-made grooves to house a full set of six 5-bar or 15-bar ceramics as well as diffused-air flushing ports. A series of suction-controlled ring shear tests was accomplished on several identically prepared, ring-shaped specimens of compacted silty sand (SM) and silty clayey sand (SC-SM). Matric suction was found to exert a critical influence on soil's peak and residual strength responses under constant-suction ring shear testing. Residual shear strength parameters, residual friction angle and residual intercept cohesion, showed a significant increase with applied suction. A comparison of results with literature allowed determining than high suction has a significant influence on the residual strength and residual friction angle of plastic material, but any effect on the cohesion intercept, which is predominantly close to zero.

TABLE OF CONTENTS

LIST OF ILLUSTRATIONS

Figure Page

LIST OF TABLES

CHAPTER 1

INTRODUCTION

Construction of the majority of conventional geo-infrastructure, including foundations, highway embankments, pavements subgrades, man-made slopes, and retaining walls, takes place in unsaturated ground or involves the use of unsaturated soils as a construction material. The annual cost of damage to civil infrastructure caused by problematic unsaturated soils is estimated as $1,000 million dollars in the Unites States, and many millions dollars worldwide (Gourly et al. 1993). Geotechnical engineering communities worldwide have long recognized the importance of a better understanding of the engineering response of unsaturated soils (Bishop, 1959; Alonso, Gens, and Hight, 1987; Burland and Ridley, 1996; Fredlund, 2006).

The development of unsaturated soil mechanics, however, was slow mainly due to a continuous debate about the appropriate stress state variables and the complexities in laboratory testing of these materials. In order to overcome these difficulties, Coleman (1962) suggested the use of the excess of total stress over air pressure (net normal stress), $(\sigma - u_w)$, and the matric suction, $(u_a - u_w)$, as independent stress state variables. Later, Fredlund and Morgenstern (1977) experimentally demonstrated the benefits of adopting the net normal stress and matric suction, as the relevant stress state variables for modeling various key features of unsaturated soil behavior.

In recent decades, several authors, including Alonso, Gens and Josa (1990), Fredlund and Rahardjo (1993), Wheeler and Sivakumar (1995), Cui and Delage (1996), and Hoyos

(1998), among few others, have been able to validate the fundamental hypotheses of several elasto-plastic constitutive frameworks postulated to date for unsaturated soils via suction-controlled oedometer, triaxial, and direct shear testing. These techniques, however, only allow the application of loads and stress paths along limited modes and levels of deformation. Today, it is well known that most geotechnical infrastructure resting on unsaturated ground involves a wide range of soil deformations. Calculation of foundation settlements, for instance, requires a good estimation of soil stiffness at relatively small strains. Analyses of slopes, embankments, and soil bearing capacity, on the other hand, require an adequate estimation of unsaturated soil shear strength, from peak to residual.

Over the last few decades, a significant amount of work has been accomplished with the aim of understanding the engineering implications of residual strength of saturated soils (Skempton 1964, Lupini et al. 1981, Stark and Eid 1994), as well as improving the devices and testing techniques used for the assessment of residual shear strength. The ring shear testing technique has been broadly used (Bromhead 1979, Stark and Eid 1993, Stark and Contreras 1996, Garga and Infante 2002, Meehan et al. 2007), essentially accommodating a ring-shaped specimen inside an annular space and allowing application of continuous and unlimited rotational shear displacement to the specimen without having to stop and reverse the shearing movement while the area of contact on the shear plane remains constant. Results from ring shear testing technique have shown good agreement with back calculations and analyses of documented landslides (Stark and Vettel 1992).

However, none of these efforts have been directly dealt with the testing of unsaturated soils over a large range of shear deformations under controlled-suction states and, therefore, very little data of this type have been reported in the literature. Only recently, Infante et al. (2005, 2007), and Vaunat et al. (2006, 2007) reported the first research efforts aimed at modifying a conventional Bromhead ring shear apparatus for testing specimens under controlled-suction

states via axis-translation and vapor transfer techniques, respectively. Low and medium plasticity clayey soils were tested. The authors reported an increment of the residual friction angle with suction. The authors also observed that the unsaturated residual strength was independent of vertical stress and suction history. These results, however, were far from conclusive, and the modified devices offered plenty of room for further refinement and development.

This research work introduces a novel suction-controlled ring shear apparatus that has been made suitable for testing unsaturated soils over a whole range of deformations using the axis translation technique. The apparatus is a fully servo-controlled system with a 113-ton-m torque capacity and more than 360-degree-range of continuous angular deformation. The general design of the core system is similar to that of the original ring shear apparatus developed by Bromhead (1979). The following chapters describe the full development of the apparatus, including details of its main components and the corresponding performance/verification testing through comparisons with the conventional Bromhead ring shear apparatus. Results from a series of suction-controlled ring shear tests on statically compacted silty sand, silty clayey sand and silty clay soils are presented and analyzed.

1.1 Research Objectives

The main objective of this research work is the development of a novel ring shear (RS) apparatus for testing unsaturated soils over a whole range of deformations and for different controlled suction states achieved via axis-translation technique.

The experimental program includes a series of suction-controlled ring shear tests on several identically prepared specimens of statically compacted silty sand (SM), silty clayey sand (SC-SM) and silty clay (CL) to investigate several features of unsaturated soil behavior, including

pre-failure and post-failure mobility, peak strength, residual strength, threshold deformation levels triggering loss of matric suction (i.e., menisci failure), and time for post-failure menisci regeneration.

The research program involves the following four major tasks:

1. Design and verify the performance of a novel suction-controlled RS apparatus for testing shear strength properties of unsaturated soils over a whole range of shear deformations.
2. Perform a comprehensive experimental program to investigate the influence of matric suction and net normal stress over the peak and residual shear strength parameters of unsaturated soils. Net normal stress values between 25 kPa and 200 kPa, and matric suction states from 0 to 300 kPa, were selected to reproduce stress states that are typical in first-time landslides occurred in shallow unsaturated soil slopes and embankments (Stark and Eid, 1997).
3. Asses the threshold deformation levels triggering loss of matric suction (menisci failure) in compacted soils and the time for post-failure menisci regeneration via tensiometers.
4. Evaluate the effects of large-strain process in soil-water retention properties (SWCC) of compacted soils.

1.2 Thesis Organization

This document is divided into seven chapters that can be summarized as follows:

Chapter 2 reviews the fundamental concepts of residual shear strength behavior of saturated and unsaturated soils and the basic theoretical aspects of this behavior. In addition, a brief description of most commonly used methods for determining residual strength parameters

of soil materials is presented, including a summary of the historical development of the ring shear testing technique. Finally, this chapter also includes a literature review of previous studies reported in the literature and related to the present work.

Chapter 3 is devoted to a detailed description of the main parts of the novel suction-controlled ring shear device implemented in this research work and the typical soil parameters obtained from suction-controlled RS tests.

Chapter 4 describes the basic physical properties of the test materials used, including compaction methods, soil specimen preparation procedures and, soil water characteristic curves (SWCC). Results from a testing program undertaken to verify the performance of the new ring shear device are also presented. The performance verification testing includes comparison of test results with those from a conventional Bromhead ring shear apparatus.

Chapter 5 describes the entire suction-controlled experimental program and test procedures followed in this research work, including a detailed list of all experimental variables. The chapter includes all the experimental results from this program.

Chapter 6 presents a thorough analysis and discussion of experimental results from all suction-controlled ring shear tests performed on silty sand, silty clayey sand and silty clay soils. Results from this work are compared to those previously reported for similar soils.

Chapter 7 studies on soil fabric and menisci response

Chapter 8 summarizes the main conclusions of this research effort and provides a few insights for further studies on the subject.

CHAPTER 2

FUNDAMENTAL CONCEPTS AND PREVIOUS WORK

2.1 Introduction

Over the last few decades, a significant amount of work has been accomplished with the aim of understanding the engineering implications of residual strength of saturated soils (Skempton, 1965, 1985; Lupini et al., 1981; Stark and Eid 1994, 1997, 2005) as well as improving the devices and testing techniques used for the assessment of residual shear strength (Stark and Eid, 1993; Stark and Contreras 1996; Garga and Infante 2002, Meehan et al., 2007). However, none of these efforts have dealt directly with the testing of unsaturated soils over a large range of shear deformation under controlled-suction states, and therefore very little data of this type have been reported in the literature.

Recently, Infante et al. (2005, 2007) reported a first attempt at modifying a conventional, Bromhead type, ring shear device for soil testing under controlled low-suction states via axis translation technique. Around the same time, Vaunat et al. (2006, 2007) reported a modified Bromhead type ring shear apparatus for soil testing under controlled high-suction states via vapor transfer technique. In both cases, low and medium plasticity clayey soils were tested.

The authors reported an increment of the residual friction angle with suction, which was associated to some partial aggregation of the clayey particles, causing the soil to behave more like a granular material. The authors also observed that the unsaturated residual strength was independent of vertical stress and suction history. These results, however, were far from

conclusive, and the ring shear devices offered plenty of room for further refinement and development.

This chapter summarizes the fundamental concepts of peak and residual shear strength of soils, as well as critical findings from these previous works.

2.2 Fundamental Concepts – Unsaturated Shear Strength

The shear strength of a soil material is a critical property required for numerous geotechnical analyses, including prediction of slope stability, and design of foundations and earth retaining structures, among others. The effective stress variable, σ', proposed by Terzaghi (1936) has been normally used in Mhor-Coulomb (M-C) theory for predicting the shear strength of saturated soils. The shear strength equation for saturated soils is generally expressed as a linear function of effective stress, and is given as follows:

$$\tau = c' + (\sigma - u_w)tan\varphi' \qquad (2.1)$$

where:

τ = shear strength

σ = total normal stress

$\sigma_n - u_w$ = effective normal stress, (σ')

u_w = pore-water pressure

c' and φ' = saturated effective stress parameters

The main focus of soil mechanics has, historically, been on saturated soils, where all the voids are assumed to be filled with water. However, many practical problems require assessing the shear strength of unsaturated soils, with voids filled with both air and water. Bishop (1959)

described the shear strength of unsaturated soils in terms of a modified effective stress variable, χ, that integrated both the matric suction $(u_a - u_w)$ and the net normal stress $(\sigma - u_a)$, as follows:

$$\sigma' = (\sigma - u_a) + \chi(u_a - u_w) \qquad (2.2)$$

where:

σ = total normal stress

u_a = pore air pressure

u_w = pore water pressure

χ = effective stress parameter that depends on the degree of saturation or matric suction

The term $(\sigma - u_a)$ in equation (2.2) represents the component of the net normal stress applicable to bulk soil while the term $\chi(u_a - u_w)$ represents the interparticle stress due to suction. This term is often referred to as suction stress. Figure 2-1 summarizes a series of experimental relationships between the effective stress parameter χ and degree of saturation for a wide range of soil types.

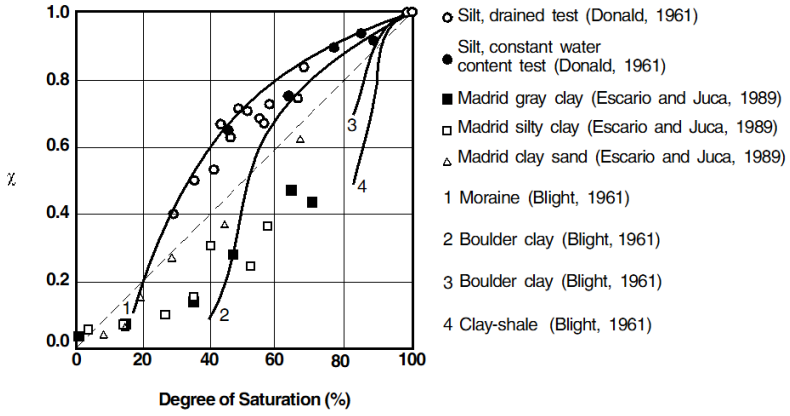

Figure 2-1. Experimental results showing the dependency of Bishop's effective stress parameter χ on degree of saturation (Lu and Likos, 2004)

Data from Figure 2-1 suggest that the effective stress parameter χ varies from a value of zero for dry conditions and unity for saturated conditions. However, despite its simplicity the validity of the Bishop's effective stress equation, based on a single stress state variable, has been widely questioned theoretically and experimentally. For instance, Jennings and Burland (1962) expressed their doubts on the validity of Bishop's effective stress equation because it could not represent the volumetric changes upon wetting of unsaturated soils adequately.

In order to describe the proper stress-strain behavior of unsaturated soils, Coleman (1962) suggested the use of two independent stress variables, the net normal stress, $(\sigma - u_a)$, and the matric suction, $(u_a - u_w)$, instead of a single effective stress variable. Later, Fredlund and Morgenstern (1977) experimentally demonstrated that the shear strength and volume change behavior of unsaturated soils could be described by any two of three stress state variables: $(\sigma - u_a)$, $(\sigma - u_w)$, and $(u_a - u_w)$ where (u_a) is the pore-air pressure. Based on these results Fredlund et al. (1978) proposed the following equation for describing the shear strength behavior of unsaturated soils:

$$\tau = c' + (\sigma - u_a)tan\varphi' + (u_a - u_w)tan\varphi^b \qquad (2.3)$$

where:

$(\sigma - u_a)$ = net normal stress

$(u_a - u_w)$ = matric suction

φ^b = angle representing the changes in shear strength with changes in matric suction

φ' = angle representing the changes in shear strength with changes in net normal stress

The first two terms on the right-hand side of the equation (2.3) describe the conventional M-C theory for strength of saturated soils. The third term captures the increase in shear strength

with increasing matric suction in unsaturated soil. The corresponding failure surface for the extended M-C criterion is illustrated in three-dimensional stress space in Figure 2-2.

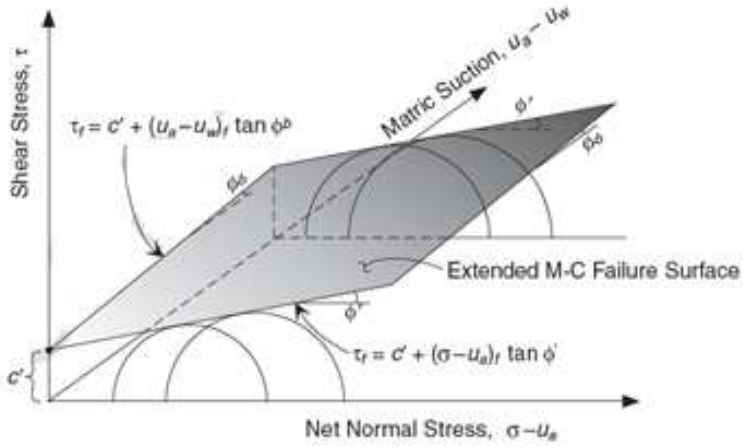

Figure 2-2. Extended Mohr-Coulomb failure surface for unsaturated soil (Lu and Likos, 2004)

The shear strength contribution due to matric suction, φ^b, was initially assumed to be linear based on the analysis of limited results published in the literature. Figure 2-3(a) shows the effect of matric suction on both the position and slope of failure envelopes of experimental data from a series of direct shear tests on unsaturated Madrid gray Clay reported by Escario (1980).

It is observed that matric suction exerts a critical influence on the final position of the failure envelope, with a considerably higher position for s = 850 kPa. It can also be observed that the failure envelopes are basically parallel, suggesting that the friction angle, φ', is suction-independent. Figure 2-3(b) shows the effect of net normal stress on both the position and slope of failure envelopes projected onto the shear stress versus matric suction plane. Likewise friction angle, φ', in Figure 2-3(a), the friction angle with respect to matric suction state, φ^b, seems to remain virtually constant regardless of the net normal stress level. Fredlund and Rahardjo (1993) summarized the results presented by other researchers and found that φ^b was a highly nonlinear

function of matric suction. They indicated that φ^b appears to be generally equal or close to the friction angle φ' at fully saturated conditions and then reduces to as low as zero or even negative values for suctions approaching the residual saturation state

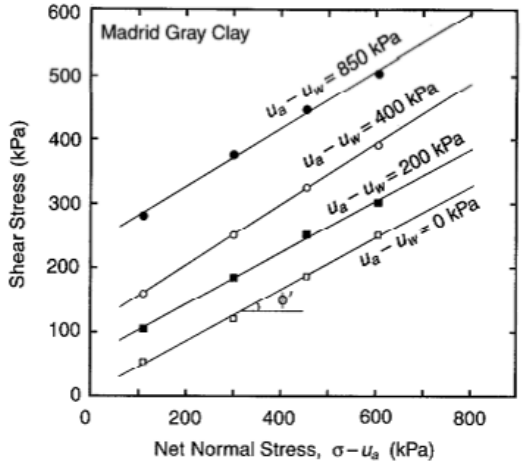

(a)

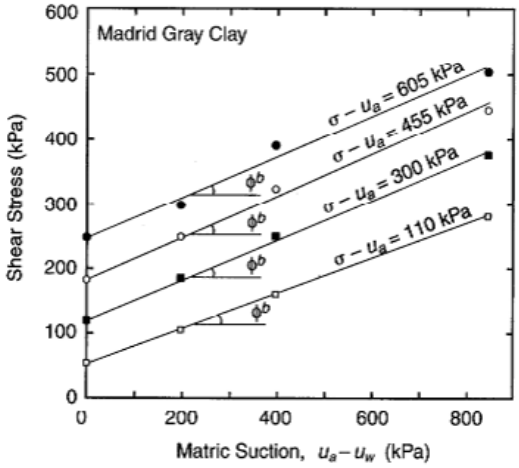

(b)

Figure 2-3. (a) Effect of matric suction state on residual failure envelopes of unsaturated Madrid gray clay, (b) Effect of net normal stress on residual failure envelopes of unsaturated Madrid gray clay (data from Escario, 1980)

Figure 2-4 shows an example of experimental data from suction-controlled direct shear tests performed on Red silty clay and Madrid gray Clay reported by Escario et al. (1989). Results demonstrate the nonlinear behavior of φ^b. Recent experimental data have yielded values of φ^b higher than φ' , as well as an increase of φ' with suction (Röhm and Vilar, 1995; Feuerharmel et al., 2006; and Pereira et al., 2006).

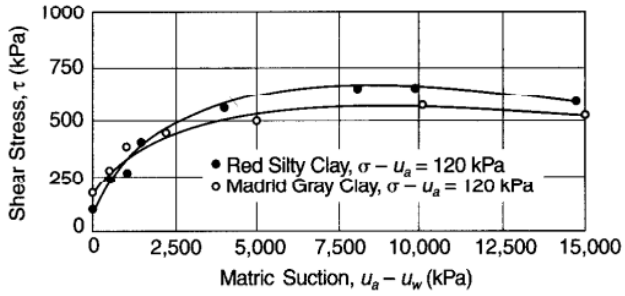

Figure 2-4. Effect of net normal stress on residual failure envelopes of unsaturated Red silty clay and Madrid gray clay (data from Escario, 1989).

In recent times, studies have showed renewed interest in the single effective stress approach suggested by Bishop (1959), as well as support for Fredlund and Morgenstern's independent stress state variable approach (Khalili et al., 2004 and Nuth et al., 2007). Although both approaches have shown significant advantages for describing the strain-stress behavior of unsaturated soil, identification of the most appropriate stress variables for unsaturated soils remains an open area of research.

2.3 Fundamental Concepts – Residual Shear Strength

Soils subjected to shearing under drained conditions will usually exhibit a rise in shear resistance with increasing displacement until a maximum resistance, the peak shear strength, is reached. If the shearing displacement is continued, the shearing resistance of the soil will decrease until a minimum resistance and will remain constant until the reorientation process of

the particles has been completed. The minimum resistance, the residual shear strength, is the lowest shearing resistance the soil can exhibit under drained conditions.

As the peak strength behavior, the residual strength of a soil is described in terms of a residual friction angel, ϕ_r', and the residual cohesion intercept, c_r', as follows:

$$\tau_r = c_r' + (\sigma - u_w) tan\varphi_r' \qquad (2.4)$$

where:

τ_r= residual shear strength

c_r' and φ_r' = residual effective stress parameters

σ = total normal stress

$\sigma - u_w$ = effective normal stress

By definition, the residual strength condition results from the reorientation of platy clay particles parallel to the direction of shear, which results in an increased face-to-face interaction of the particles (Skempton, 1985). The resulting shear strength is low because it is difficult for the face-to-face particles to establish contact or bonding between them. As a consequence, the particle contact and bonding that leads to a value of cohesion greater than zero has been reduced or eliminated by the shear displacement required to reach a residual strength condition. This results in only a frictional shear resistance that is represented by a residual friction angle and the effective normal stress acting on the shear surface as follows:

$$\tau_r = (\sigma - u_w) tan\varphi_r' \qquad (2.5)$$

However, although has been generally accepted for designing proposes the assumption of zero cohesion at residual states, Tiwary et al. (2005) reported residual cohesion values as large as 9.2 kPa obtained from the best fit residual strength envelope for some soils.

The concept of residual shear strength has contributed enormously to the understanding of the behavior of soils subjected to large displacements under drained conditions. This is generally associated with the long-term stability of slopes in overconsolidated clays, and it plays an important role in the assessment of the engineering properties of soils deposits and evaluation of the risk of progressive failure in stability problems.

Furthermore, some studies have suggested that the residual shear strength may also govern the shaft adhesion of piles in both normally and overconsolidated clays (Randolph and Wroth, 1982; Anderson and Yonk, 1985), as well as the stability of pipelines in offshore environments (Najjar et al., 2007).

Skempton (1965) experimentally demonstrated that residual shear strength does not depend on the initial structure or stress history of the soils. Therefore, the residual friction angle should be a constant for any particular clay whatever its consolidation history, depending only on the nature of the particles. Unlike the stress-strain and volume change characteristics exhibited by clay before reaching the residual condition that are functions of the stress history of the soil.

2.3.1 Development of Residual Strength

Heavily overconsolidated clays show a rapid increase in shear stress reaching a peak value at low shear strains and then show a decrease in shear stress with increasing shear strain until the critical state condition is attained. Critical state is the stress state reached in a soil when continuous shearing occurs at constant shear stress to normal effective stress ratio and constant volume. Finally, at larger displacements, when particle reorientation is complete, the strength

decrease below the critical state shear stress and remains constant at the residual stress, as is shown in Figure 2-5(a).

Skempton (1985) stated that the reduction in strength of overconsolidated clays is due first to an increase in water content due to dilatation and, secondly to orientation of clay particles parallel to the direction of shearing. On the other hand, normally consolidated clays generally have lower peak strengths than overconsolidated clays and exhibit a smaller decrease from peak to residual strength. This decrease in strength is accompanied by a reduction in void ratio and is due entirely to the orientation of particles parallel to the direction of shearing (Figure 2-5b).

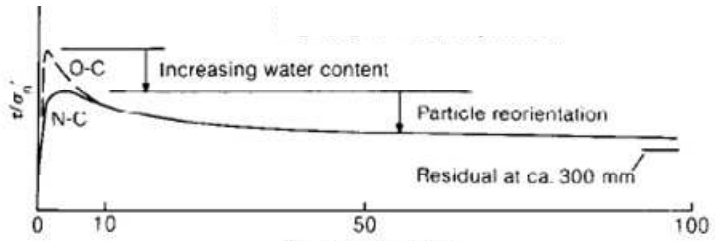

(a)

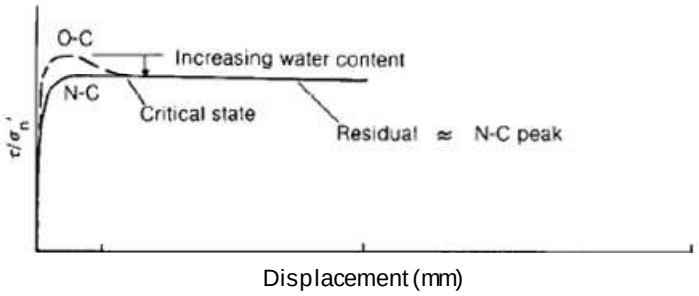

(b)

Figure 2-5 Stress-displacement curves at constant σ': (a) high clay fraction (> 40%) , (b) low clay fraction (< 20%), (Skempton, 1985).

Haefeli (1951) and Skempton (1964) found that the magnitude of the drop in strength from peak to residual in clays increased with liquid limit. Lupini et al. (1981) and Skempton (1985) demonstrated that particle reorientation will be significant only in clays containing platy clay minerals and having a clay fraction (percentage by weight of particles smaller than 0.002 mm) exceeding about 20-25% (Figure 2-5a). Silt and sandy clays with lower clay fractions exhibit nearly the classical critical state type of behavior in which, even at large displacements, the strength is scarcely less than the normally consolidated peak value, and the postpeak drop in strength of overconsolidated material of this kind is due almost entirely to water content increase (Figure 2.5b).

Based on this experimental evidence, many correlations between the residual shear strength and clay fraction or plasticity index have been proposed by different authors. Skempton (1964) reported experimental data of residual strength from direct shear tests and postulated a first general correlation between residual strength and clay fraction. Figure 2.6 displays the correlation postulated by Skempton including correlations reported by other authors Lupini (1981).

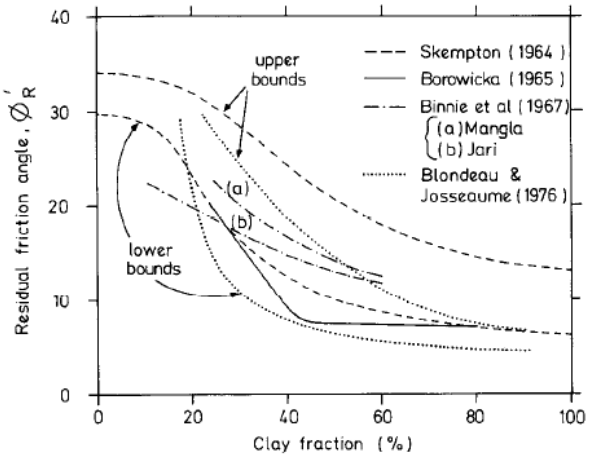

Figure 2-6 Relationship between the residual friction angle and the clay fraction (Lupini et al., 1981).

Some authors also have suggested that there is a better correlation between the residual friction angle and the plasticity Index than with any other parameter. Figure 2-7 summarizes the correlations of this type reported by different authors (Seycek, 1978).

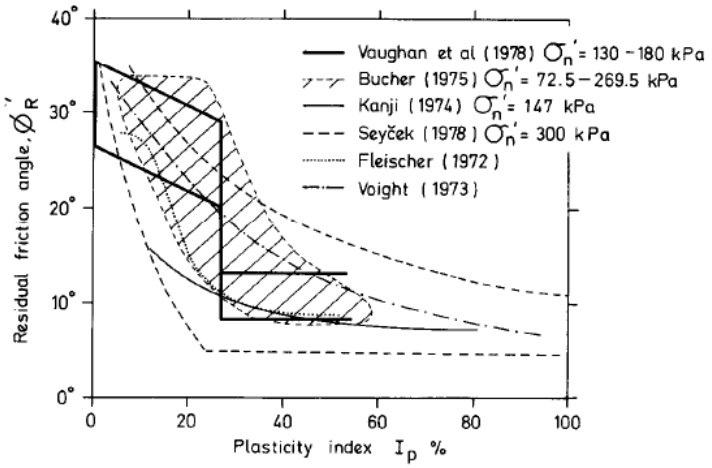

Figure 2-7 Relationship between the residual friction angle and Plasicity Index (Seycek, 1978).

Despite the good correlation found by different research works between the residual friction angle and some soil properties like the amount of clay fraction or Index properties for some soils, Lupini et al (1981) point out that these correlations cannot be generalized. He stated that other properties like the particle shape, grading, mineralogy, pore-water chemistry, etc.; affect notably the residual strength of soils.

More recently, Stark and Eid (1994) demonstrated that correlations based on only clay-size fraction or clay plasticity tend to overestimate the drained residual friction angle. In addition, they do not consider the nonlinearity of the residual failure envelope which could represent a poor estimation of the factor of safety in soil stability analysis problems. Since the residual strength is usually small, small changes in the residual friction angle results in significant changes in the calculated factor of safety.

The authors suggest that the residual failure envelope can be approximated by a straight line for cohesive soils that have a clay size fraction less than 45%. For cohesive soils with clay size fraction greater than 50% and a liquid limit between 60 and 220, they demonstrated that the nonlinearity of the drained residual failure envelope was significant. As a consequence, the authors proposed a new drained residual strength correlation which is a function of the liquid limit, clay-size fraction, and the effective normal stress (Figure 2-8).

Recently, Stark et al. (2005) based on new experimental data revised the correlation shown in Figure 2-8 and presented a new empirical correlation only for the relationship of an effective normal stress of 100 kPa (Figure 2-9). The new relationship was shifted slightly upward (less than 1°), which increased the stress dependency of the secant residual friction angle for soils with a clay-size fraction less than or equal to 20%. The relationship for an effective normal stress of 400 and 700 kPa were not changed from Stark and Eid (1994).

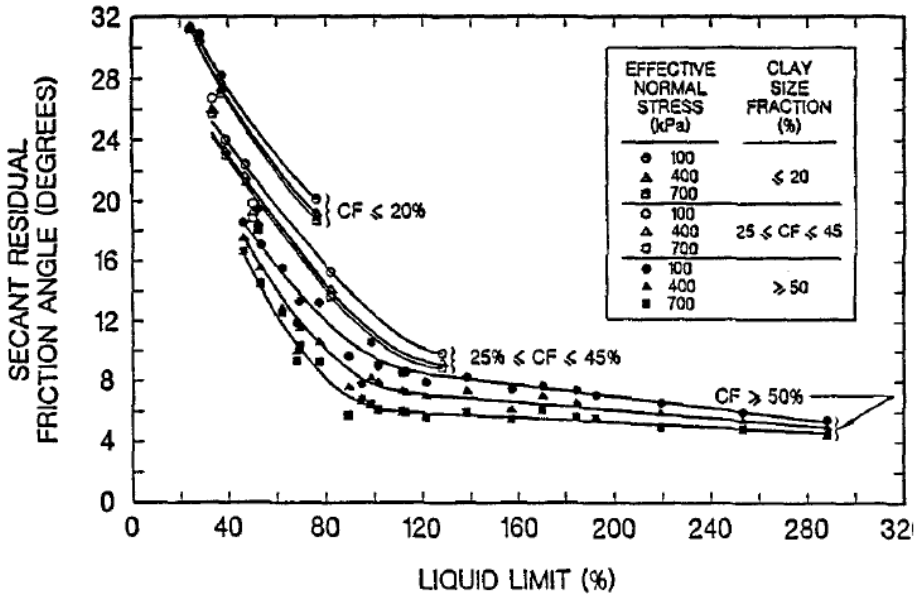

Figure 2-8 Relationship between the secant residual friction angle and Liquid Limit, clay-size fraction and the effective normal stress (Stark and Eid, 1994).

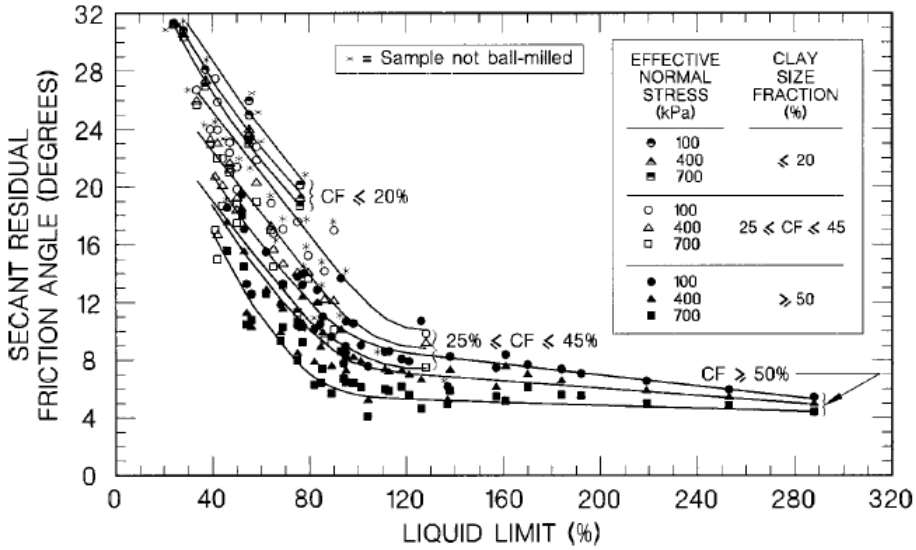

Figure 2-9 Relationship between the secant residual friction angle and Liquid Limit, clay-size fraction and the effective normal stress (Stark et al., 2005).

2.3.2 Residual shearing mechanism

Lupini et al. (1981) define three possible modes of residual shear behavior, depending of the proportion of platy particles presents in the soil and the coefficient of interparticle friction of the platy particles. The three possible modes of residual shear are as follows:

Turbulent mode: This mode occurs when behavior is dominated by rotund particles, or, in soils dominated by platy particles when the coefficient of interparticle friction between these particles is high. Residual strength is high, no preferred particle orientation occurs and brittleness is due to dilatant behavior only. The residual friction angle in this mode depends primarily on the shape and packing of the rotund particles and not on the coefficient of interparticle friction. A shear zone, once formed, is a zone of different porosity only and it is considerably modify by subsequent stress history.

Sliding mode: This mode occurs when behavior is dominated by platy, low friction particles. A low strength shear surface of strongly orientated platy particles then develops. The residual friction angle depends primarily on mineralogy, pore-water chemistry and on the coefficient of interparticle friction. A shear surface, once formed, is not significantly affected by subsequent stress history. Brittleness during first shearing is due primarily to preferred particle orientation.

Transitional mode: This mode occurs when there is no dominant particle shape, and involves turbulent and sliding behavior in different parts of a shear zone. The properties of the soil in residual shear change progressively across the transitional range from those of turbulent shear to those typical of sliding shear. In this mode the residual friction angle is sensitive to small changes in grading of the soil, and the changes in grading required to cross this range entirely are typically small. Finally, the authors state that the residual friction angle depends on the normal effective stress and this dependence is typically greatest for the sliding mode of behavior.

2.3.3 Residual shear strength

At present, there are two methods to determine the residual shear strength of soils: first, laboratory test method and, secondly back analysis evaluation method. Back analysis evaluation method, as a theoretical method, is very useful to evaluate old landslides and slowly sliding slopes. However, some basic assumptions having uncertain properties must be given in the process of back analysis which will result in uncertain analysis results.

The main laboratory methods that have been used for residual strength determination are the reversal direct shear, triaxial and ring shear test. The direct shear and triaxial apparatus, originally developed for the study of peak strength behavior, are small displacement devices that have been adapted for use in determining residual strength. The ring shear apparatus was designed specifically for residual strength testing.

Direct shear test:

The direct shear test is the most common method used for determining residual strength. Due to the short length of travel of the shear box, large strains are accumulated by repeated reversals of the direction of travel or by repeated uni-directional shears, repositioning the shear box at the end of each travel.

The main advantages of the common shear box applied to residual strength testing would appear to be the ready availability of suitable equipment, the simple method of operation, and the short drainage path which results in short time tests. The main disadvantage is that the soil is sheared forward and then backward until a minimum or equilibrium shear resistance is measured (Skempton, 1985). Each reversal of the shear box results in a horizontal displacement that is usually less than 2.5 cm. As a result, the specimen is not subjected to continuous shear deformation in one direction and thus only a partial reorientation of the clay particles is obtained. In addition, the cross sectional area of the specimen is changing during shear, arising high local concentrations of strain, and a substantial amount of soil is usually extruded out of the exposed shear plane during the test. Furthermore, specimens must have the shear surface aligned precisely with the plane of separation of the shear box, and this may be impossible where the shear surface is not flat. Bishop et al. (1971) also reported as main limitations of the direct shear test, the uncertainty about the directions of the principal stresses as the test proceeds. These and other limitations usually result in residual strength that is higher than the residual values obtained from ring shear devices (Bromhead, 1979; Stark and Eid, 1994).

Triaxial test:

The triaxial test is more difficult to adapt for residual testing than the direct shear test and, for this reason, has not been widely used. The mayor limitation encountered in triaxial testing for residual strength is the inability to obtain large strains without severely distorting the sample.

Other disadvantages include the corrections which must be made for the constraining effect of the rubber membrane surrounding the sample, for the changing cross-sectional area of the failure plane, and for the horizontal component of the ram load if the loading cap is incapable of lateral movement.

In triaxial testing for residual strength, given that only limited displacement can be achieved, methods must be employed to promote shear plane development at small strains. Some success is claimed for triaxial test on samples with pre-cut shear planes or pre-existing fissures at an angle of $45° + \varphi_r'/2$ to the horizontal, where φ_r' is the estimated angle of residual friction. Petley (1966) found that the displacement to reach the residual condition could be significantly reduced by smoothing the pre-cut shear surfaces with a piece of glass drawn over the surfaces in the direction of shear. However, complicated test procedures and the uncertainty of residual strength determinations obtained at small shear displacements make the triaxial test unsuited for normal practical use in this application.

Ring shear test:

The ring shear test was developed specifically for the purpose of determining residual strength. In general, the two obvious advantages of any type of torsion or ring shear test are that there is no change in the area of the cross section of the shear plane as the test proceeds and that the sample can be sheared through an interrupted displacement of any magnitude. This allows full orientation of the clay particles parallel to the direction of shear and the development of a true residual strength condition. Other advantages of the ring shear apparatus include a thinner specimen, which allows the use of a faster drained displacement rate, more reproducible results, and less laboratory supervision than the reversal direct shear test (Stark and Vettel, 1992).

In the ring shear test, an annular soil specimen is confined between outer and inner rings and is sheared with the normal load applied in the axial direction and the shear load applied tangentially. Thus, the soil is sheared in a plane perpendicular to the axis from its bottom, or top, or mid-height surface depending on the configuration and fixity of the rings. Figure 2-10 shows a representation of the ring shear test mechanism in typical ring shear devices. Figure 2-10(a) illustrates an annular-split-ring device with shear zone at mid height (Imperial College/Norweigian Geotecnical Institute RS - type design); and Figure 2-10(b) an annular-solid-ring device with shear zone at the top of the specimen (Bromhead RS - type design). Both devices will be described lately in this section. The solid and dashed arrows indicate directions of measured and applied shear stresses, respectively (Sadrekarimi and Olson, 2009).

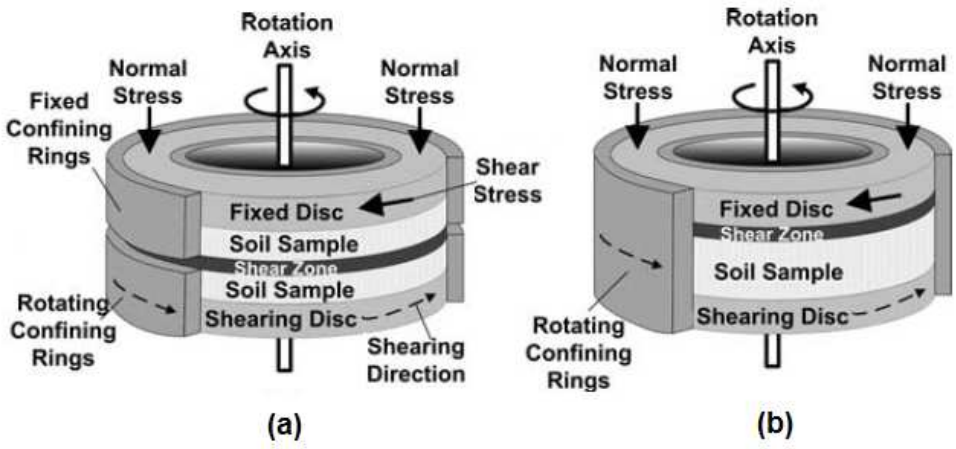

Figure 2-10 Schematic of ring shear test mechanism: (a) Imperial College/Norweigian Geotecnical Institute RS type design, (b) Bromhead RS type dedign (Sadrekarimi and Olson, 2009).

Ring shear devices were initially developed in the early 1930's by a number of independent researchers including A.S.C.E (1917), Streck (1928), Gruner and Haefeli (1934), Cooling and Smith (1935, 1936), Langer (1938), Tiedemann (1939), and Hvorslev (1939). The

most successful devices incorporated upper and lower pairs of confining rings positioned to cause failure to occur within the sample body away from the end platens. All of the early devices were stress-controlled. Hvorslev (1947) presented a new ring shear that could operate in either a stress-controlled or strain-controlled mode. With the exception of this work by Hvorslev, the evolution of the ring shear apparatus virtually ceased until interest in residual strength was rekindled in the 1960's.

Of several devices developed since the early 1960's, the more significant in terms of design advancement and innovation are the ring shear device developed at Harvard University (La Gatta, 1970), the device developed jointly by the Imperial College and the Norwegian Geotechnical Institute (Bishop et al., 1971), and the device developed by the School of Civil Engineering, Kingston Polytechnic (Bromhead, 1979). The Harvard ring shear device can test annular or solid disc-shaped specimens with either solid or split confining rings. The sample height is variable from 1 to 25 mm but thin samples (2 to 3 mm thick) are normally used. The Imperial College and the Norwegian Geotechnical Institute, I.C. – N.G.I ring shear apparatus can test (3/4 in) thick annular specimens using split confining rings (Figure 2.10a). Sample loss through squeezing between the confining rings is regulated by a precise gap control mechanism. Both the Harvard and I.C. – N.G.I. devices are strain-controlled. Bishop (1971) stated that the wall friction in these devices is wider reduced due to the thin sample used. However, he noted that if the split confining rings are used, excessive squeeze affects the normal stress distribution and the advantages of a thin sample are lost.

By the mid-1970's, ring shear test had become widely recognized as the best method for measuring the drained residual strength of clayey soils, due to their ability to apply large shear displacements without reversal in the direction of shear. However, ring shear tests conducted at that time using the Harvard and the I.C-N.G.I ring shear equipment were too expensive and time consuming to be widely used in engineering practice. In an attempt to address this issue,

Bromehead (1979) developed a simple, robust, and relatively inexpensive ring shear device that was capable of running shearing test more quickly than other ring shear devices on the market. As a result, the Bromhead ring shear has become widely used in engineering practice.

The Bromhead apparatus accommodates a ring-shaped specimen of 5 mm thick inside an annular space with inner and outer diameters of 70mm and 100mm respectively allowing application of continuous, unlimited rotational shear displacement. Once the soil is placed inside the annular space between the concentric rings of a lower rotating cell, the load cap is installed and a normal load is applied. A torque is then applied from below to the rotating cell and resisted by a pair of rods that induce torque reactive from a pair of calibrated load rings, separated a distance L, on a tortional beam. Failure occurs by rupture of the soil specimen along its upper platen displaced relative to clay particles below. Continued shearing results in clay particle orientation along the failure plane, and the development of slickensides along which the residual strength is measured (Figure 2-10b). Moreover, consolidation in the Bromhead ring shear device occurs rapidly, because the thin, annular specimen has a short drainage path length. Additionally, since the shearing plane is located close to the top of the specimen, the pore pressures generated during shear dissipate rapidly.

Despite of all the advantages described before, the main factor affecting the measured residual strength is the magnitude of the wall friction that is developed along the inner and outer circumferences of the confined specimen. The magnitude of the wall friction increases with the depth of the specimen, and thus the plane of least wall friction occurs at or near the soil-top porous stone interface. As the top porous stone settles into the specimen container, the wall friction influencing the shear plane increases, which causes an increase in the measured residual strength (Bromhead 1986; Stark and Vettel 1992, Meehan et al 2007).

In the Bromhead ring shear apparatus, tests are performed on remolded test specimens. As with the earliest ring shear devices, multistage test procedure can be performed. Using this

technique, a single specimen is sheared to its residual state, changing the normal stress, and then shearing the same specimen to its residual state again. The acceptability of the multistage technique has been mainly based on test results for overconsolidated clays, which suggested that stress history has no effect on the measured residual strength.

Although it had long been recognized that residual stress envelopes were not linear, a straight line relationship was often used for fitting the result of tests on overconsolidated clays. However recent studies have established that, particularly at low stress levels, there is a distinct curvature of the residual failure envelope, and that the residual angle of shearing resistance ϕ_r' is dependent on the stress level (Lupini et al., 1981; Stark et al., 2005).

Despite of simplicity of the multistage technique, Anderson and Hammund (1988) stated that this technique is satisfactory for clays exhibiting turbulent or transitional shearing mode, that is, soils with a percentage of clay particles less than 50%. If soils contain more than 50% clay particles, they will exhibit a sliding mode of shearing and different results are likely to be obtained from multistage and single stage tests. The authors suggest that the single stage is recommended for clays with more than 50% of clayey particles, not only because of the inaccurate values of residual strength obtained from multistage test, but also because the brittleness of the clay, which may be obtained from the single stage tests for different normal stress level.

Over the last two decades, a number of researchers such as Anayi et al. (1988), Anayi et al, (1989), Anderson and Hammoud (1989), Stark and Vettel (1992), Stark and Eid (1993), Stark and Contreras (1996), Garga and Sedano (2002), Sasa et al (2003) and Meehan et al (2007), have proposed different test procedures or modifications to the Bromhead ring shear apparatus in order to overcome some issues such as soil extrusion, top platen intrusion and the development of wall friction during single and multistage tests.

Anyi et al (1989, 1988) incorporated vanes into the top porous stone of a Bromhead type apparatus and increased the depth of the specimen container from 5 mm to 10 mm. The modifications were made in order induce the shear failure at a plane at some depth within the specimen, instead of at top of the specimen and reduce the soil extrusion as shearing progressed. However, this modification introduced additional side friction between the upper half of the specimen and the specimen container, decreasing the accuracy of the measured shear stress.

Stark and Vettel (1992) proposed a new test procedure called “flush test” in order to reduce the wall friction produced in ring shear tests via Bromhead type device. This procedure limits the total settlement of the top porous stone, due to consolidation and/or soil extrusion during drained shear, to 0.75 mm. They recommend only perform one test per sample. They concluded that the flush test procedure yields the lowest residual strength of the existing procedures and provides the best agreement with field case histories. They also installed vanes into the top pore stone. They reported drained residual shear strength that were substantially higher than the flush test procedure. They concluded that the higher strengths were due to the additional wall friction developed by the shear plane forming at the bottom of the vanes instead of the soil-top porous stone interface.

Stark and Eid (1993) designed a new specimen container for the Bromhead apparatus that allows remolded specimen being overconsolidated and precut prior to shearing. Authors stated that the new container minimizes the settlement of the top platen and decreases the horizontal displacement required to reach the residual strength condition. They also stated that the use of overconsolidated and precut specimen provides a better representation of field conditions. Experimental data of residual strengths were in excellent agreement with field case histories.

Stark and Contreras (1996) described a modified Bromhead type apparatus that allows applying constant volume conditions for measuring undrained peak and residual shear strength of cohesive soils. The experimental data were in excellent agreement with data from direct simple shear, which verify the accuracy of the new constant volume ring shear apparatus.

Garga and Infante-Sedano (2002) modified the conventional Bromhead device to undertake constant volume ring shear tests on sands. The mayor modifications were the increasing of the sample height from 5 to 20 mm and the increasing of the outer and inner diameters form 100 and 70mm to 133 and 92 mm respectively. Additionally in order to reduce the wall friction of the annular specimen along the confining walls of the cell, the rigid walls were replaced by two stacks of ten outer and inner confining rings. The modify RS device has an air actuator to provide the normal load instead that the conventional dead weights system, two torque load cells, and one linear vertical displacement transducer (LVDT) to measure the vertical deformation of the specimen. The study reported data that are in a good agreement with data presented by other authors.

Sassa et al. (2003) presented the design and construction of a split-ring shear device where the upper and lower confining rings are pressed together to maintain undrained conditions and shear induced pore-water pressures are measured using transducers installed through the outer fixed confining rings. This apparatus is suited for undrained shear tests under all types of loading, and enables examining the undrained shear behavior of soils with high mobility in virtually limitless shear displacement levels.

Meehan et al. (2007) compared results from single stage and multistage tests using the conventional Bromhead RS device and found that the secant residual friction angles presented a difference of about 10 to 15%. He concluded that this difference was associated with top platen intrusion and development of wall friction along the confining rings. Therefore in order to reduce the wall friction the top platen was modified by machining the inside an outside edges of the

porous bronze loading platen back to a 45° bevel. The authors reported that both single stage and multistage “modified platen” tests gave the same residual strengths, showing that the modified platen eliminates the effect of wall friction associated with top platen intrusion. They suggest that in order to minimize the effect of wall friction in the Bromhead ring shear device, it is recommended that the top platen be modified, prepared specimens a water content less than the liquid limit to reduce the testing time and, avoid presheared multistage tests.

Recently, *Sadrekarimi and Olson (2009)* presented the design of a new ring shear device developed at the University of Illinois which allows conducting constant volume or drained tests. The device has an auxiliary load and torque cell to measure any wall friction that develops along the confining rings, and utilize quad-rings along the confining rings to prevent soil extrusion. Additionally, the dimensions of the specimen were increased in order to reduce stress and strain uniformities.

2.4 Results from Previous Work

Over the last few decades, conventional soil testing equipment such as direct shear and triaxial testing devices have been modified and widely used for the assessment of residual shear strength properties of unsaturated soils (Escario and Saenz, 1986; Gan and Fredlund, 1988; Wheeler, 1988; de Campos and Carrillo, 1995; Yin, 2003; Caruso and Tarantino, 2004). However, these techniques present the limitation that they impart a limited shear deformation state along the failure plane, which prevents reaching the critical state condition under controlled-suction states. In addition, specimens with pre-cut planes, or specimens containing shear surfaces at appropriate angle, are generally required. Therefore, in order to overcome these limitations controlled-suction ring shear testing devices have recently been introduced.

Recently, Infante et al. (2005, 2007) reported a first attempt at modifying a Bromhead type ring shear apparatus for testing soils under controlled low-suction states via the axis-translation

technique. The modified ring shear apparatus incorporates an automated data acquisition and control system which allows independent control of the pore-air pressure and the net normal stress. The major modifications were the increasing of the sample height from 5 to 20 mm and, the increasing of the outer and inner diameters from 100 and 70mm to 133 and 92 mm, respectively.

The current cell design of this device is based on the apparatus previously developed by Garga and Inafante Sedano (2002) to undertake constant volume RS test on sands. In that apparatus, the confining cell walls of the annular specimen are made of stacks of 2mm thick rings. These rings can easily slide over each other so that they can independently move with the soil at their respective depths. The authors state that this technique reduces the stress concentrations, or wall friction, which are typical of conventional ring shear testing devices.

The modified ring shear device allows the determination of the residual shear strength of unsaturated soils under constant volume, consolidated drained test or constant water content conditions over matric suction states from 0 to 500 kPa. In addition, the device is useful to study changes in the Soil Water Characteristic Curve (SWCC) that occur during shearing process.

The authors state that the SWCC obtained by conventional means (e.g., pressure plate extractor technique) can be substantially different from the SWCC obtained from a sheared specimen. They found that the best predictions of the shear strength from SWCC models are obtained from the apparent SWCC at critical state (Infante et al., 2010). They also present a methodology to correct the water content measurements for the effect to air infiltration and evaporation or condensation of water.

Figure 2-11 shows a picture of the modified RS apparatus featuring the following components: (1) LVDT to measure the vertical deformation; (2) Load cells for the measurement of the torque; (3) Pressure transducer to monitor the pressure of the air phase, and therefore the matric suction; (4) Rotational potentiometer to measure the angular displacement of the cell with

respect to the top platen, (5) Load cell for the measurement of the normal load; and (6) Precise electronic balance (resolution of 0.001g) to measure the water content change of the specimen.

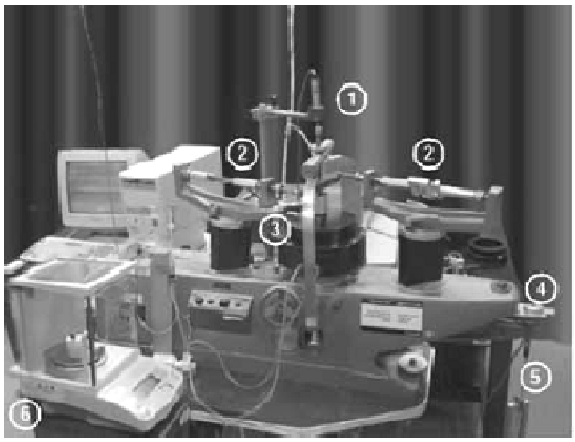

Figure 2-11 Modified Bromhead ring shear apparatus (Infante et al., 2007).

Shortly after, Vaunat et al. (2006, 2007) reported results from a modified Bromhead type ring shear apparatus used for soil testing under controlled high-suction states via vapor transfer technique. The specimen height is 5 mm while its outer and inner diameters are 100 mm and 70 mm, respectively. Low and medium plasticity clayey soils were tested. The authors reported an increase in the residual friction angle with an increase in the applied suction. This was mainly associated to the partial aggregation of clayey particles, which was believed to have caused the soil to behave more like a granular material.

The authors also observed that the unsaturated soil residual strength was independent of both the applied vertical stress and the suction stress history. Figure 2-12 shows a picture of the modified RS apparatus. In this device, the shear box was isolated from the ambient atmosphere by a glass-cap and connected to a circuit of forced convection of vapor. Relative humidity was controlled by circulating the air above a solution saturated in salts of different types.

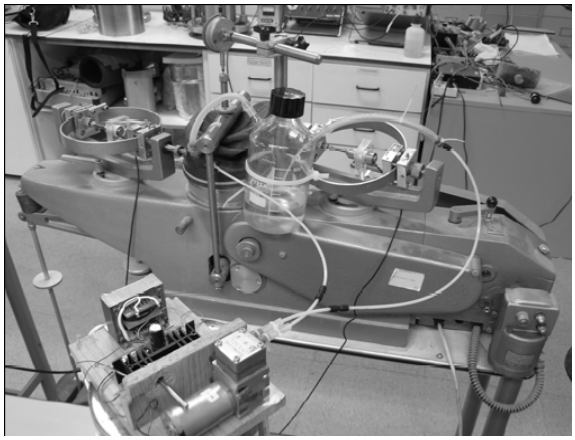

Figure 2-12 Modified Bromhead ring shear apparatus (Vaunat et al., 2006).

The above results, however, are far from conclusive, and the modified ring shear devices offer plenty of room for further refinement and development. The present research work introduces a novel suction-controlled ring shear apparatus that has been made suitable for testing unsaturated soils over a whole range of deformations using the axis translation technique.

The next chapter describes the full development of the novel suction-controlled ring shear device including details of its main components. Typical soil parameters obtained during suction-controlled RS tests are also presented.

CHAPTER 3

DEVELOPMENT OF A NOVEL SUCTION CONTROLLED RS DEVICE

3.1 Introduction

This chapter introduces a novel suction-controlled ring shear apparatus that has been made suitable for testing unsaturated soils over a whole range of deformations using the axis translation technique. The apparatus is a fully servo-controlled system with a 113-ton-m torque capacity and more than 360-degree-range of continuous angular deformation. The general design of the core system is similar to that of the original ring shear apparatus developed by Bromhead (1979). In contrast to the modified Bromhead type ring shear apparatus, tests can be performed either on remolded or statically compacted test specimens. This allows a better control of the initial compaction conditions such as dry density, initial water content and initial matric suction.

The modified ring shear device allows the determination of shear strength properties of unsaturated soils under constant volume or consolidated drained conditions over matric suction states from of 0 to 1500 kPa. In addition, the device is useful to study changes in the Soil Water Characteristic Curve (SWCC) that can occur during the shearing process. All data, such as shear stress, vertical load, vertical and angular displacements are collected by a data acquisition system connected to a computer. The general design of the core system is similar to that of the original ring shear apparatus developed by Bromhead (1979).

The following sections describe the full development of the novel suction-controlled ring shear device implemented in this research work, including details of its main components, and the typical soil parameters obtained from suction-controlled RS tests.

3.2 Axis Translation Technique

The axis translation technique forms the basis for laboratory testing of unsaturated soils under high matric suctions conditions. Basically, both pore-air (u_a) and pore-water (u_w) pressures are translated into the positive pressure range, so that the matric suction induced in the specimen, $(u_a - u_w)$, remains constant regardless of the magnitude of (u_a) (Hilf, 1956; Bishop et al., 1960; Fredlund, 1989). Figure 3-1 illustrates the application of the technique to an unsaturated soil specimen undergoing a matric suction of 101 kPa. Pore-water pressure (u_w) is measured below a saturated high-air-entry disk with an air-entry value of 202 kPa which acts as an interface that separates air and water phases. The water phase is originally under 101 kPa tension. An air pressure of 202 kPa is then applied directly to the specimen in order to rise (u_a) to the same magnitude. As a result, pore-water pressure (u_w) is increased by an equal amount, with a final positive value of 101 kPa.

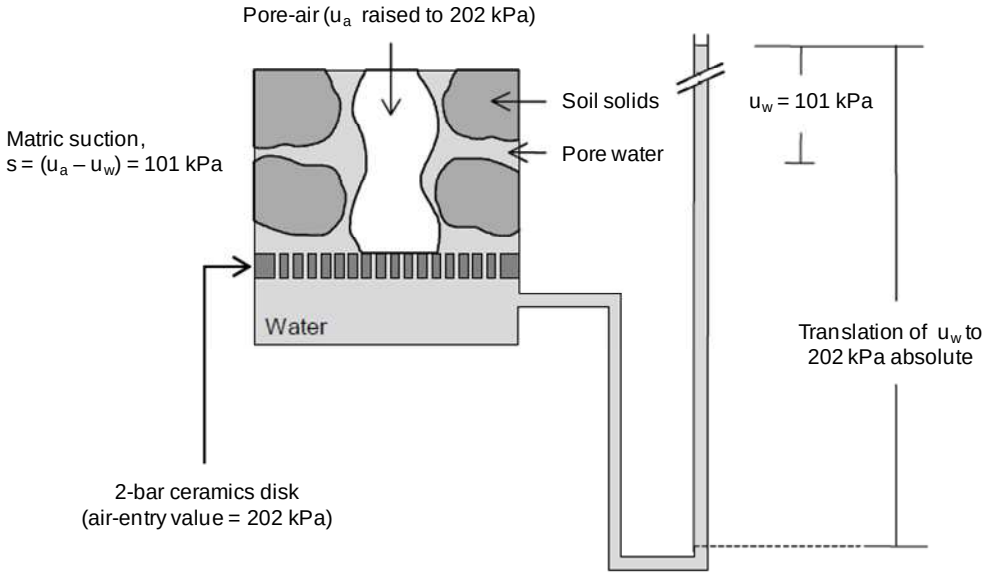

Figure 3-1 Concept of axis-translation technique.

Under these conditions, there is no problem associated with possible cavitation of the water in the measuring system. Despite the translation of the reference pore-air pressure (u_a) from 0 to 200 kPa, the matric suction experienced by the soil remains constant at 101 kPa. If the pore-water pressure is set to zero (i.e., open to atmospheric conditions) the applied pore-air pressure (u_a) will be the matric suction experienced.

Limitations of the axis translation technique:

Dineen (1997) classified the limitations of the axis translation technique in two categories, equipment and materials. The author describes as equipment limitations the necessity of using robust devices to resist the effects of the elevated air pressures, the air pressure capacity that conventional air supply can provide and the limited air entry value of the ceramics disks that are commercially available. At the University of Texas at Arlington, the main air supply has a maximum rating of 800 kPa. Compressed air bottles are required beyond this range. For the novel ring shear apparatus the working range of suctions is further limited by the requirement for the air pressure to be equal to the sum of the suction and the total normal stress (σ).

Among the material limitations, the technique is best suited for measuring matric suctions of unsaturated soil specimens in which the air phase is continuous. If occluded air bubbles are present, the application of elevated air pressure will cause the pore fluid to compress. As a consequence, a pore pressure gradient will develop through the sample, and irreversible volume changes will occur.

Booking and Fredlund (1980) concluded that for a degree of saturation above of 85% the air permeability was effectively zero. They suggested an upper limit of 85% saturation should apply for use the axis translation technique because the presence of occluded air bubbles in the soil specimen can result in an overestimation of the measured matric suction. The authors state that even at this degree of saturation there may be a percentage of pore air that is occluded.

In this work, matric suction in the specimen during controlled-suction ring shear testing was controlled via the axis translation technique in order to achieve suction states, $(u_a - u_w)$, of 0, 25, 50, 75 and 100 kPa. Testing specimens showed initial degree of saturation less than 80% at suctions within the range of applicability of the axis translation technique.

Matric suctions beyond 100 kPa could not be applied, when SM and SC-SM specimens where tested, due to the fact that the peak shear strength response of the specimens during suction-controlled ring shear testing exceeded the maximum torsional shear capacity of the load-torque transducer.

Likewise, CL specimens could not been tested under suction-controlled states because the peak and residual shear response were beyond to the maximum torsional shear capacity of the load-torque transducer.

3.3 General Assembling of the Novel RS Devise

The novel ring shear device features two independent servo-controlled actuators: a pneumatic actuator for applications of normal loads and an electromechanical rotary actuator for application of torque loads and rotary motion. It allows the application of vertical loads up to 8000 N, monotonic torque up to 113 N-m, constant suction states up to 500 kPa, and more than 360-degree-range of continuum angular deformation.

Figure 3-2 shows a panoramic view of the complete suction-controlled ring shear test layout, which is composed of three main modules: (1) Main cell with rotational shear system, including normal load and torque actuators; (2) Data acquisition and process control (DA/PC) system with performance and data reduction software for real-time calculation of normal and shear stresses and average linear and angular displacements; and (3) PCP-15U suction control panel for implementation of axis-translation technique. Details are summarized in the following.

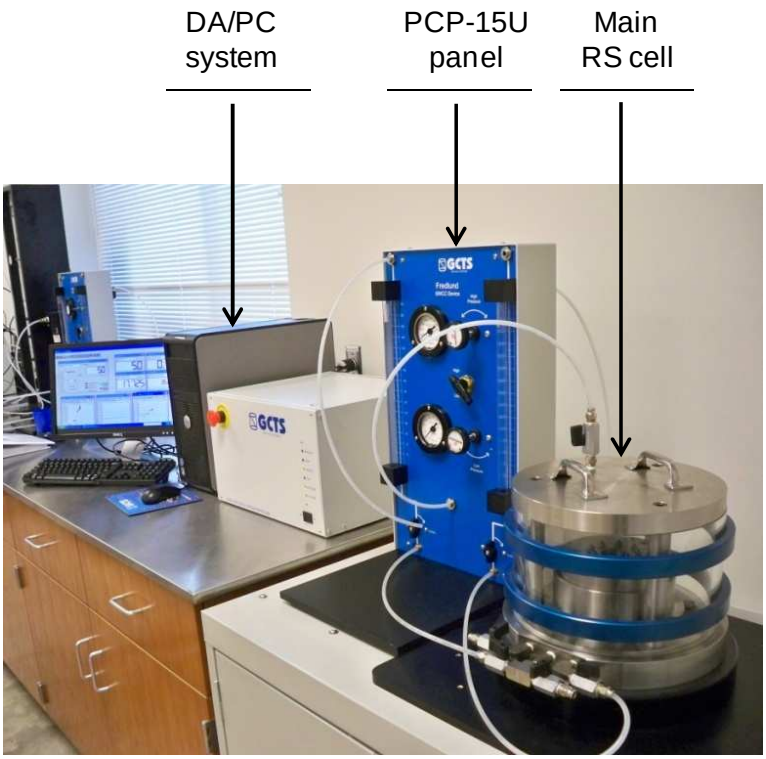

Figure 3-2 Panoramic view of complete suction-controlled ring shear test layout.

3.3.1 Main Cell

Figure 3-3 shows an isometric view of the main cell and the corresponding servo-controlled normal load and torque application systems, featuring all of the following: (1) Top cover plate; (2) Core confining cell with a 1500-kPa air pressure capacity; (3) Bottom base plate; (4) Adjustable stainless steel upper annular platen; (5) Stainless steel lower annular platen; (6) Vertical load shaft; (7) Self-contained electrical sensors for real time calculations of vertical load and shear torque; (8) Rotary servo-controlled actuator for application of tortional loads up to 820 N-m; (9) Pneumatic servo-controlled actuator for application of vertical loads up to 8000 N; and (10) Linear variable differential transducer (LVDT) for monitoring of vertical deformations.

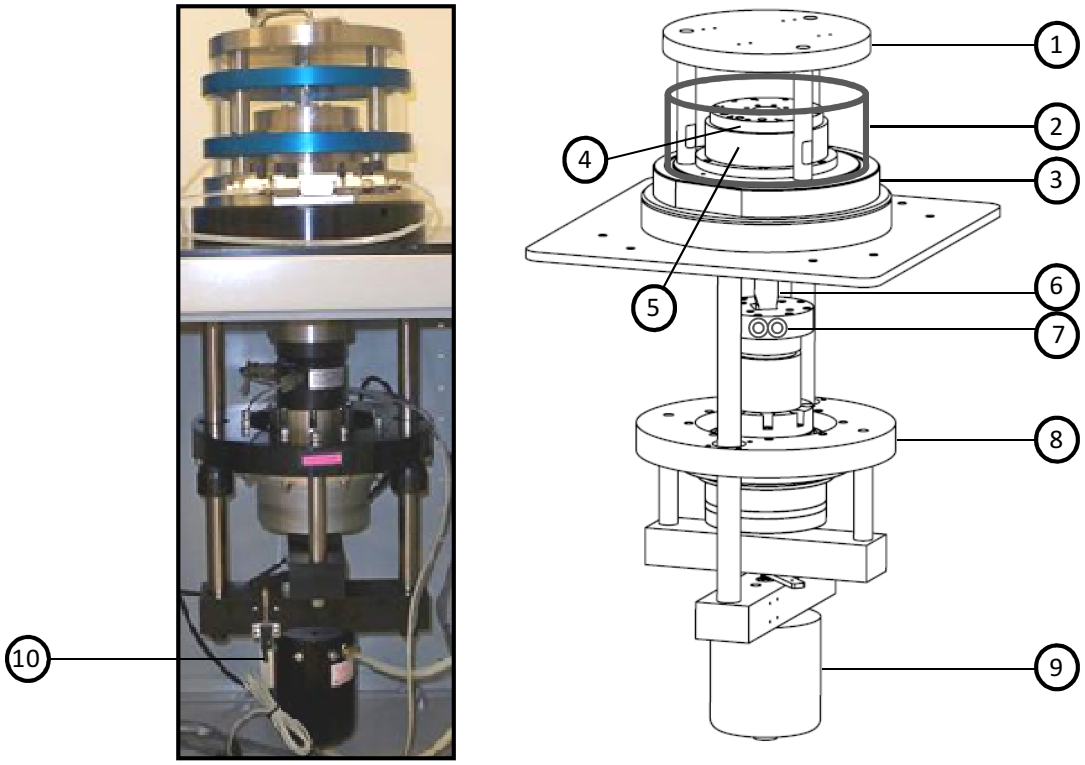

Figure 3-3 Isometric view of main cell and servo-controlled normal load and torque application systems.

Core confining cell:

The novel ring shear apparatus features a see-through Plexiglas external cell wall for application of lateral air pressure (u_a). The cell is reinforced with steel bands (rings) to sustain lateral confining pressures up to 1500 kPa. The top cap of the confining cell is equipped with one plug connected to the air pressure system supply. At the University of Texas at Arlington the main air supply has a maximum rating of 800 kPa. The bottom base plate is equipped with four ball valves and quick disconnects fittings for air pressure vent, bottom air/water pressures, and bottom flushing. Figure 3-4 shows a detailed photograph of the fully assembled ring shear confining cell.

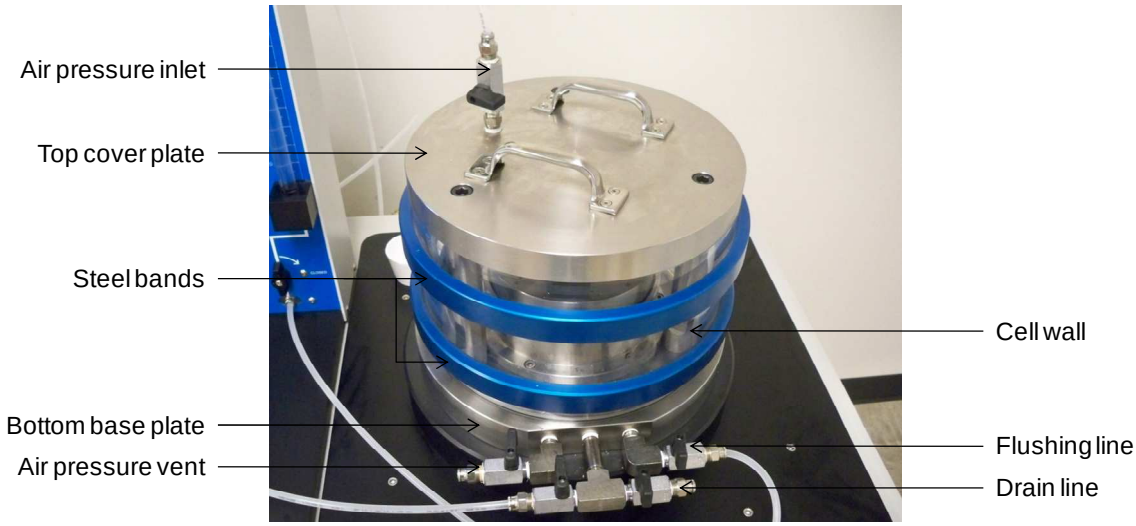

Figure 3-4 Ring shear confining cell.

Upper Annular Platen:

The original upper annular platen houses a full set of six coarse stainless steel porous stones provided by Applied Porous Technologies, Inc., which are evenly distributed along the central perimeter of its bottom surface for application and control of pore-air pressure, as shown in Figure 3-5. Each stone is 6.35-mm in diameter and 1.56-mm in thickness. The stones cover about 1.74% of the total surface area of the specimen, which is 109.25 cm^2. The upper annular platen also features a full series of linear groves chiseled across its bottom surface to ensure enough contact at the soil-platen interface to develop full shearing effect.

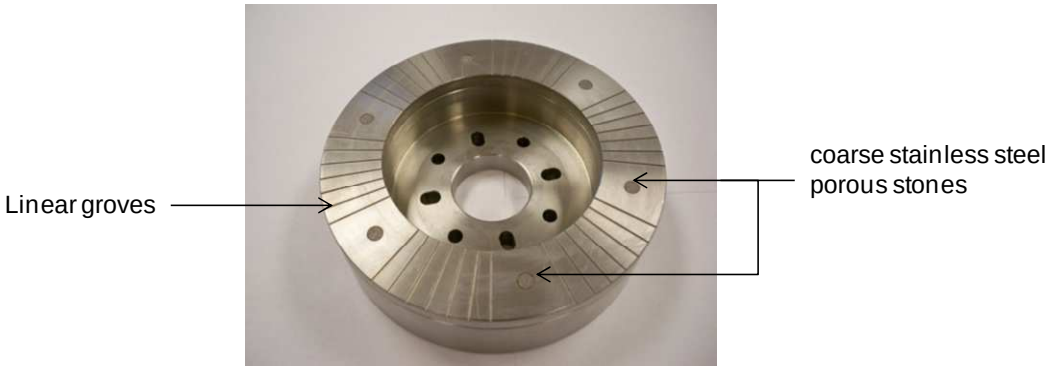

Figure 3-5 Original RS design: upper annular platen - shown upside down

Lower annular platen:

The core base of the lower annular platen features a 3-mm depth, 4-mm wide, circular groove to facilitate the flushing of diffused air during suction-controlled testing, as shown in Figure 3-6(a). The lower annular platen accommodates a stainless steel annular disk that houses a full set of six high-air-entry (HAE) ceramic disks for application/control of pore-water pressure (u_w) . The annular disk is 96.5-mm in inner diameter, 152.4-mm in outer diameter and 7.60-mm in thickness. This array is shown in Figure 3-6(b). All ceramics are sealed to the annular disk via a sintered stainless-steel ring and an O-ring seal to prevent pore-air leakage into the water system. The sintered stainless-steel rings are 18-mm in inner diameter, 22-mm in outer diameter and 7.6-mm in thickness. The air-entry value of the ceramics disks used in this study is 500 kPa and was supplied by Soil Moisture Equipment Corporation, USA. The ceramic disks are 16.3 mm in diameter and 7.55-mm in thickness. Figure 3-6(c) shows a sintered stainless steel rings-ceramic disk arrangement. The ceramic disks can be easily replaced by others ceramics with high air-entry value for application of higher values of matric suction enabling testing unsaturated soils under a wider range of matric suctions. The annular disk is fixed to the base of the lower annular platen with 10 screws and an O-ring seal as shown in Figure 3-6(d).

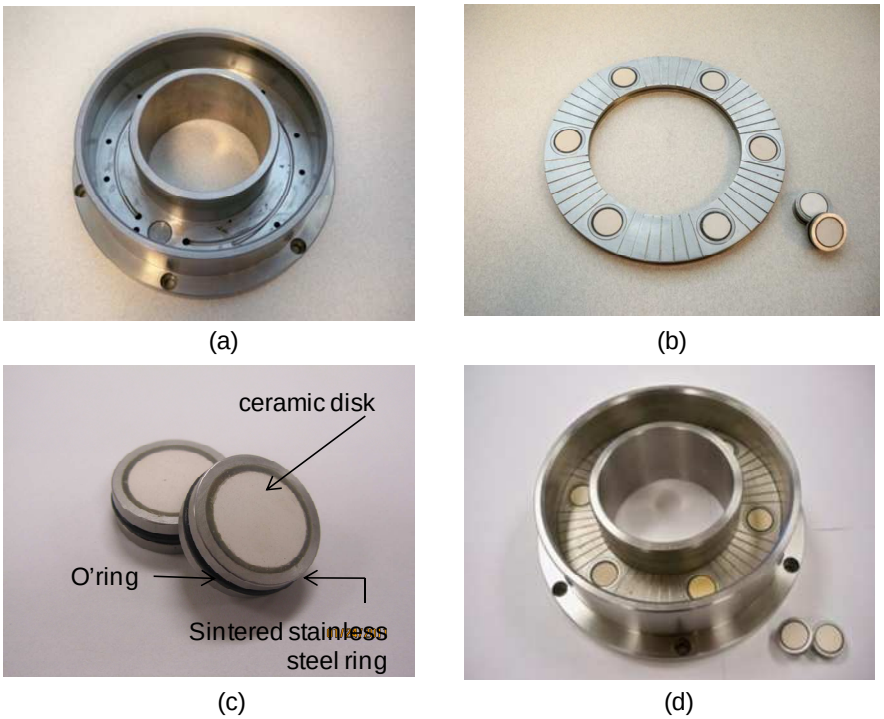

Figure 3-6 Original RS design: (a) core base of lower annular platen, (b) annular disk with ceramics, (c) ceramic disk and sintered stainless steel rings, (d) lower platen with ceramics.

Saturation procedure of ceramics disks:

In order to achieve the continuity between the pore-water and the water in the compartment beneath the ceramics disks, as well as to prevent air passage through the ceramic disks, the ceramics were saturated following the next procedure: The ceramic disks were initially immersed in deaired water in a beaker for 24 hours. Then, a vacuum of 30 mmHg was applied to this system and left for 24 hours in order to remove any air bubbles inside of voids of the ceramics disks (Figure 3-7). It was expected that any occluded bubble at this stage were replaced by water. After that, the ceramic disks were mounted in the annular disk and this assembly was installed and fixed to the bottom annular platen. The bottom annular platen was filled with deaired distilled water and fixed to the bottom plate as is shown in Figure 3-8. The confining cell was installed and a pressure of 200 kPa was applied. The assembly was left 24

hours under the cell pressure to ensure the fully saturation of the ceramic disks. Ceramics disks were re-saturated after each test by filling again the bottom plate with deaired water and applying pressure as previously described. In between the periods of test the disks were kept under distilled water in order to avoid drying.

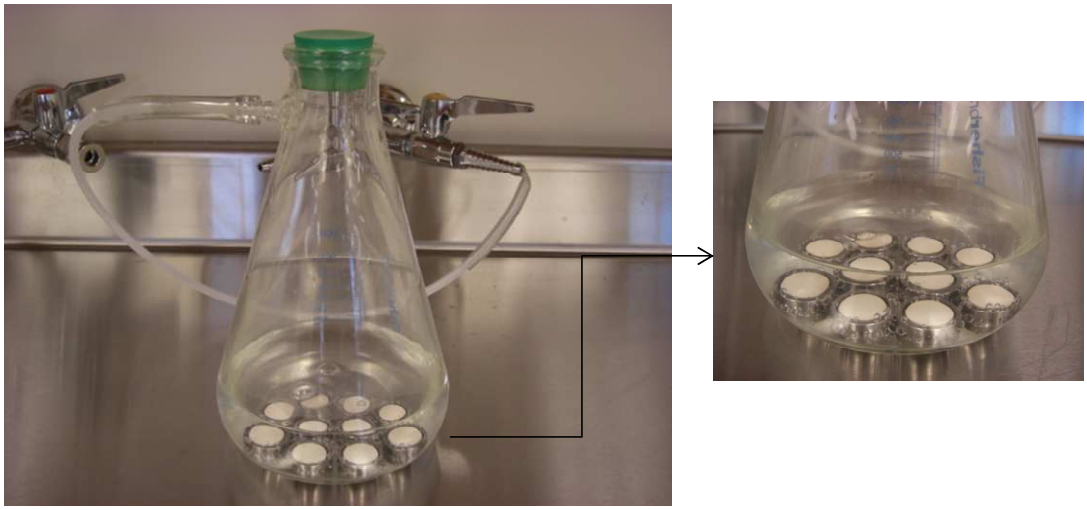

Figure 3-7 Vacuum application for saturation of ceramic disks.

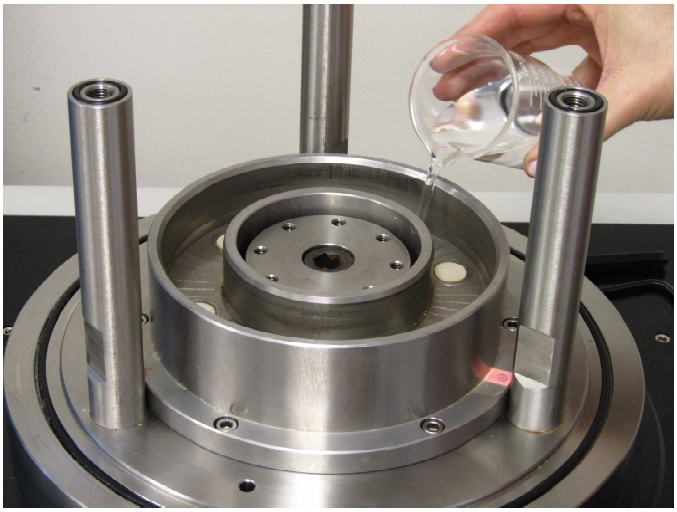

Figure 3-8 Application of deaired water into the bottom plate.

Flushing procedure:

When testing unsaturated soils there is a requirement for the precise measurement of the volume change of the sample. In a saturated soil the change of volume is related to the change in pore-water, whereas in an unsaturated soil the change in volume is due to change in both pore-water and pore-air. Therefore, the changes in water content in the soil are calculated by measuring the water volume that passes through the ceramic disks. This value could be corrected taking into account the amount of air diffused through the ceramic disks. After long testing periods the diffused air accumulates underneath the ceramics and introduces an error in either the pore water pressure measurements in constant water content tests or in the pore water volume change in drained tests.

Padilla et al. (2006) state that the accumulation of diffused air can also lead to the possible dry-out of the ceramics, retarding the flow of water through the disks and causing impedance of the hydraulic conductivity of the ceramics disks. The authors conclude that the air diffused through the ceramic disks rated 1- and 3-bars is essentially negligible and that one flushing over three days can be considered adequate. For 5-bar ceramic disks the amount of air diffused is relatively small compared to 15-bar disks. The authors suggest that flushing once in two days could be adequate. In contrast, air diffused through 15-bar ceramic disks is considerable even at 50% of the rated bubbling pressure. They recommended flushing twice or more a day. The authors propose that the flushing frequencies should be adjusted by observing the actual air diffusing during a test.

During the present research the drainage line and the circular groove beneath the disks were flushed once every two days with deaired distilled water using the PCP-15U suction control panel described later in section 3.3.2.

Sample measurements:

Soil samples conform to the annular space between the two concentric rings of the lower platen, having a 152.4-mm outer diameter and 96.5-mm inner diameter, as shown in Figure 3-9. The inside to outside diameter ratio is 0.63, as per ring shear testing standard ASTM D6467-06a. The effective surface area of the sample is 10924 mm^2, which is used for calculation of applied normal stress. The average specimen height is 15 mm.

Figure 3-9 Exposed compacted sample of SM.

The loading system:

Axial loading system:

The normal load is derived from air pressure supplied to a servo-controlled axial actuator. The axial actuator is a double acting diaphragm air cylinder, 16-in^2 in size and, 3.7-in of stroke provided by MB Marsh Bellofram, USA. It allows the application of vertical loads up to 8000 N. The stainless steel loading piston, aligned by a guide bushing system, transfers the load through a high pressure-low frictions ball seal and the upper annular platen to the soil sample. The high pressure-low frictions ball seal eliminates the static friction associated to the bearings

of the bushing system when the piston is moving up and down. The precise guide bushing system prevents tilting of the upper annular platen in the event of uneven soil compression.

The axial actuator is servo-controlled by two valves for closed-loop control using either the linear variable differential transducer (LVDT) or the normal force sensor as a feedback for controlling the axial loading piston either in stress-load control or in deformation or strain control. The first valve corresponds to a servo solenoid valve MH 1353 type, manufactured by Ingersoll Rand Industrial Technologies, and is used for shutting off, releasing and dosing the air flow from the main air supply system. The second valve is a proportional directional control valve, MPYE 5/3 way-valve type, provided by FESTO Inc. This proportional valve is used for transforming the analogue input signals into a corresponding opening cross-section at the valve outputs. This valve combination allows a precise pneumatic position and speed of the air cylinder. The servo controlled axial actuator and the servo valves system are shown in Figure 3-10.

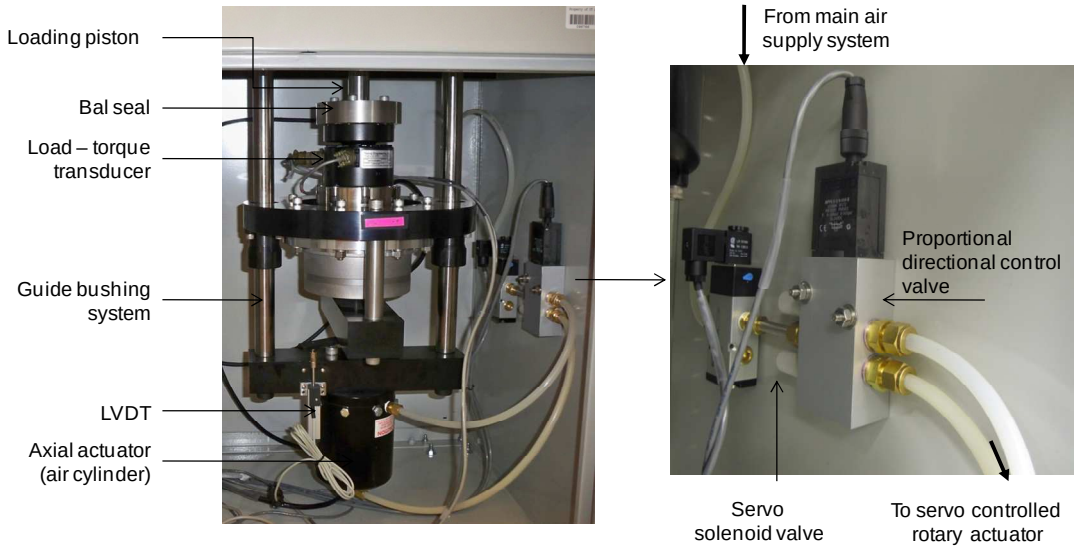

Figure 3-10 (a) Servo-controlled load application system layout, (b) servo valve configuration.

Torsional loading system:

The torsional load is derived from an electromechanical rotary actuator FHA-40C-160-US-250 type manufactured by Harmonic Drive Sytem Inc, USA. Table 3-1 shows the model code of the FHA-C series used in the novel RS apparatus.

Table 3-1 Model code of the FHA-40C-160-US-250 type actuator.

Type	FHA-C Series
Frame size	40
Design Version 1	C
Reduction ratio of harmonic drive gear	160: 1/160
Encoder Specification	US: 14 wire incremental encoder
Encoder resolution	250: 2500p/rev

The FHA-40C servo actuator provides high torque and a high accuracy rotary motion. An important feature of this actuator is the large through-hole in the center of the shaft, through which the loading shaft and electric cables pass to supply power and signals to moving parts. The motor of the FHA-C actuator is equipped with an incremental encoder of 2500 resolutions for detecting the angular position of the loading shaft. The one-way positioning accuracy of the actuator is of 30 arc seconds. This is the maximum positional difference between a commanded theoretical position and its actual angular position for serial positioning in one revolution when approached from the same direction (Figure 3-11). The one-way positioning accuracy of the actuator is almost equal to the angular positioning accuracy of the servo drive.

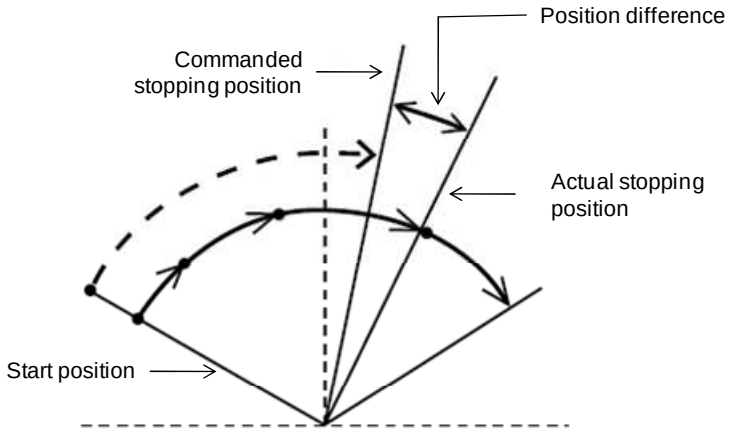

Figure 3-11 One-way positioning accuracy for the rotary actuator.

The actuator is also comprised of a digital servo drive BAS-6/230 manufactured by Elmo Motion Control Inc., to control its position and speed with great accuracy and reliability. This servo drive supports up to 6 amps continuous current. Its high density allows the drive to deliver 1900 W continuous power and 3800 W peak power. Based on Elmo's SimplIQ Motion Control technology, the drive is capable of operating in position, velocity and current modes and contains a wide range of feedback and I/O options. Basically, once the servo drive receives a command signal from a control system (computer) this amplifies the signal and transmits electric current to the servo rotary actuator in order to produce motion proportional to the command signal. The command represents a desired angular velocity. The encoder attached to the rotary actuator reports the actual actuator velocity back to the servo drive. The servo drive then compares the actual actuator velocity with the commanded motor velocity. It then alters the voltage frequency to the motor so as to correct for any error in the velocity. As previously explained, the actuator rotates at a velocity that very closely approximates the velocity signal being received by the servo drive from the control system. Several parameters, such as P gain (also known as

proportional gain), I gain (also known as integral error) and D gain (or derivate gain), can be adjusted through the software CATS to achieve this desired performance (that will be explained later in this section). The model code of the BAS-6/230 servo driver is shown in Table 3-2.

Table 3-2 Model ordering code of the BAS-6/230 servo driver.

Type	BAS
Design Version	Standard
Continuous current (Amps)	6
Nominal AC operating voltage	230
Feedback	Incremental encoder

Table 3-3 shows a summary of the main technical specification of the FHA-40C rotary actuator with an incremental encoder.

Table 3-3 Specifications of FHA-40C-160-US-250 with an incremental encoder.

Maximum Torque	N•m	820
Maximum Speed	r/min	22
Torque Constant	N•m/A	102
Maximum Current	A	9
EMF Voltage Constant	V/(r/min)	11.4
Reduction Ratio	-	1:160
Allowable Radial Load	kN	14.7
Allowable Axial Load	kN	39.2
Allowable Torsional Moment	N•m	690
Moment stiffness	N•m/rad	$1400x10^3$
One-way Positioning Accuracy	arc-sec	30
Motor encoder	Pulse/rev	2500
Quad encoder resolution	Pulse/rev	1600000
Mass	Kg	12

Although the electromechanical actuator allows applying torque loads up to 820-N-m, as shown in Table 3-3, the maximum torque load capacity of the ring shear is limited by the maximum range of the torque sensor which is 113 N-m. This constraint limited the application of matric suction and normal stress states beyond 100 kPa because the peak shear strength response of the soil under those conditions exceeds the maximum capacity of the torque sensor.

During shearing, the upper annular platen is monotonically rotated by the rotary servo-controlled drive unit while the lower annular platen remains restrained. A complete layout of the servo-controlled load-torque application system is shown in Figure 3-12.

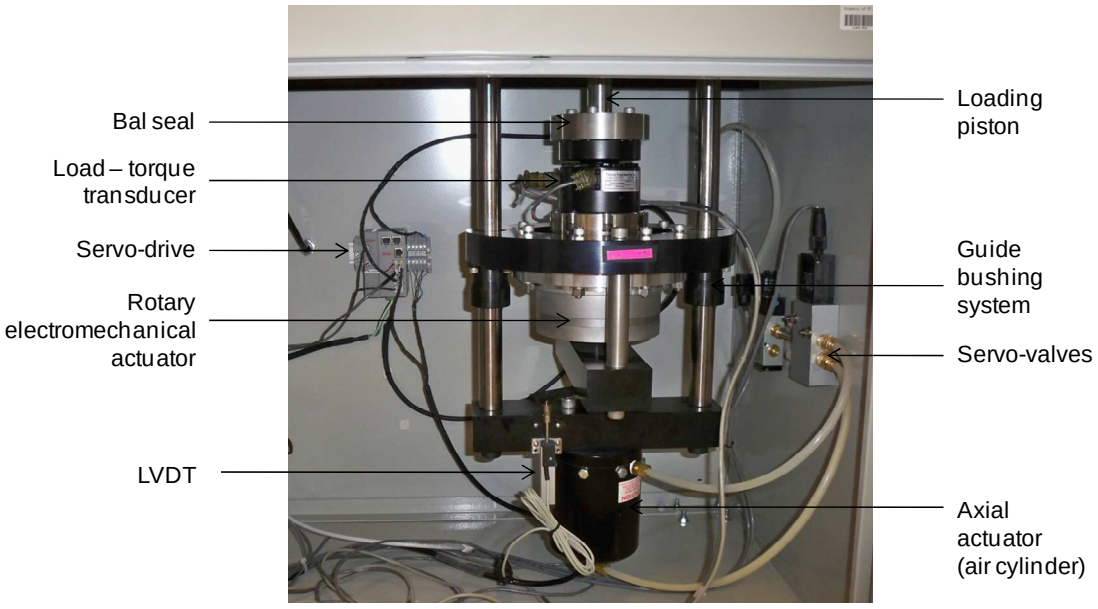

Figure 3-12 Detail of the servo-controlled load-torque application system.

Measurement of normal and torque loads:

The normal load applied to the soil sample and the shear forces developed across the failure plane during testing are measured through a combined axial force and torque transducer, series SWT10-2K-B000, manufactured by Tovey Engineering Inc. The transducer features a high accuracy in both force and torque bridges, low crosstalk and low creep. The maximum capacity of the transducer is 8000-N of axial load and 113-N-m of torque. This is mounted on an internal floating frame to allow for large vertical specimen deformations. Figure 3-13 shows the combined axial force and torque transducer and Table 3-4 shows a summary of its main specifications

Figure 3-13 Combined axial force and torque sensor transducer.

Table 3-4 Specifications of combined the axial force and torque transducer.

		Axial force bridge	Torque bridge
Capacity	lbf. / in.-lbf	2K	1K
		Accuracy	
Nonlinearity	% R.O.	± 0.04	± 0.07
Hysteresis	% R.O.	± 0.04	± 0.05
Nonrepeatibility	% R.O.	± 0.02	± 0.05
Creep	% in 20 min	± 0.025	± 0.025
Zero balance	% R.O.	± 2.0	± 2.0

Measurement of vertical displacements and angular displacements:

A linear variable differential transducer (LVDT) was used for monitoring of vertical soils deformations and also as feedback of the normal actuator. The LVDT has a range of ± 25 mm. This instrument measures the relative movement of the transducer body and a core by relating the displacement to the interference of the electric field generated by the energized body. A signal conditioning system makes the output signal compatible with the read out system.

The electromechanical rotary actuator includes an incremental rotary encoder for detecting the position and speed of the loading piston. This rotary encoder is an electrical-mechanical device that converts the angular position of the loading piston to a digital electronic signal, making it an angle transducer. As previously described the rotary actuator is equipped with an incremental encoder of 2500 resolutions.

3.3.2 PCP-15U suction control panel

A Model PCP-15U pressure control system (from Geotechnical Consulting and Testing Systems) is used for direct control of pore-air pressure at the top of the soil specimen, featuring dual pressure regulators and gauges for precise measurement and control of matric suction using the $s = u_a$ testing concept (i.e., $u_w = 0$). Air pressure is directly supplied to the main cell from the PCP-15U panel, as shown in Figure 3-14.

The panel also features a flushing line that connects to the bottom base plate of the main cell for removal of diffused air during constant-suction RS testing.

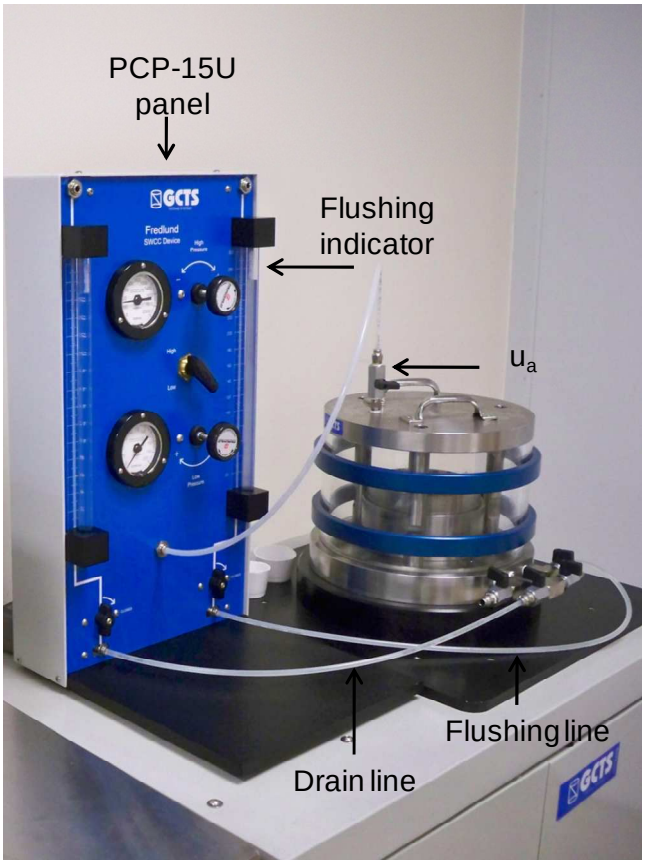

Figure 3-14 PCP-15U suction control panel.

3.3.3 DA/PC system

The data acquisition and process control system, as shown in Figure 3-15, consists of all of the following: (1) One SCON-1500 digital servo controller and acquisition system; (2) GCTS CATS software for real time measurement/control of normal stress, shear stress, and angular deformations; and (3) IBM-PC unit.

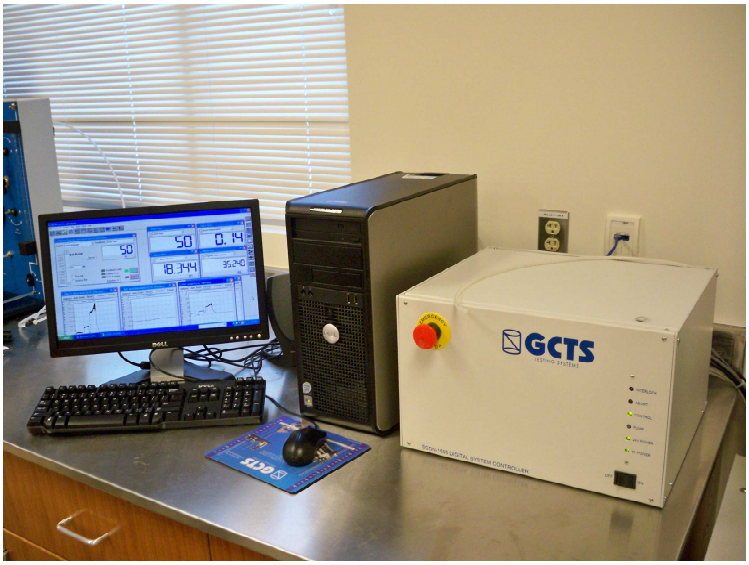

Figure 3-15 Data acquisition and process control system (DA/PC).

SCON-1500 digital servo controller and acquisition system:

The SCON-1500 model Digital System Controller consists of a microprocessor based digital servo controller, function generator, data acquisition, and digital I/O unit. This unit allows an advanced servo control from any system sensor with “on-the-fly-bump-less” transfer switching between any connected transducer or calculated input. Utilizing signal conditioning electronics, optimization and calibration settings (gains and offsets) are controlled through the GCTS CATS software developed by GCTS Testing Services. The system features a Universal Signal Conditioning board module that can be used by any type of sensor (strain gauge, LVDT, DC output, and thermocouple). The sensor amplifier gain and offset are digitally and precisely controlled by the software, eliminating the need to use reference gauges or shunt resistors to setup each sensors. If a new sensor is installed into the SCON-1500 the only information required to be entered into the software are the calibration factors. The signal conditioning automatically sets the amplification and offset values to accurately read new sensors.

The SCON-1500 system provides 16-bit resolution and an analog anti-alias filter for high frequencies, and a digital filter for low frequencies. This configuration produces a very stable and precise signal measurement and control system. The system is equipped with Remote Interlock and Watchdog Timer for safety operation of the test equipment. The system can accommodate up to 16 signal dynamic inputs and provide real time linearization. The SCON-1500 uses a “Sample and Hold” circuit to digitize all the connected inputs at the same instant. Sample and Hold is important for dynamic tests to eliminate and data skew between sensors input. The user defines the function inputs and can combine calculations on a number of inputs. The system is capable of independently and simultaneously controlling 4 separate Analog Output (servo) channels in closed or open loop. Also it includes 4 Digital Inputs and 4 Digital Outputs. A summary of the main features of the SCON-1500 are listed as following:

- 850 MHz micro-processor with 64 MB RAM and 128 MB solid state disk.
- 6 HHZ maximum loop rate (250 kHz conversion rate between channels).
- 16-bit resolution.
- Microprocessor based digital servo controller.
- Built-in function generator.
- Data acquisition and digital I/O unit.
- Advanced servo control from any system sensor with “one-the-fly-bump-less” transfer switching between any connected transducer or a calculated input.
- Can be configured to read up to 8 analog sensor (transducer) inputs and control up to 4 analog outputs.
- 4 digital inputs and 4 digital outputs.
- Watchdog timer to detect control program status for automatic interlock shutdown.
- RS-232 Communications.

GCTS CATS r*ing shear software:*

The GCTS CATS 1.8 software is a complete Computer Aided Testing System software that accompanies the GCTS control system. The GCTS control system is composed of two components, called the CATS program.

The controller is usually an embedded microprocessor that is running the control program in a real time environment (operating system). The controller actually read/writes to the boards, performs the requested test, saves the data file, and many other functions. The user does not have direct access to the controller, as the user can only interact with the controller through CATS program. However, the controller is independent from the CATS program as the CATS does not need to be running in order for the controller to operate. The CATS program is foremost a GUI program with an interface for the user to communicate with the controller. It runs on a separate computer from the controller, on a computer that is running a Windows operating system.

Because the controlling is done by the controller, the CATS by itself cannot do any controlling, and thus its functions are very limited without its controlled counterpart. The CATS program handles the data base aspect of the CATS system, where it keeps the information for all the sensors, projects, samples, specimens, etc. The CATS program communicates with the controller through a communication protocol.

The GCTS CATS software is a friendly program that allows the user to easily setup and conduct ring shear tests. The program allows for real-time determination and control of various test inputs, such as shear stress and normal stress. The user has the choice to assemble their own test consisting of multiple stages. The tests can include Consolidation, Shear Loading or Universal Stage. The Consolidation stage allows for the user to easily perform normal consolidation, and the Shear Loading stage is optimized for shear loading, while the Universal Stage allows the user to define any test sequence that they prefer. Figures 3-16 and 3-17

illustrate the configuration parameters for the consolidation and universal stages used in a typical suction-controlled ring shear test.

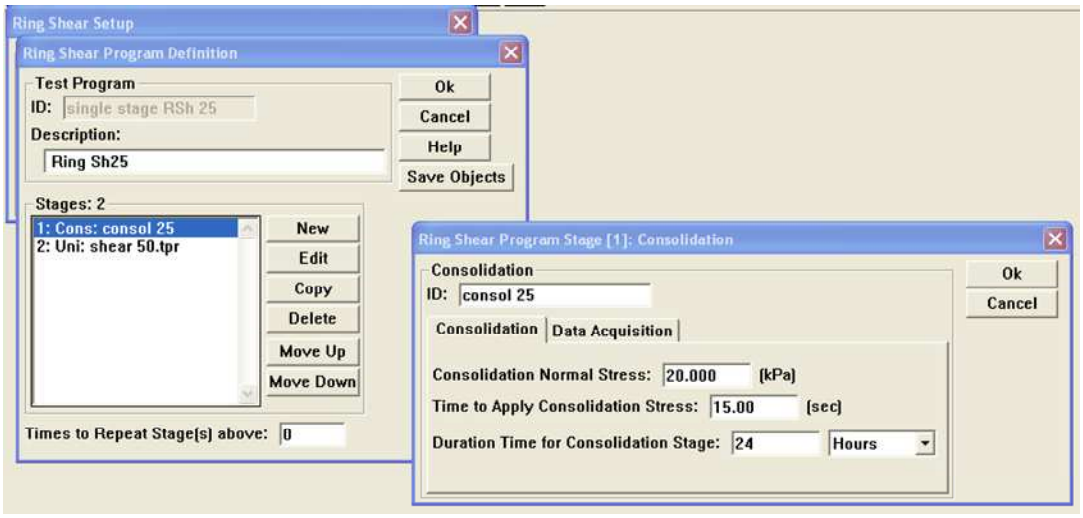

Figure 3-16 View of the consolidation stage configuration windows for a ring shear test

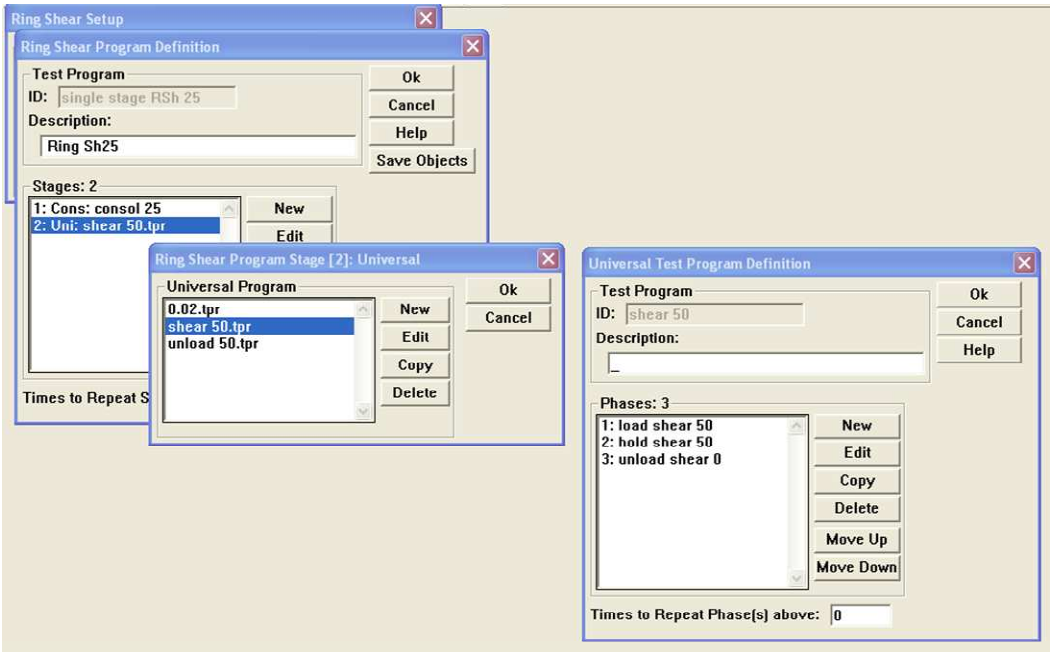

Figure 3-17 View of the universal stage configuration windows for a ring shear test.

The Ring Shear test configuration is the configuration of the test to respect to its system setup and its connections to the hardware apparatus. The configuration itself does not have to be adjusted often, as the configuration is not something that will change regularly. Test setup, on the other hand, is the actual test sequence on the specimen.

The test configuration is divided up to individual sections: control, inputs, units and specimen. In this chapter only the control and input configuration sections will be described. Information about the other parameters can be found in Direct/Ring shear test CATS User's guide and reference (GCTS, 2009). Figure 3-18 shows the four ring shear configuration windows that can be setup by the user.

Control: The system is comprised by two control parameters, shear actuator and normal actuator (Figure 3-18a). They need to be connected to the analog outputs if they are controlled by them. All of these parameters can be manually controlled. The shear actuator option is the analog output that is connected to the servo driver that controls the rotary electromechanical actuator. The shear actuator control is controlled by its feedback angular deformation. The normal actuator option is connected to the servo valves that control the axial actuator. The normal actuator control is controlled by its two main feedbacks, the normal load input and the normal actuator deformation input.

Inputs: The CATS ring shear software operates with four inputs, shear torque input, shear angular deformation input, normal load input and, normal deformation input (Figure 3-18b).

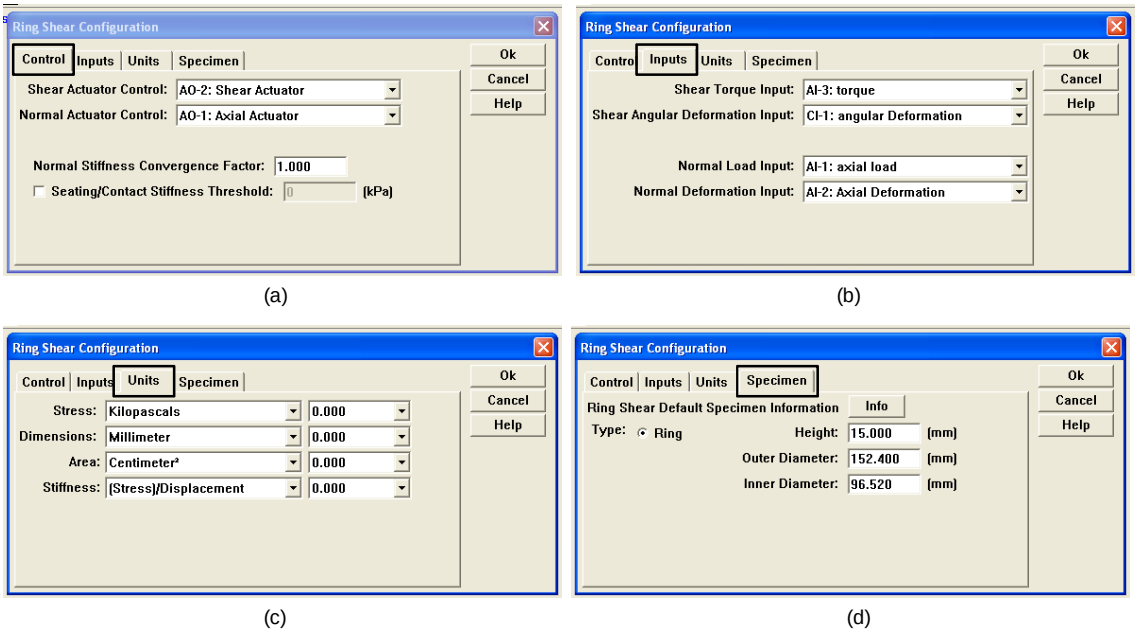

Figure 3-18 Ring shear configuration windows: (a) control; (b) inputs; (c) units; (d) specimen.

Test inputs:

The CATS software allows obtaining two ring shear test inputs, normal and shear stress on the shear plane.

The normal stress is calculated from the normal load acting on the failure plane by the following equation:

$$\sigma_n = \frac{P}{\pi(R_2^2 - R_1^2)} \qquad (3.1)$$

where:

σ_n = normal stress on shear plane (kPa)

P = vertical load on shear plane (N)

R_1 = inside radius of soil specimen (m)

R_2 = outside radius of soil specimen (m)

The shear stress is calculated from the torque load on the shear plane by the following equation:

$$\tau = \frac{3T}{2\pi\left(R_2^3 - R_1^3\right)} \qquad (3.2)$$

where:

τ = shear strength on shear plane (kPa)

T = torque load on shear plane (N•m)

The linear displacement is calculated from the equation:

$$D = \frac{\theta\pi(R_2 + R_1)}{360} \qquad (3.3)$$

where:

D = average linear displacement (mm)

θ = angular displacement (degrees)

Inputs views:

The software allows the user to monitor the status of the inputs in real time through the Chart and Plots option and Digital View option. The charts and plot option are used for viewing multiple inputs at a time with multiple points displayed for each input in real time. If the user is interested in the complex and dynamic behavior of the inputs, the Chart option is the ideal tool for that. If the user is more interested in the static behavior, or in the history of an input, the Plot is the better suited for that. During suction-controlled RS tests the Plot option was chosen to monitor the behavior of the shear stress and axial deformation in real time. This option allowed verifying the proper performance of the device during RS tests as well as identifying problems

related to exceed wall friction or malfunctioning of the sensor system. Digital View allows the user to check the status of one input with the display value of the input displayed predominantly on the Digital View. Figure 3-19 shows an example of Plots and Digital Views for shear stress, normal stress, axial deformation and angular deformation inputs from a multi-stage suction-controlled RS test on SC-SM.

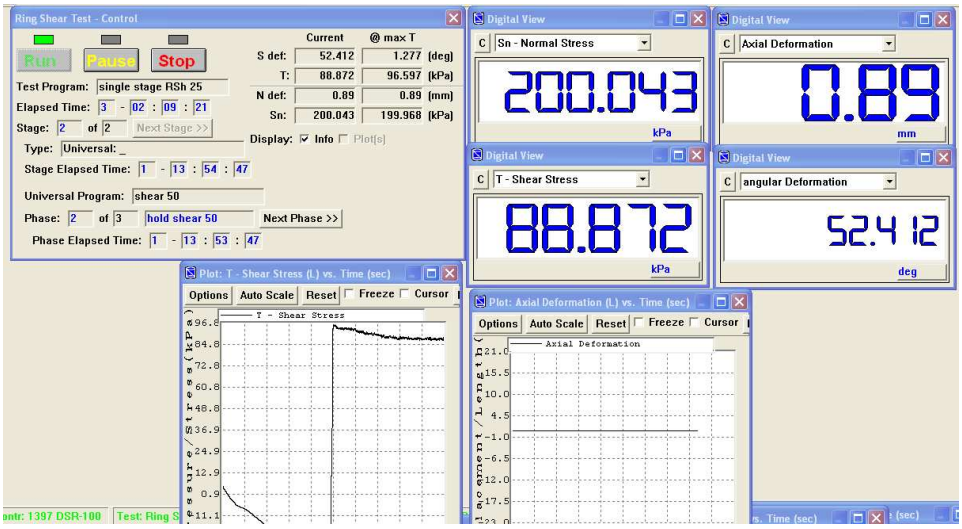

Figure 3-19 Plots and Digital Views in real time for a multi-stage suction-controlled RS test.

The next chapter describes the basic physical properties of the test materials used, including compaction methods, soil specimen preparation procedures and, soil water characteristic curves (SWCC). Results from a testing program undertaken to verify the performance of the new ring shear device are also presented. The performance verification testing includes comparison of test results with those from a conventional Bromhead ring shear apparatus.

CHAPTER 4

SOIL MATERIALS AND PERFORMANCE VERIFICATION OF RS APPARATUS

4.1 Introduction

In this work, three different soils having widely varying properties were selected for the suction-controlled RS testing program, namely, silty sand, silty clayey sand, and silty clay. Two of the soils, silty sand and silty clay, were tested in both the novel suction-controlled ring shear apparatus and conventional Bromhead ring shear apparatus. The third soil, silty clayey sand, was tested in the novel suction-controlled ring shear only. In this chapter, the main index properties and compaction characteristics of all three soils are initially presented. The procedure employed to prepare the samples for the different experimental programs is also explained, as well as the assessment of the soil-water characteristic curves (SWCC).

Results of an initial testing program undertaken to investigate the performance of the newly developed device are also presented in this chapter. The initial performance verification tests, following the manufacturing of the new device, allowed identification of critical drawbacks of the original design of the upper annular platen and the method used to seal the high-air-entry ceramics. In order to correct these, the upper annular platen was modified and a new sealing procedure for the HAE ceramics was adopted through the course of the experimental program. Results that confirm the effectiveness of these modifications are presented, as well as comparisons with results from the conventional Bromhead ring shear apparatus. Finally, results from a series of suction-controlled ring shear tests on fully saturated and unsaturated

specimens, to verify the repeatability of test results in the device, as well as the definition of the appropriate suction-controlled RS testing scheme are presented.

4.2 Soil Material Selected

The test soils classified as SM, SC-SM and CL according to the Unified Soils Classification System, USCS (ASTM D2487), respectively. SM soil was selected because of its local availability and poor gradation, which minimizes the effects of particle size and shape on menisci formation in the water phase, reducing the equalization time of pore fluids (air and water) during suction-controlled testing. SM soil is an artificial mix composed of 20% natural silty clay CL, and 80% uniform sand available in the Soils Mechanics Laboratory at University of Texas at Arlington. SC-SM and CL soils were also selected because of their local availability and their typical strain-softening behavior at large strains.

4.2.1 Basic Engineering Properties

Particle size distribution:

The determination of the particle sizes above 0.075 mm (sieve No. 200) was obtained by the sieving method (ASTM D422-63, 2007), while the distribution of particle sizes below 0.075 mm was determined by the sedimentation process using the hydrometer method (ASTM D422-63, 2007). Figures 4-1 shows the particle size distribution of the SM, SC-SM and CL soils selected for this research.

The particle size distribution of the SM shows that 9.8% of the material is within the silt sizes, and only 6.6% corresponds to clay sizes (< 2μ). For the SM-SC, 34% of the material is within the range of the silt sizes, and only 6% corresponds to clay sizes (< 2μ). In the case of the

silty clay, CL, 18 % of the material is within the range of the fine sand sizes, 49% correspond to silt sizes, and 33% corresponds to clay sizes (< 2μ).

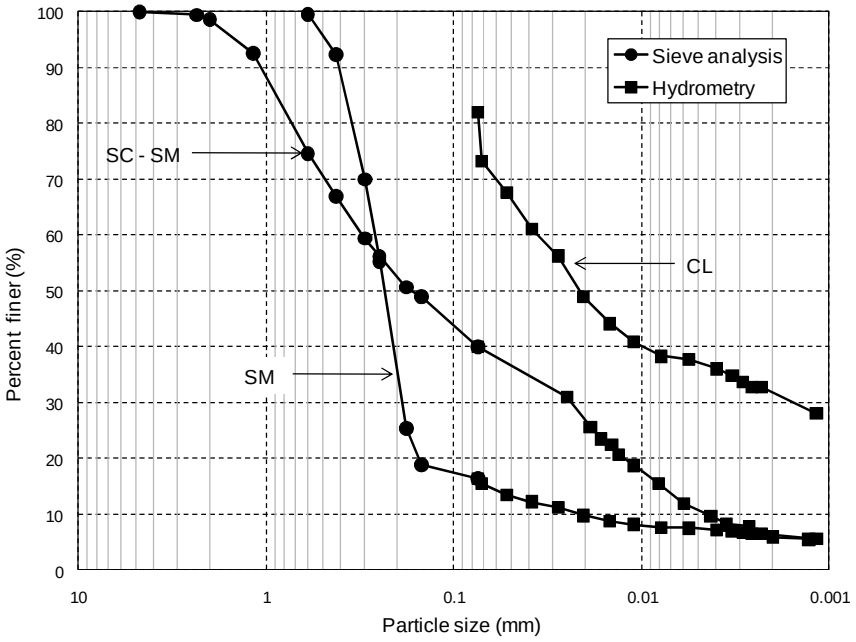

Figure 4-1 Particle size distribution for SM, SM-SC and CL soils.

Specify gravity:

The specific gravity of the soils was measured by the water pycnometer method (ASTM D854-00, 2007). Table 4-1 shows the results obtained. These results will be used to analyze the experimental data obtained throughout this project.

Table 4-1 Specific gravity of soil solids.

SM	2.68
SC-SM	2.71
CL	2.72

Atterberg limits:

The Liquid limit (LL), Plastic limit (PL) and Plasticity index (PI) of the corresponding fraction materials passing 0.425 mm were established following the ASTM D4318-00 procedure. The results are presented in the table 4-2.

Table 4-2 Atterberg limits

Type of soil	SM	SC - SM	CL
Liquid Limit (%)	NL	26.4	37
Plastic Limit (%)	NP	20.2	17
Plasticity Index (%)	-	6.2	20

4.3 Compaction Characteristics

Material preparation:

Throughout the experimental program of this research, the soil in an air-dry state was mixed initially with distilled water until reaching the required water content for compaction. The material was mixed by hand with a spatula for about 10 minutes until mixture had a homogenous moisture distribution. After that, the moist material was stored in airtight bags and left in a controlled temperature and humidity room for at least 24 hours prior to RS testing to allow for moisture equalization.

Compaction characteristics:

In this work two compaction methods were used, dynamic and static compaction. Dynamic compaction was first conducted on the SM and CL testing soils following the procedure described in the ASTM D698-07 in order to determine the relationship between moisture content and dry unit weight of the soil. The experimental values for the SC-SM soil were taken from

Suescun (2010). Table 4-3 summarizes the maximum dry unit weight γ_{d-max}, and the optimum moisture content w_{opt}, for all three test soils. The compaction curves for SM and CL soils are shown if Figures 4-2 and 4-3, respectively.

Table 4-3 Dinamic compaction characteristc for SM, SC-SM and CL soils.

Type of soil	Maximum dry density (kN/m^3)	Optimum water content (%)
SM	1.84	10.5
SC - SM	1.33	26.5
CL	1.77	17.0

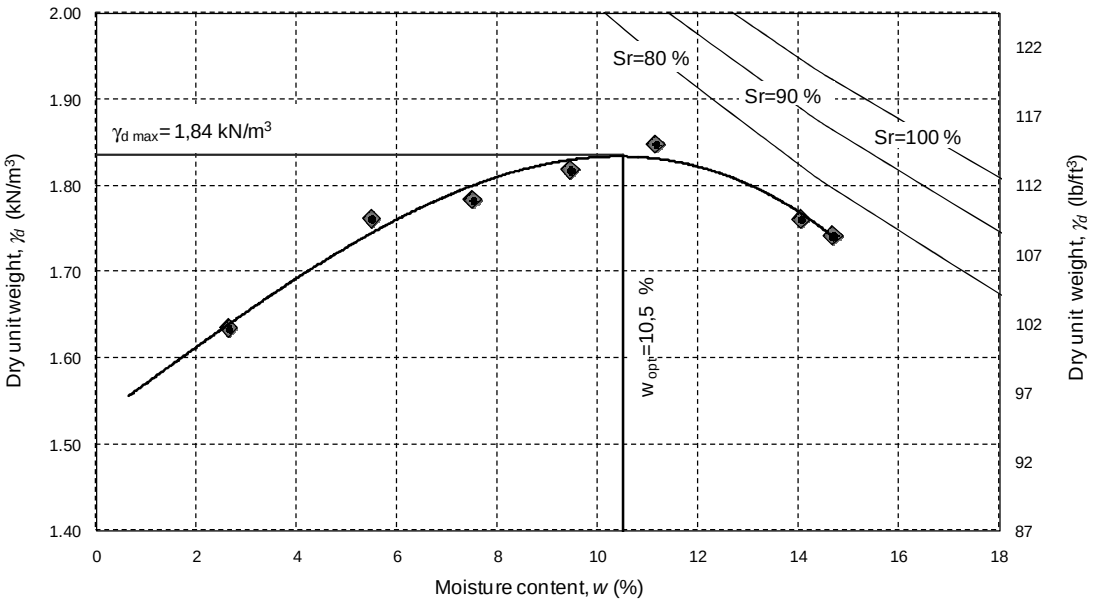

Figure 4-2 Compaction curve for silty sand (SM) soil.

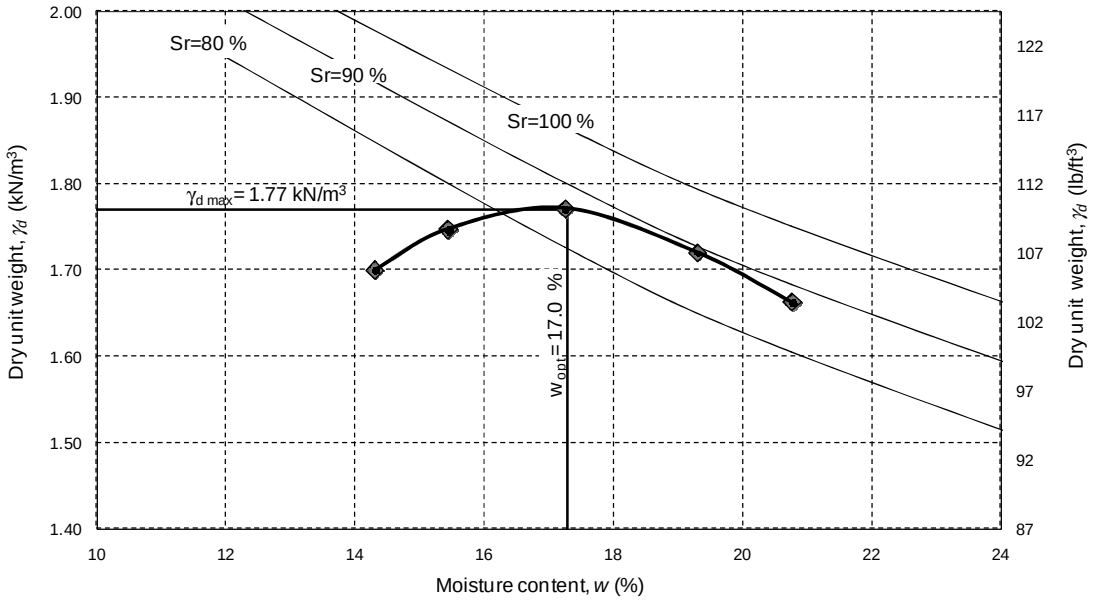

Figure 4-3 Compaction curve for silty clay (CL) soil.

Static Compaction Process:

Special attention was given to the selection of a procedure that yields soil specimens at a specified dry unit weight, water content and degree of saturation in order to ensure adequate sample uniformity and repeatability. For that reason static compaction method was selected to prepare the ring-shaped specimens to be tested in the novel ring shear device. In this method the material is compacted by a gradually applied monotonic force. The soil is confined within the concentric rings of the lower annular platen while compaction is achieved by the monotonic movement of a piston that presses the soil until a specific final thickness is achieved.

In this research the ring-shaped specimens were compacted directly onto the lower annular platen. The ring-shaped top platen was used to press the soil down against the lower annular platen. The monotonic force was applied by means of a conventional triaxial loading frame as shown in Figure 4-4. The samples were prepared in a single lift at a compaction

displacement rate of 1.25 mm/min in order to minimize the potential for fabric variations throughout the sample (Venkatarama, 1993). Before compaction the inside faces of the ring shear lower annular platen were lubricated in order to reduce the wall friction generated between the ring and the soil specimen. In addition, small pieces of wet filter paper were placed on top of each ceramic disk to ensure continuity between the pore-water in the sample and water in the ceramic disks (Figure 4-4a). After compaction the final height and weight of the statically compacted sample were determined to verify the final dry unit weight.

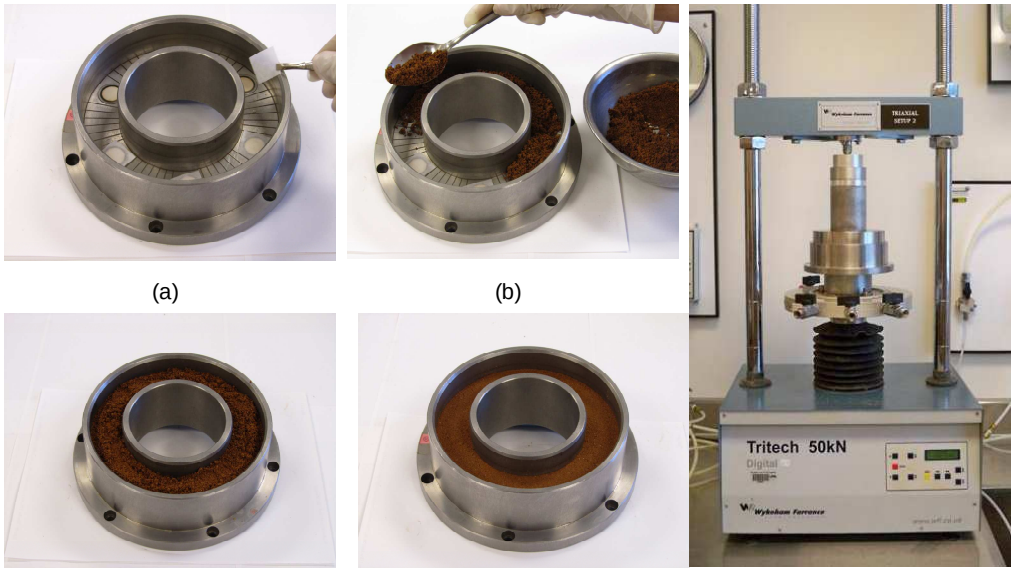

(a) (b) (c) (d) (e)

Figure 4-4 Static compaction of ring-shaped samples using the conventional triaxial frame: (a) filter paper interface sample-ceramics; (b) pouring material into the bottom plate; (c) sample in loose state; (d) sample in compacted state; (e) triaxial frame.

4.4 Soil Water Characteristic Curve (SWCC)

The soil water characteristic curve (SWCC) represents the relationship between the water content and the suction of a soil. This curve plays an important role in the characterization and understanding of the behavior of unsaturated soils because it provides information about the capacity of retention of water of a soil and because it can be used to predict some of its mechanical properties, such as coefficient of permeability and shear strength (Vanapalli et al., 1999).

4.4.1Features of the Soil Water Characteristic Curve

The water content in a SWCC can be expressed as gravimetric water content (w), volumetric water content (θ_w) or degree of saturation (S_r). An important characteristic of the SWCC is its hysteretic behavior. That means that the relationship water content-suction is not the same if the soil is subjected to a drying process or to a wetting process (Figure 4-5).

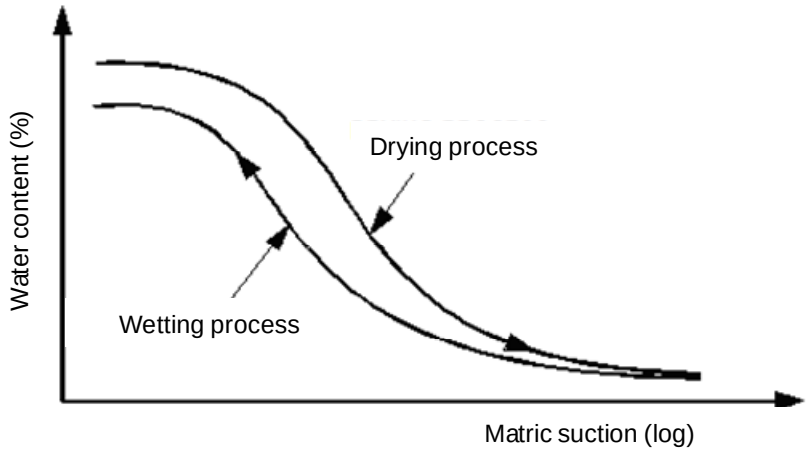

Figure 4-5 Hysteretic behaviour of the Soil water characteristic curve (Dineen, 1997).

The soil water characteristic curve of an initially fully saturated soil undergoing a monotonic drying process is schematically shown in Figure 4-6. The main features of a typical

SWCC are the air entry value (AEV) and the residual degree of saturation. They define the boundaries between successive stages of the drying process Vanapalli et al. (1999). The AEV represent the suction required to induce air to enter the larger pores of the soil and could be graphically estimated by the intersection of a line parallel to the suction axis at a degree of saturation of 100%, and a line extending the linear slope portion of the curve (Figure 4-6). A soil with a suction value below the AEV could be assumed that remains essentially saturated. On the other hand, the residual degree of saturation is considered to be the degree of saturation at which, during a drying process, the liquid phase becomes discontinuous and removing water from the soil by drainage results very difficult. This value also can be graphically estimated by the intersection of a line extending the linear portion of the curve and the line extending from 10^6 kPa along the curve (Figure 4-6).

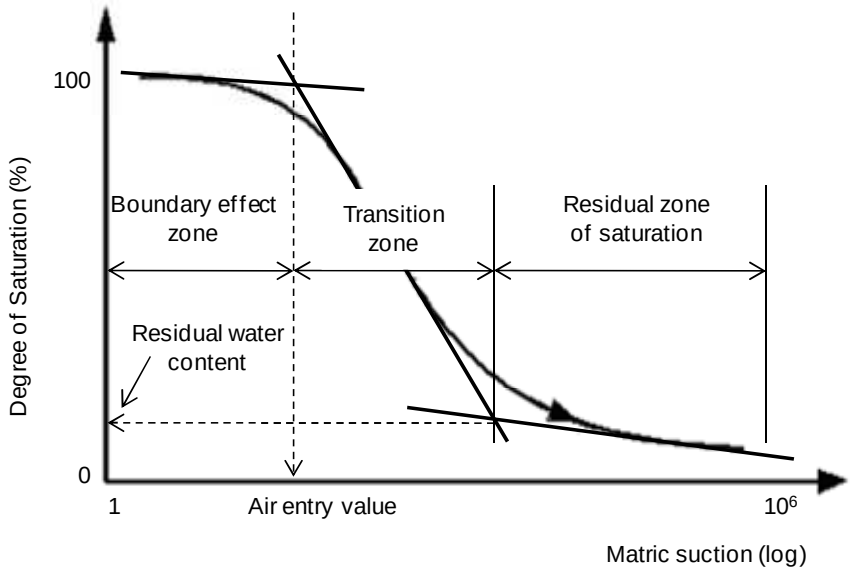

Figure 4-6 Features of the Soil water characteristic curve.

Vanapalli et al. (1996) defined three stages of saturation during the drying process of a soil: the boundary effect stage, the transition stage (primary and secondary) and the residual state of saturation as shown in Figure 4.7.

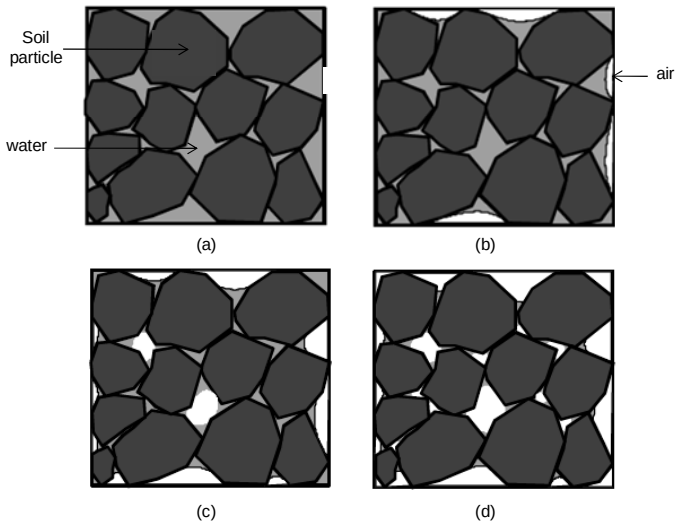

Figure 4-7 Drying stages: (a) boundary effect stage; (b) primary transition stage; (c) secondary transition stage, and (d) residual stage of saturation. (Vanapalli et al, 1996).

In the boundary effect stage the soil remains essentially saturated as the water content is reduced and the suction increases (Figure 4-7a). Volume changes are directly related to changes of the water content during this stage and the effective stress variable $(\sigma_n - u_a)$ can be used to describe the behavior of the soil. As the water content is reduced further, tension in the pore water increases and eventually air is drawn into the soil matrix from the surface. During this primary transition stage, large reductions in water content are required to cause relatively modest increases of soil suction (Figure 4-7b). As progressively more water is replaced by air, the continuity of water is reduced and a secondary transition stage is entered. Volumetric reductions are no longer directly related to reductions of water content and the principle of effective stress becomes invalid (Figure 4-7c). Eventually the water filled pores become

discontinuous, water is present mainly in the form of lenses between adjacent soil particles and air (or gas) is the dominant pore fluid. This stage is identified as the residual degree of saturation stage. Relatively small reductions of water content will cause large increases in suction (Figure 4-7d).

4.4.2 SWCC of compacted SM, SC-SM and CK soils

In this research the SWCC for SM and CL testing soils was experimentally obtained over a wide range of suctions, from fully saturated conditions (0 kPa) up to matric suction of 36000 kPa. Pressure plate and filter paper techniques were used to induce and measure the suction in the soil, respectively. Pressure plate was employed to determine the SWCC within of the suction range between 0 to 800 kPa, and filter paper technique to measure suctions above than 800 kPa. The SWCC for soil was taken from Suescun (2010).

SWCC via the Pressure Plate Technique:

Ten specimens of each soil (SM and CL) having 57 mm in diameter and 23 mm in height were prepared following the procedure described previously, and compacted statically in individual retaining plastic rings. Specimens were prepared at water content of optimum plus 4%, and at 95% of maximum dry density as determined by Standard Proctor testing. The initial dry density and initial water content values for each material are presented in Table 4.4.

Table 4-4 Initial sample characteristics

Soil	Initial water content (%)	Initial dry density (kN/m^3)
SM	15.56	1.75
CL	24.08	1.68

After compaction, the specimens were saturated by inundation under the following conditions: samples contained in the retaining ring were sandwiched between one filter paper;

one perforated latex membrane and, one porous stone on each side of the sample. The pore stones were fixed to the sample through two perforated metal plates in order to allow the drainage at top and bottom, and attached by four screws in order to prevent additional soil volume change. The samples were left submerged in distilled water for about two weeks. The degree of saturation was verified at the end of this process. Degrees of saturation close to 98% were measured. According to these results, it can be reasonably assumed that the initial condition corresponds to essentially zero matric suction. Figure 4-8 shows a series of pictures of the saturation process.

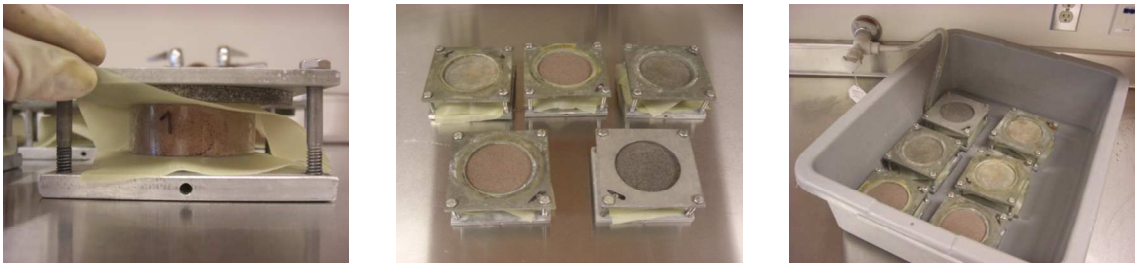

(a) (b) (c)

Figure 4-8 Sample saturation process: (a) sample assembling; (b) samples assembly and, (c) saturation bath.

After saturation, the specimens were placed inside the pressure plate and the first increment of air pressure was slowly applied according to the procedure described in the Standard Test Method for Determination of the SWCC for Desorption using Pressure Extractor (ASTM D6836-02). This method only allowed obtaining the SWCC for suctions below 800 kPa (Figure 4-9). As a result, filter paper technique was used to complete the SWCC curve for SM and CL soils.

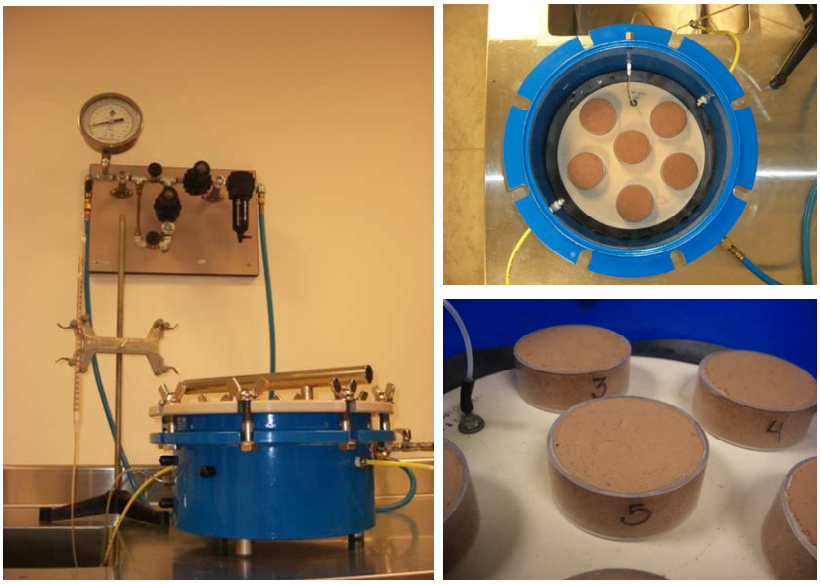

Figure 4-9 SWCC setup and typical SM or CL samples.

SWCC via Filter Paper Technique:

Matric suction was measured by filter paper technique following the procedure recommended by Ridley et al. (2003). According to the authors this procedure has been used with great success for many years and the results present high repeatability. The procedure used involves placing an initially dry filter paper (Whatman N. 42) on each side of the sample and covering the system with a disk of Plexiglas in order to guarantee a perfect contact between the sample and the filter paper. After that, the sample and the disks are covered and sealed by several layers of cling film and tape. The covered sample is then placed in three sealed plastic bags and stored for 7 days in a temperature controlled room. After the equilibrium time is reached, the filter papers are removed with a pair of tweezers and placed in a small plastic bag. The water contents of the filter papers are determined using a balance with a resolution of 0.0001 g. The filter papers are allowed to dry for at least two hours in the oven at 110 ° C. The samples are allowed to air-dry for a couple of hours and the process is repeated. During the all

stages of the suction measurement the filter paper is always handled with a pair of tweezers and the filter paper is placed in the plastic bag as quickly as possible. The complete assembly of the filter paper technique is shown in Figure 4-10.

The procedure described above for measuring suction was repeated every week until the sample reached an air-dry condition. This occurred when the water content of the filter paper reached equilibrium with surrounding atmosphere at suction of approximately 30 MPa.

According to Vanapalli et al. (1999), the initial water content has a considerable influence on the resulting structure of fine-grained soils. The authors state the SWCC of fine-grained soils is dependent mainly on the structure and stress history, rather than the initial void ratio. As a result, the filter paper measurements were made on samples which had a previous dried process via pressure plate. Two samples were initially brought to a suction state of about 800 kPa by means of pressure plate, and which the measurement of suction were continued through filter paper technique until the SWCC was completed.

Several relationships between the filter paper, water content and suction have been developed for different filter paper brands by different researchers. In the present work, the calibration curve for Whatman N. 42 recommended by ASTM D5298-03 was used. This calibration curve is presented as follows:

$$Log\ (\psi) = 5.327 - 0.0779w \qquad w < 45.3\% \qquad (4.1)$$

$$Log\ (\psi) = 2.412 - 0.0135w \qquad w \geq 45.3\% \qquad (4.2)$$

where:

ψ = matric suction (kPa)

w = paper filter water content (%)

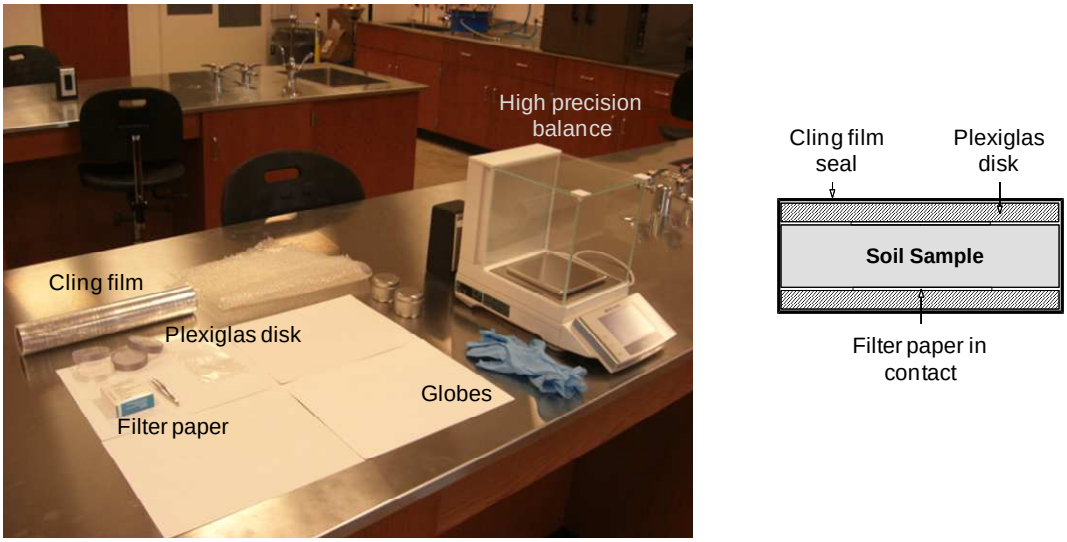

Figure 4-10 Layout of the filter paper testing assembly

4.4.3Equations to best-fit SWCC laboratory data

Different empirical equations have been proposed to best-fit the soil water characteristic curve. Fredlund (2006), Leong and Rahardjo (1997), and Fredlund and Xing (1994) present a good summary of these models. Each of these proposed equations has one or two fixed points that are related to water content or suction at specific condition, such as complete degree of saturation, air entry value or residual degree of saturation; and two or more empirical or semi-empirical fitting constants that are related to physical characteristics of the soil, such as pore size distribution, selected to capture the general shape of the curve between these fixed points (Lu and Likos, 2004). In this research work three models were used in the modeling of the SWCC for each soil.

Brooks and Corey model, BC (1964):

In this model the SWCC is constant for suctions less than the air entry value, and is assumed to be an exponentially decreasing function of water content at soil suctions greater than this value. The model is given as:

$$\Theta = \frac{\theta-\theta_r}{\theta_s-\theta_r} = \left(\frac{\psi}{\psi_{AEV}}\right)^{-n} \qquad when\ \psi \geq \psi_{AEV} \qquad (4.3)$$

$$\Theta = 1 \quad \text{and} \quad \theta = \theta_s \qquad \text{when } \psi < \psi_{AEV} \qquad (4.4)$$

where, Θ = normalized volumetric water content; θ = volumetric water content (kPa); θ_s= saturated volumetric water content (kPa); θ_r= residual volumetric water content (kPa); ψ=soil suction (kPa); ψ_{AEV}=soil suction at the air entry value (kPa), and the fitting parameter "n" which is called as pore size index and is related to the pore size distribution of the soil. The more uniform the pore sizes in the soil, the larger is the value of n. The larger the value of n, the steeper is the SWCC within the desaturation zone.

Van Genutchen model, VG (1980):

This model has three fitting parameters: α , n , and m, respectively, which allow taking into account the inflexion point at the air entry value. As a result, the sinoidal shape of typical SWCC can be better represented. The equation is given as:

$$\Theta = \frac{\theta-\theta_r}{\theta_s-\theta_r} = \left\{\frac{1}{[1+(\alpha\psi)^n]}\right\}^m \qquad (4.5)$$

where the parameter α is related to the inverse of air entry value, the parameter n is related to the pore size distribution of the soil, and the parameter m is related to the symmetry of

the characteristic curve. For numerical stability m is often taken as equal to $(1 - 1/n)$. Soils with steeper SWCC are characterized by smaller n, and SWCC with higher air entry suction is characterized by smaller α values. In addition, soils with higher plasticity index have lower α, which correspond to greater air-entry suction and larger n, which corresponds to an SWCC with shallower slope.

Fredlund and Xing, FX (1994):

This model also considers three fitting parameters to describe the SWCC for the entire suction ranges. The equation is given as:

$$S = \frac{1}{\left\{ln\left[e+\left(\frac{\psi}{\alpha}\right)^{n}\right]\right\}^{m}} \qquad (4.6)$$

In this model, S represents the degree of saturation, and the fitting parameters α and m have similar meanings described by the VG model, while e is the natural logarithmic constant (2.718). As the parameter α increases the curve moves toward higher soil suction region. The parameter n is related to pore-size distribution, as a result the more pore sizes in the soil, the larger is the value of n. The parameter m controls the slope of SWCC. According to Lu and Likos (2006) the FX model allows describing well the SWCC over a wide range of suctions. This is one of the most widely used SWCC models in understanding unsaturated soil behavior.

Figures 4-11, 4-12 and 4-13 show the soil water characteristic curves for SM, SC-SM and CL used throughout this research. In those figures, black dots represent actual experimental data, whereas solid and dashed lines represent best-fit SWCC models devised for the soil using the Brooks and Corey (BC), Van Genutchen (VG) and Fredlund and Xing (FX) model equations.

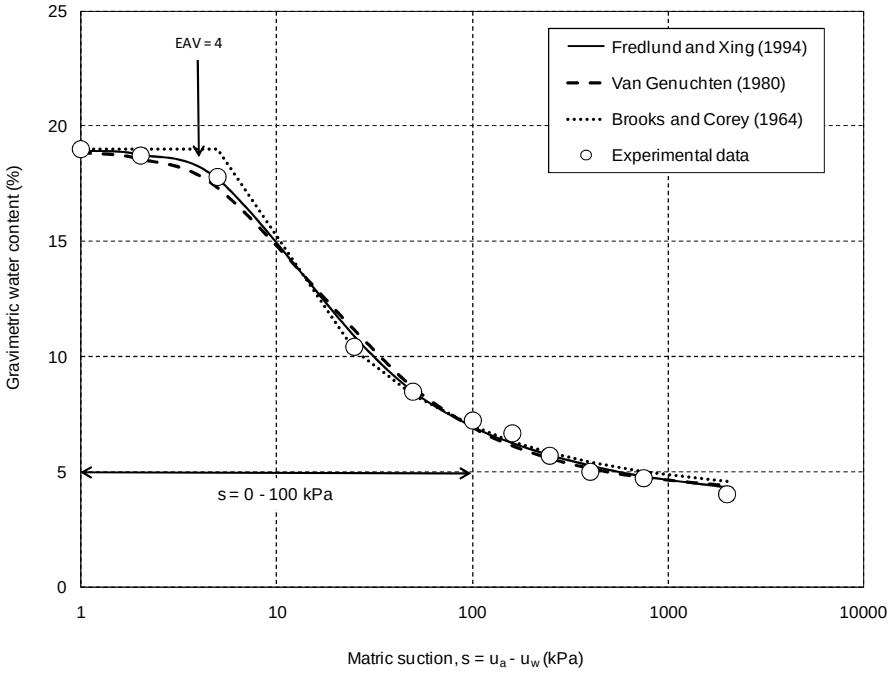

Figure 4-11 SWCC best-fitting models for silty sand (SM) soil.

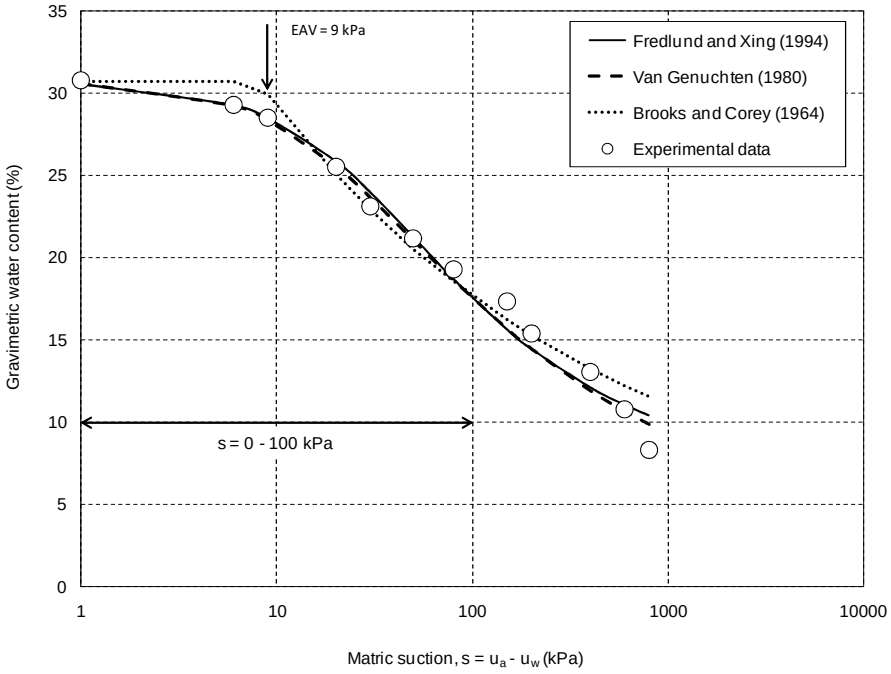

Figure 4-12 SWCC best-fitting models for (SC-SM) soil.

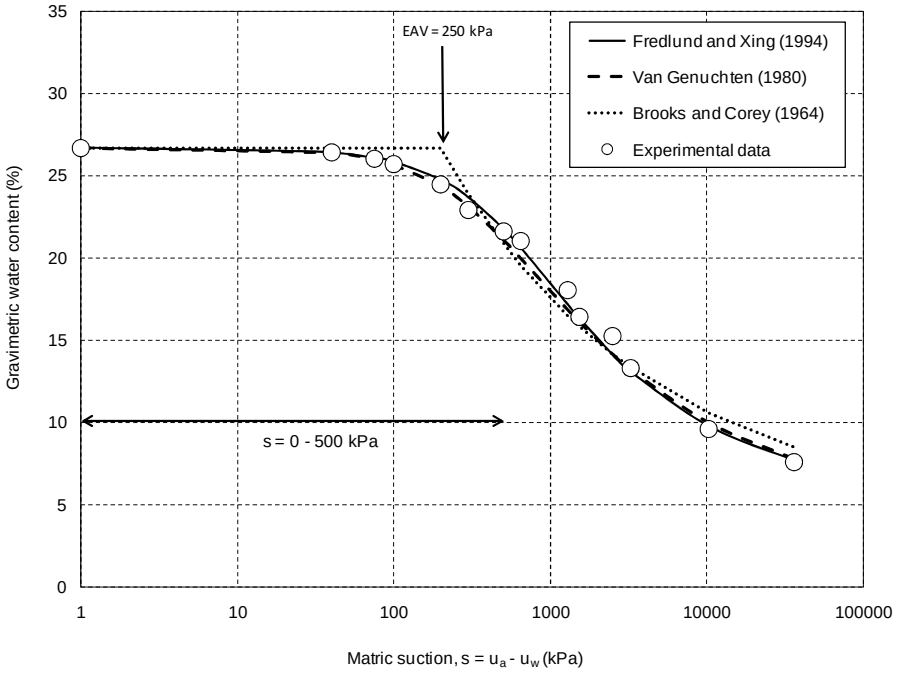

Figure 4-13 SWCC best-fitting models for silty clay (CL) soil.

Figures 4-11. 4-12 and 4-13 show that the air entry value for the SM soil is around 4 kPa, for the SC-SM soil it is around 9 kPa and for the CL soil the air entry value is close to 250 kPa. Based on the SWCC's and the limited capacity of the load-torque sensor (previously mentioned in Chapter 3), the selected range of matric suction states chosen for suction-controlled RS tests range from 0 kPa to 100 kPa for SM and SC-SM, and from 0 kPa to 600 kPa for CL. It can be noticed that the selected matric suction range for SM and SC-SM soils includes the saturation and transition zone of the respective SWCC. According to Lu and Likos (2004), the main contribution of matric suction to shear strength of a soil is within the transitional zone. This regime of nonlinear behavior corresponds to drainage of the soil pores. As drainage continues through this zone of de-saturation, the geometrics of the interparticle pore water menisci dramatically change, thus affecting the resultant interparticle forces that contribute to stress on the soil skeleton and ultimately contribute to shear strength. On the contrary, the reduction in the

volume of pore water within the residual regime of saturation effectively reduces the contribution that matric suction has toward increasing shear strength. Thereby, although it was not possible to study the effect of matric suction on the residual shear strength of the test soils (SM and SC-SM) within the residual regime, a good understanding of the behavior of the soils within the saturated and transitional regimens could be achieved. Conversely, for silty clay soil, useful residual shear strength data under suction-controlled states could not be reordered. However, in view of the novel experimental nature of the apparatus, all tests results, whether successful or inconclusive, are presented and thoroughly discussed in Chapter 5.

Finally, Table 4-5 summarizes the best-fitting parameters selected for each SWCC model. It can be observed that the VG and FX models capture the SWCC reasonably well over the entire range of suctions, particularly at high suction states in all materials.

Table 4-5 Summary of SWCC fitting parameters for test soils.

SOIL	Brooks and Corey (1964)	Van Genuchten (1980)	Fredlund and Xing (1994)
SM	$\lambda = 0.54$ $\Psi_b = 4$ kPa $\theta_r = 4$ $\theta_s = 19$	$\lambda = 0.105$ n = 1.695 m = 0,41 $\theta_r = 4$	a = 8.5 n = 2 m = 0.63 $\theta_s = 19$
SC-SM	$\lambda = 0.24$ $\Psi_b = 9$ kPa $\theta_r = 2$ $\theta_s = 30.70$	$\lambda = 0.053$ n = 1.32 m = 0.24 $\theta_r = 2$	a = 26 n = 1.1 m = 0.8 $\theta_s = 30.70$
CL	$\lambda = 0.33$ $\Psi_b = 250$ kPa $\theta_r = 4.5$ $\theta_s = 26.67$	$\lambda = 0.0029$ n = 1.41 m = 0.29 $\theta_r = 4.5$	a = 480 n = 1.3 m = 0.72 $\theta_s = 26.67$

4.5 Performance Verification of Original RS Design

4.5.1 Upper Annular Platen

The first problem with the original design of the upper annular platen was encountered during a first trial test on silty clayey sand. Close examination of the top surface of the failed sample showed that the failure surface had been entirely developed right at the interface between the upper annular platen and the top soil, and not within the sample itself. Photos of the exposed failed sample, including a failure surface detail, are shown in Figure 4-14. This was a clear indication that the upper platen was simply slipping over the surface of the top soil, with minimal shear resistance being developed only at the contact areas between the soil and the porous stones.

(a) (b) (c)

Figure 4-14 Original RS design: (a) upper annular platen – shown upside down, (b) exposed failed sample, (c) failure surface detail.

The problem was corrected by replacing the original design of the upper annular platen with a single, sintered rough-surfaced bronze stone having the same dimensions of the specimen surface, i.e., 152.4 mm OD and 96.5 mm ID, as shown in Figure 4-15(a). With the new platen, enough shearing resistance was generated at the interface between the upper annular platen and the top soil, hence inducing the failure surface within 3 millimeters into the soil sample, as shown in Figures 4-15(b) and (c). Moreover, application of pore-air pressure is

uniformly distributed on the entire top surface of the specimen, which considerably reduces the equalization time required under a sustained-suction state when using axis translation technique.

(a) (b) (c)

Figure 4-15 Modified RS design: (a) upper annular platen – shown upside down, (b) exposed failed sample, (c) failure surface detail.

The observations summarized above are further corroborated by the results from two RS trial tests performed on saturated silty sand using both the original upper platen and the modified upper platen. A very erratic response is observed from the RS test performed using the original upper platen, as shown in Figure 4-16(a), which makes it quite difficult to identify either the peak or residual shear strength. On the contrary, a more defined trend is observed when using the modified upper platen, as shown in Figure 4-16(b), with a very well defined residual strength under a net normal stress, $(\sigma_n - u_a)$ = 200 kPa. The modified upper platen was then used for further RS testing in this research work.

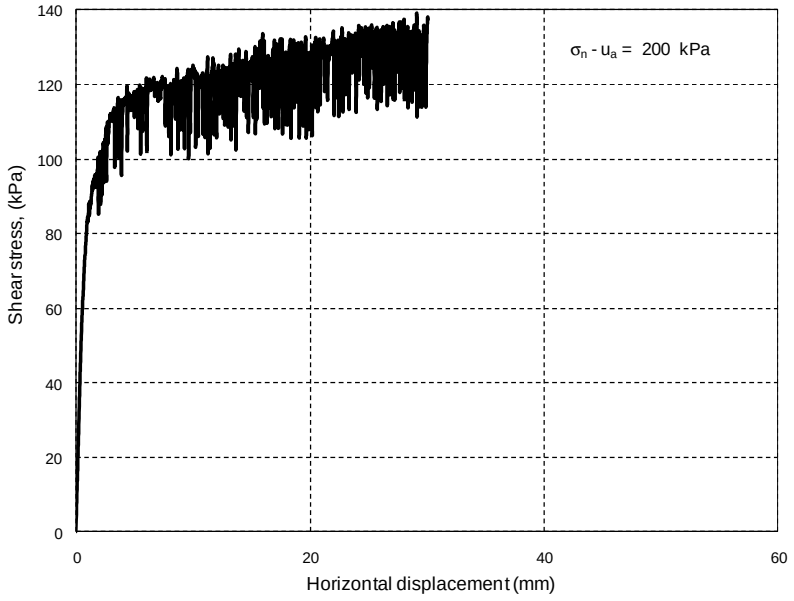

(a)

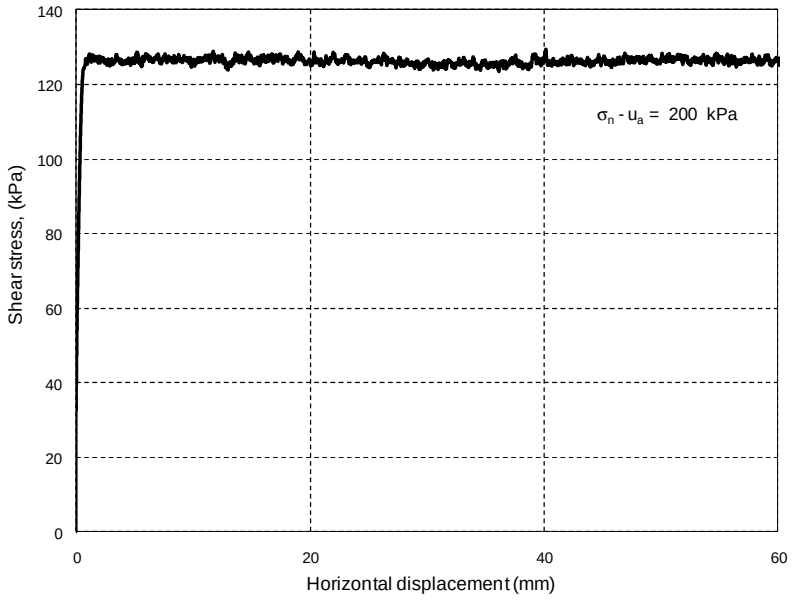

(b)

Figure 4-16 Response from two RS trial tests on saturated silty sand using: (a) original upper platen, (b) modified upper platen.

4.5.2 Sealing of High-Air-Entry Ceramics

Extreme care is to be exercised when sealing the HAE ceramics onto the sintered stainless steel rings to avoid the formation of occluded air bubbles within the hardened epoxy. Under sustained high pore-air pressure, the occluded air bubbles may burst, allowing air into the water compartment beneath the ceramic disks. Microscopic and full scale photos of occluded air bubbles entrapped in the epoxy sealant are shown in Figures 4-17(a) and (b). The photos were taken at the very early stages of the present research work.

Infante-Sedano et al. (2007) suggested applying the epoxy in multiple layers to improve the bonding and minimize the formation of air bubbles. They also recommended a curing time interval of 24 hours between consecutive layers to ensure full hardness of the final epoxy sealant. The method was adopted in this work: a typical microscopic photo of an efficient epoxy sealant achieved in this investigation is shown in Figure 4-17(c). The method was found to be effective through the course of the experimental portion of this current work, which included a range of sustained suction states from 0 to 100 kPa.

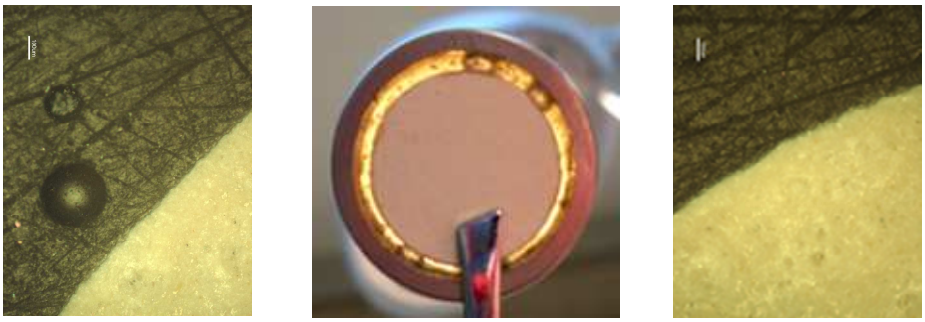

(a) (b) (c)

Figure 4-17 Sealing of HAE ceramics: (a) deficient epoxy, (b) dysfunctional epoxy, (c) efficient epoxy.

4.6 Performance Verification of Modified RS Design

4.6.1 Verification against Conventional Bromhead RS Apparatus

In order to verify the reliability of the newly developed RS apparatus, a series of four RS trial tests were performed on saturated silty sand (SM) and silty clay (CL) using the conventional Bromhead RS device, also available at UT-Arlington's geotechnical laboratories, and the novel RS device. In the novel device, the specimen was statically compacted with water content 3% above the optimum, and then allowed to saturate by direct inundation of the main RS cell (Fig-3.4) during 24 hours. In the conventional device, the soil-water mix was prepared at the same target moisture of 3% above the optimum; the mix was then allowed to hydrate for 24 hours in a 100% humidity room, after which the soil was placed into the annular space between the two concentric rings of the lower annular platen and allowed to saturate by direct inundation during 24 hours.

The tests were performed under different net normal stresses, $(\sigma_n - u_a)$ = 25, 50, 100, and 200 kPa. All tests were conducted by following a multi-stage testing scheme. (A thorough explanation will be given at a later section). Results from RS tests conducted at normal stresses of 25 and 200 kPa are shown in Figure 4-18 for SM soil and Figure 4-19 for CL soil. Results from both devices are presented in separate plots to adequately distinguish the true nature of the peak and residual responses of SM and CL soil in each case. Reasonably good agreement is observed for RS test results using both devices, which demonstrates the capability of the novel RS apparatus to reliably assess residual shear strength parameters for granular and clayey materials. The same is observed in Figure 4-20 which shows the residual strength envelopes for saturated silty sand and silty clay using both novel and conventional RS devices.

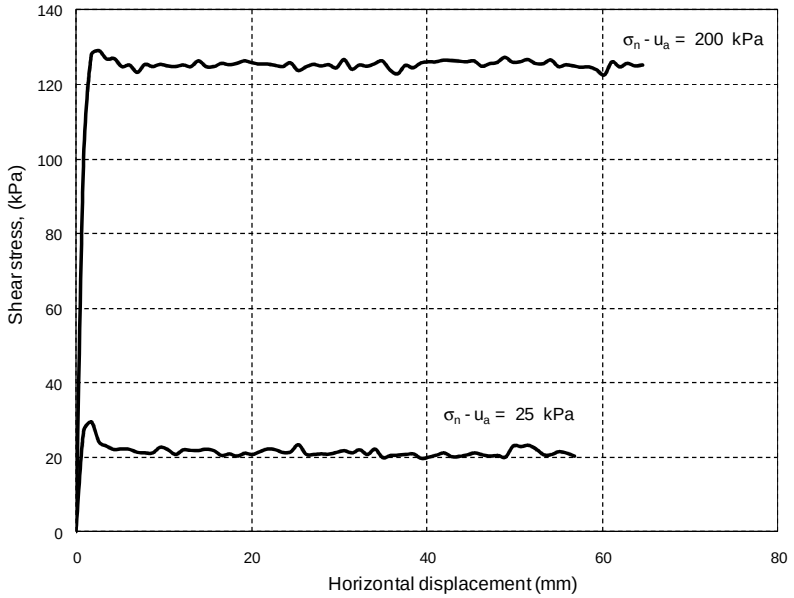

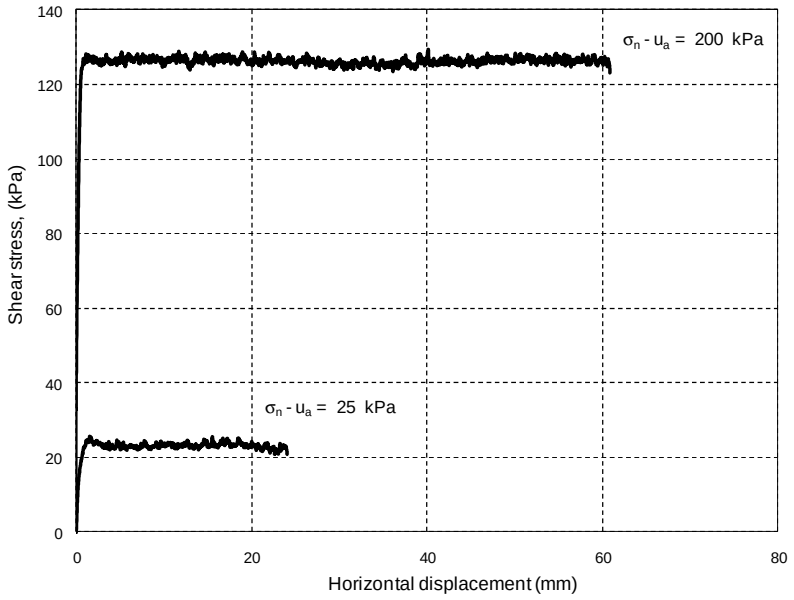

Figure 4-18 Response from two RS trial tests on saturated silty sand (SM) using: (a) conventional Bromhead RS device, (b) novel RS device.

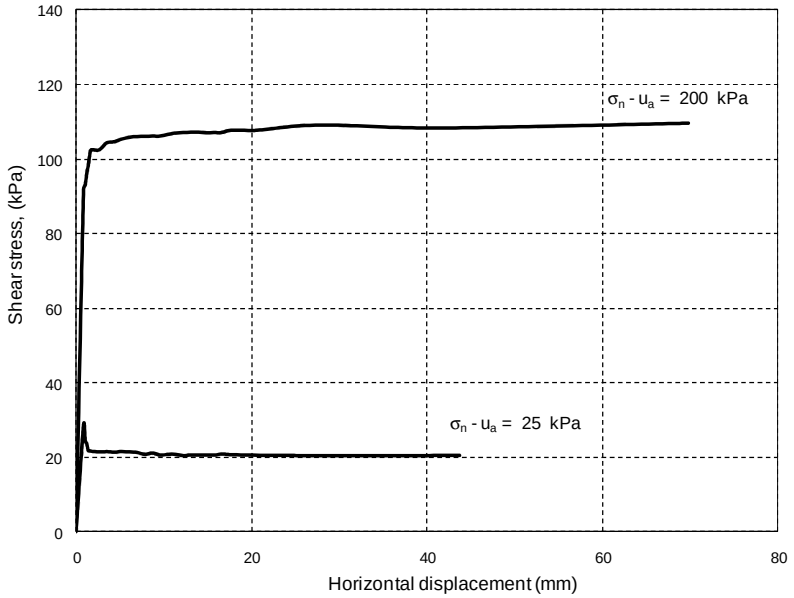

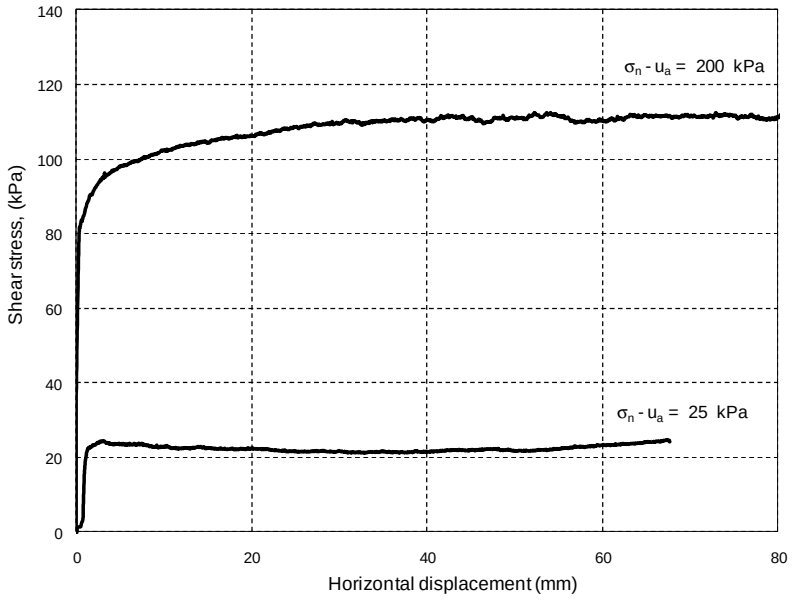

Figure 4-19 Response from two RS trial tests on saturated silty clay (CL) using: (a) conventional Bromhead RS device, (b) novel RS device.

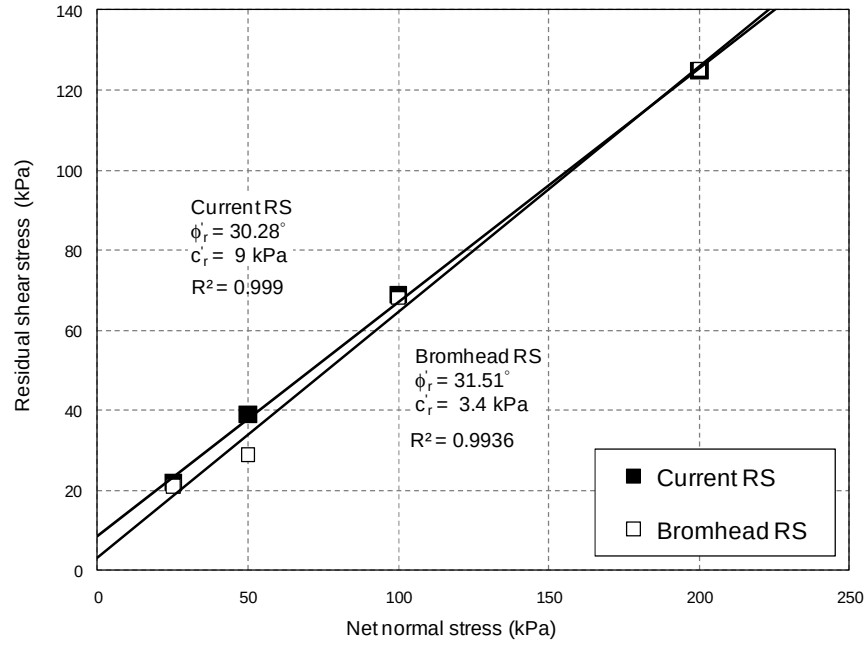

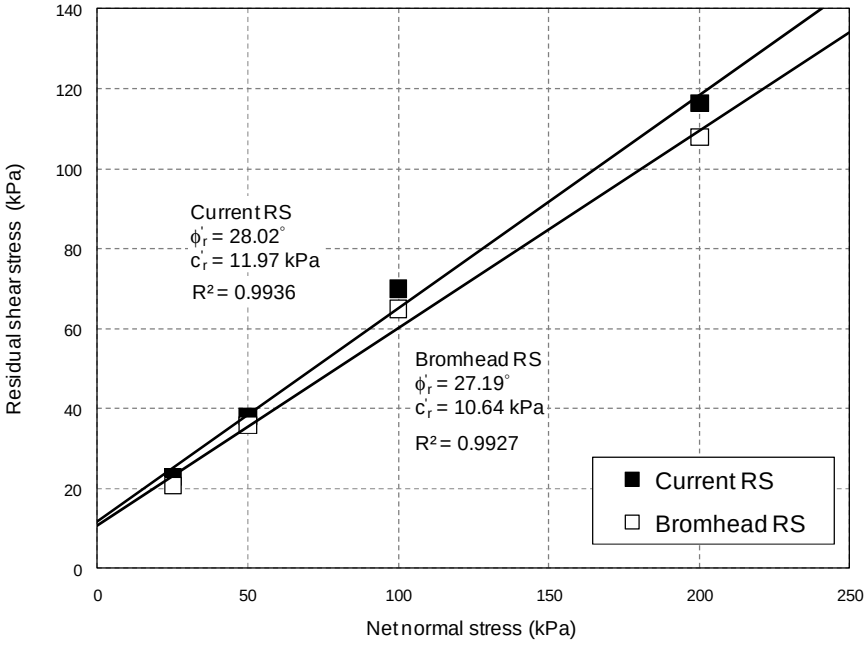

Figure 4-20 Residual strength envelopes using conventional and novel RS devices for: a) saturated silty sand (SM) and, (b) saturated silty clay (CL).

The slightly higher values of residual strength from novel RS device can be attributed to possible wall-friction effects between upper annular platen and walls of the bottom annular platen. According to Stark et al. (1992) the main factor affecting the residual strength measured in conventional Bromhead RS devices is the magnitude of wall friction that is developed along the inner and outer rings of the specimen. The main cause of wall friction in conventional and novel RS devices is the entrapping of soil between the upper annular platen and walls of the specimen platen extruded during initial the consolidation and shearing stages. As the upper annular platen settles into the specimen platen, the wall friction influencing the shear plane increases, which causes an increase in the measured residual strength. Figure 4-21 shows pictures of the conventional Bromhead and novel RS bottom annular platens after shearing. It can be noticed that the amount of soil extruded on the walls of the bottom plate of the novel RS (Figure 4-21a) is larger than the soil extruded on the walls of the conventional RS Figure 4-21b). This phenomenon is related to the larger dimensions of the novel RS platens and because the compacted specimen is not completely flushes with the edges of the specimen container as it is in the conventional device, leaving more room for accumulation of extruded soil between the top platen and walls. As a consequence the magnitude of the wall friction developed affecting the measured residual strength is higher for the novel RS. Although there is a slightly difference between measurements of residual strength using both RS devices, the difference is not very significant and therefore it can be concluded that residual shear strength measured using the novel RS are consistent and reliable. On the other hand, during suction-controlled RS tests it could be noticed that the amount of soil entrapped between the upper annular platen and the specimen platen was reduced significantly. This was associated to the low water content of the unsaturated samples which reduced the extrusion of soil during initial consolidation and shearing stages reducing the development of wall friction and thus allowing the use of multi-stage testing scheme during the experimental program performed in this research work.

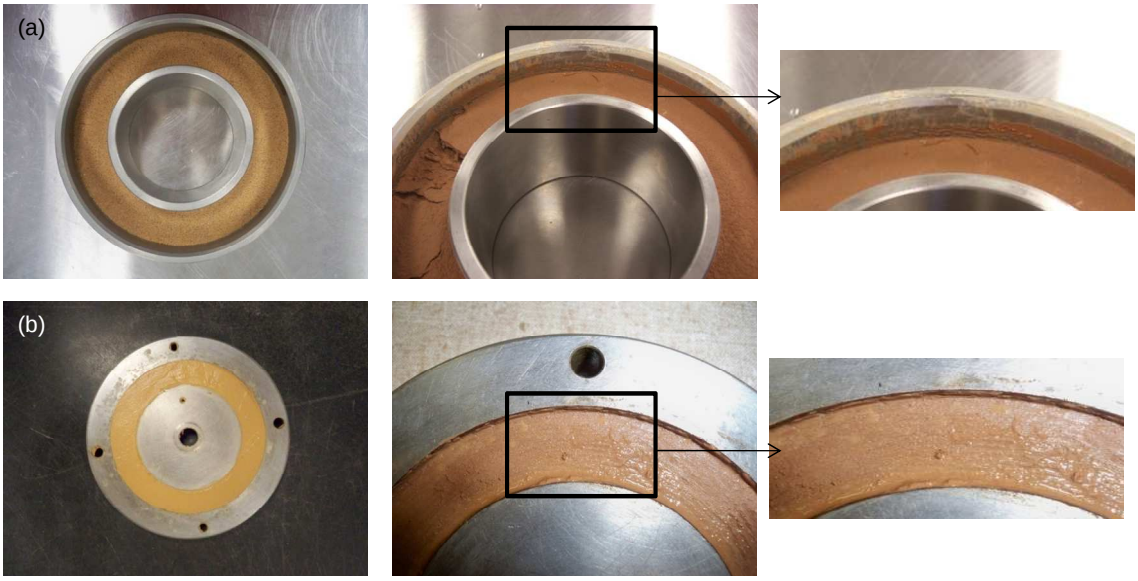

Figure 4-21 Extruded soil on the wall of the bottom annular platen of (a) novel RS, (b) conventional Bromhead RS.

4.6.2 Repeatability of Suction-Controlled RS Test Results

To assess the repeatability of test results under controlled-suction states in the novel RS apparatus, a series of four tests were conducted on statically compacted samples of SM soil under either fully saturated conditions or a controlled suction state, s = 25 kPa, for net normal stress, $(\sigma_n - u_a)$ = 25, 50 or 100 kPa. The tests were conducted by following a multi-stage testing scheme. An additional series of three single-stage tests were conducted on statically compacted samples of CL soil under fully saturated conditions for net normal stress, $(\sigma_n - u_a)$ = 25 kPa. Figure 4-22 and Figure 4-23 shows the results from RS tests performed on SM and CL specimens at suction state, s = 0 kPa (fully saturated condition). Residual shear strength obtained from these trial tests is reasonably close for both, SM and CL materials. The same is observed in Figure 4-24, which shows the saturated residual strength envelopes for the first and second trial RS tests for the SM soil.

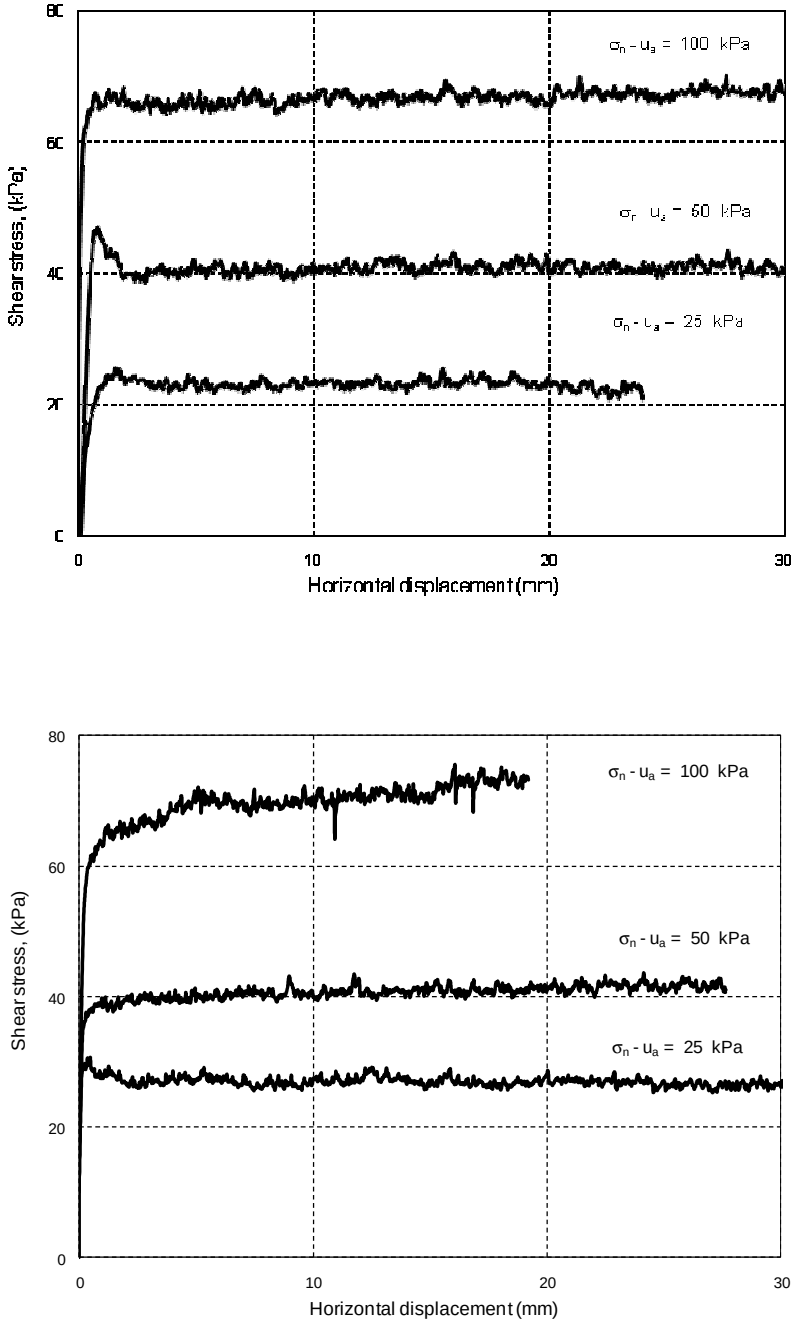

Figure 4-22 Repeatability of RS test results trial 1 and trial 2 at suction state, s = 0 kPa for silty sand soil (SM).

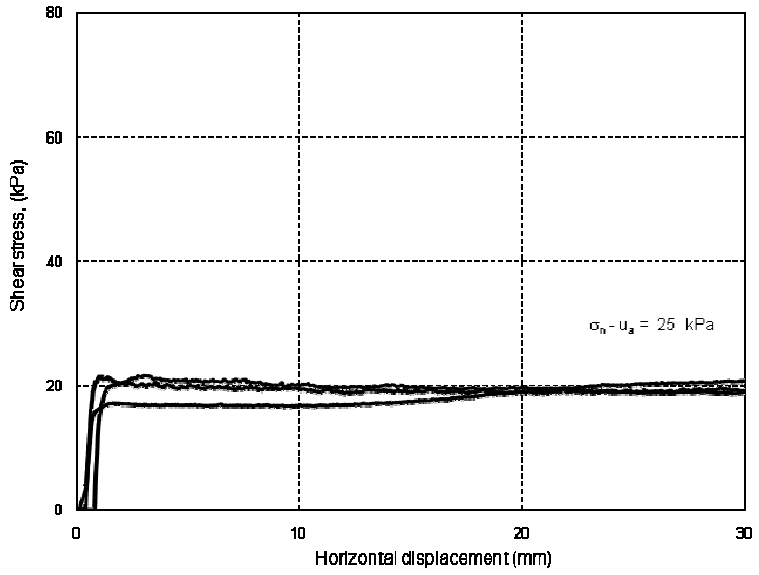

Figure 4-23 Repeatability of RS test results at suction state, s = 0 kPa for silty clay soil (CL).

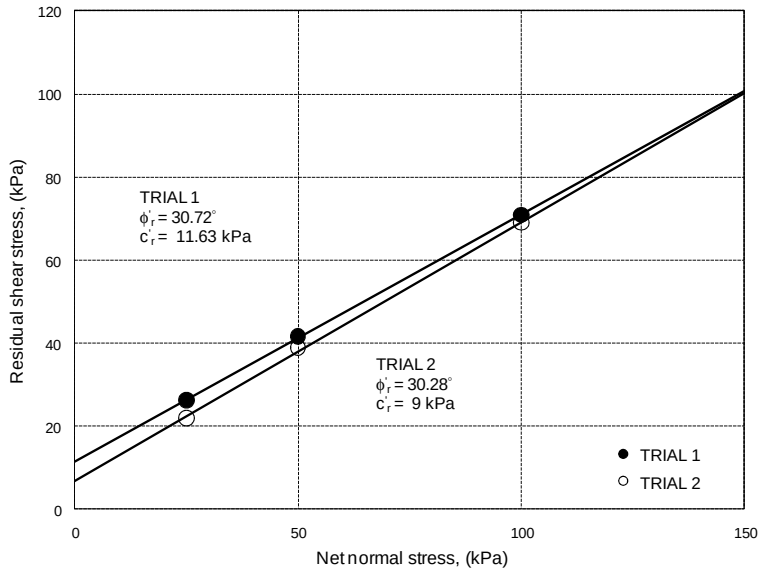

Figure 4-24 Residual strength envelopes for saturated silty sand.

Likewise, Figure 4-25 shows the results from the first and second trial RS tests performed on SM soil at suction state, s = 25 kPa, for net normal stress, $(\sigma_n - u_a)$ = 25 and 50 kPa. Residual shear strength obtained from both multi-stage trial tests is also reasonably close. In this case, the samples were prepared with a water content corresponding to the target suction state of 25 kPa, according to the SWCC shown in Figure 4-11, which reduces the time required for pore-fluid equalization prior to ring shear testing.

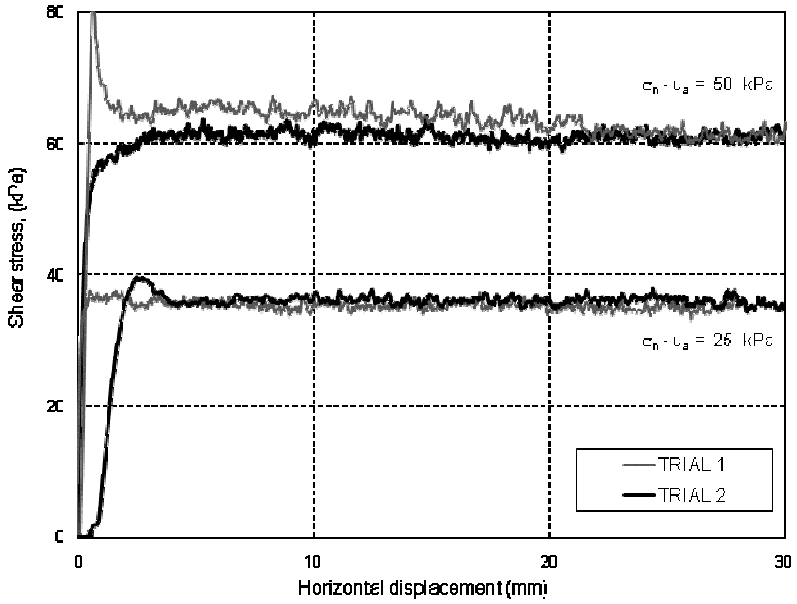

Figure 4-25 Repeatability of RS test results for suction state, s = 25 kPa for silty sand soil (SM).

Finally, results from the four tests conducted on SM soil are summarized in Figure 4-26. Each black dot represents the value of residual strength for two samples tested at the same net normal stress and matric suction. Points yield approximately on a 45° line suggesting that results from the RS tests following a multi-stage testing scheme are repeatable under saturated and suction-controlled states.

Test results, overall confirm the proper functionality of the newly developed system for granular and clayey materials and, the feasibility of the axis-translation technique.

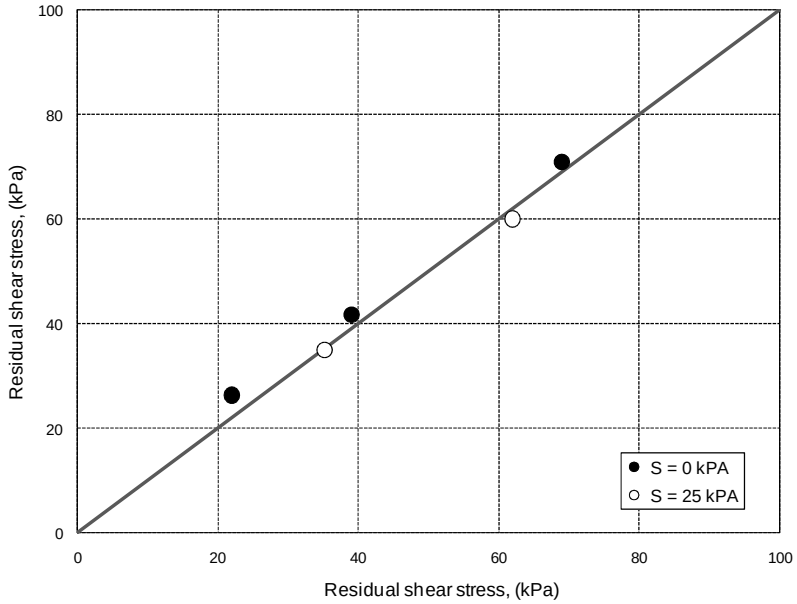

Figure 4-26 Repeatability of suction-controlled test under suction = 0 kPa and 25 kPa.

4.7 Definition of Appropriate Suction-Controlled RS Testing Scheme

There are three main tests procedures for measuring the residual shear strength of soils in the conventional Bromhead type ring shear apparatus and then in the novel RS device (Stark & Vettel, 1992). These procedures are termed: single stage, pre-shearing and, multistage procedure. The single stage test procedure involves loading the specimen to the desired effective normal stress and then shearing the specimen. Once the test is completed, the specimen is removed from the apparatus and a new specimen is used for the next test. The pre-shearing test procedure involves shearing the sample at a rapid displacement rate prior to shear.

Before the displacement rate is applied, the specimen is allowed to dissipate any excess pore water pressures that were induced during rapid shearing. This pre-shearing technique facilitates the creation of a shear plane and reduces the amount of horizontal displacement required to reach a residual condition. Although only one test is performed on each specimen the pre-shearing procedure removes the peak shear strength. In multistage tests, after a residual shear strength condition has been established under the first normal stress, shearing is stopped and the normal stress is increased. The test specimen is allowed to reconsolidate under the higher normal stress before shearing. This procedure is repeated for a number of stress levels. The advantage of using multistage procedure for assessing the residual strength of soils relays in the short duration of tests compared with the other two procedures previously described. Furthermore the variability introduced by specimen preparation is eliminated. Thereby, in the present work a multistage procedure was followed in the mayor part of the experimental work taking into account the typical long durations that a controlled-suction test can last.

4.7.1 Single-Stage RS testing scheme

Typical single-stage (SS) ring shear test paths at different controlled-suction states are shown schematically in Figure 4-27. A typical single-stage procedure can be summarized as follows. After full assembly of the RS apparatus (Fig. 3-2), a vertical load is monotonically applied via the upper annular platen to induce a normal stress 25 kPa greater than the target value of matric suction. The soil was then allowed to consolidate under this load for at least 24 hours or until no more vertical soil deformation was registered. Pore-air pressure u_a was then increased via compressed air in the main cell (Fig. 3-4) until achieving the desired suction state.

After complete equalization of pore fluids under a constant pore-air pressure, which may take up to 48 hours, the shearing stage was initiated. Shearing was continued at a constant angular displacement rate of 0.024°/min until it was apparent that a well-defined residual state

had been reached. At this point, shearing was stopped and the normal load completely removed. Finally, the air pressure in the main cell was slowly brought back to zero. The top annular platen was then removed and the sample inspected for possible shear band formations.

The same procedure summarized above was followed for the saturated samples, except that this time the sample was kept soaked in distilled water in the main RS cell, under a constant 25-kPa normal stress, prior to initiating the shearing stage. Saturation of the sample was allowed for at least 24 hours in order to ensure a zero matric suction (s = 0) state.

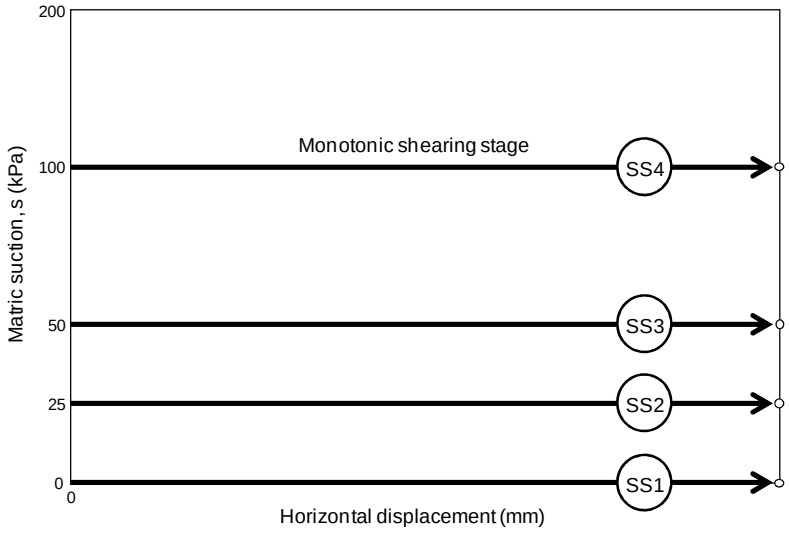

Figure 4-27 Single-stage RS test paths for constant net normal stress, $(u_a - u_w)$ = 25 kPa.

4.7.2 Multi-Stage RS Testing Scheme

A typical multi-stage (MS) ring shear test path at a constant suction state, and net normal stress $(\sigma_n - u_a)$ = 25, 50, 75 and 100 kPa, is shown schematically in Figure 4-28. Test procedure can be summarized as follows. After initial consolidation and equalization of the pore fluids to achieve a net normal stress, $(\sigma_n - u_a)$ = 25 kPa, the first shearing stage was initiated at a constant angular displacement rate of 0.024°/min until it was apparent that a residual state had

been reached. At this point, shearing was stopped and the net normal stress further increased to the next corresponding level (Fig. 4-28), depending on the sample being tested. The sample was then allowed to consolidate under this new load for a period of at least 12 hours or until no more vertical soil deformation was registered, while the initial suction state was kept constant. Shearing was then reinitiated until it was apparent that a new residual state had been reached. The same procedure was followed for the remaining value(s) of net normal stress $(\sigma_n - u_a)$. Upon completion of the last shearing stage, both the torque and vertical load are slowly brought back to zero and the air pressure in the main RS cell fully removed. The upper platen is then removed and the top surface of the sheared sample carefully examined for significant features such as shear band formations.

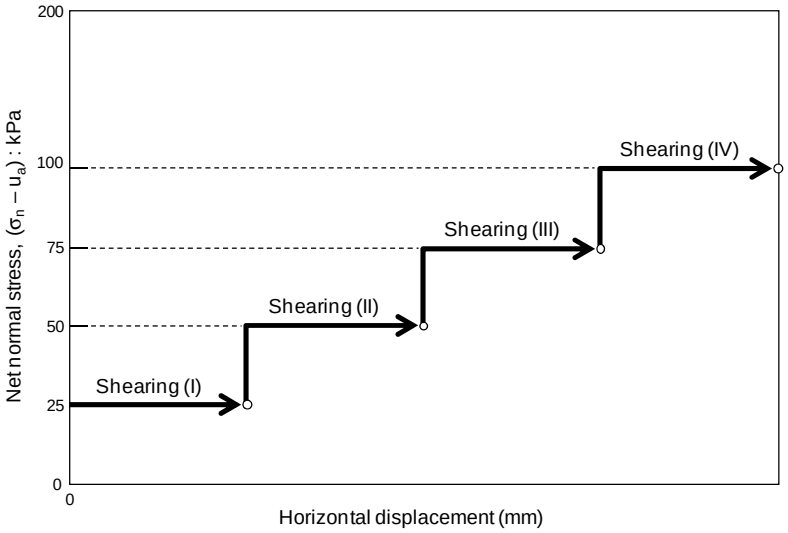

Figure 4-28 Multi-stage RS test paths for constant suction states, s = 25, 50, 75 or 100 kPa.

4.7.3 Experimental validation of the multi-stage Testing Scheme

In order to assess the feasibility of the multi-stage testing scheme under suction-controlled conditions one multi-stage RS tests was performed on a statically compacted sample of SM soil,

under constant suction state, s = 25 kPa and net normal stresses, $(\sigma_n - u_a)$ = 25, 50, 75, and 100 kPa. Results at net normal stress of 75 kPa were compared with those from a single-stage test on a statically compacted sample of SM soil, sheared under net normal stress, $(\sigma_n - u_a)$ = 75 kPa, and the same constant suction state, s = 25 kPa. Figure 4-29 shows a schematic of the RS stress path followed and Figure 4-30 ring shear test results from both tests.

Results demonstrate that the multi-stage procedure yields residual strengths that are in reasonably good agreement with those from single-stage procedure. The slightly higher values of residual strength from multi-stage testing can be attributed to possible wall-friction effects between the upper platen and the walls of the bottom annular platen as was discussed in section 4-6. Adoption of a suction-controlled multi-stage testing scheme, as typically done in the conventional Bromhead apparatus, reduces the time required to accomplish a test and minimizes the soil variability introduced by the sample preparation process. Thereby, based in the above experimental results this testing scheme was adopted through the main experimental program of this research work.

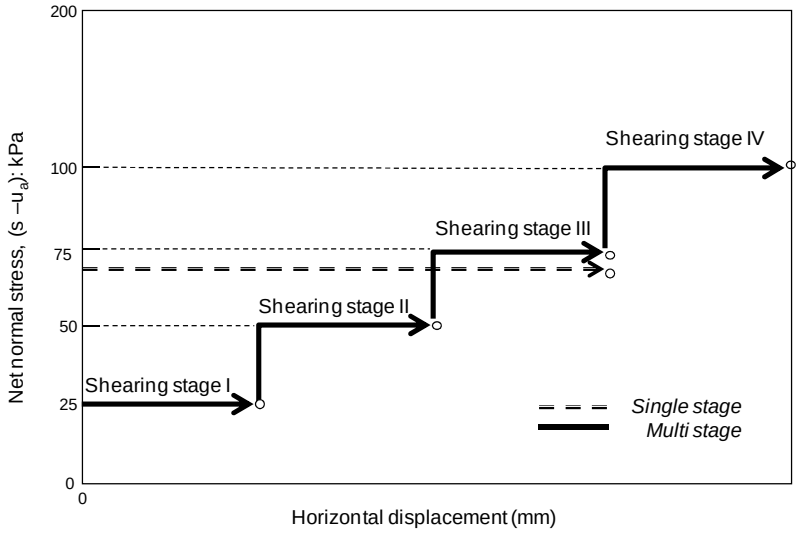

Figure 4-29 Multi-stage RS test paths

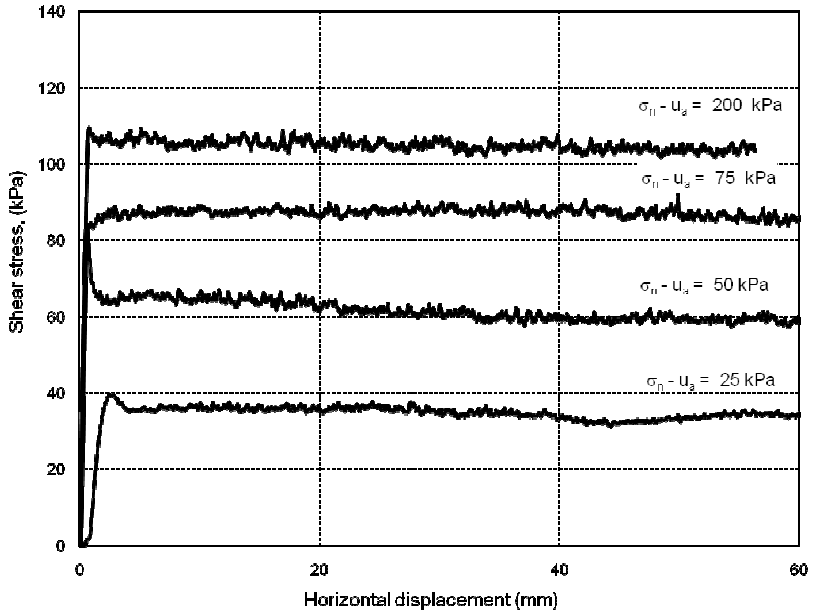

(a)

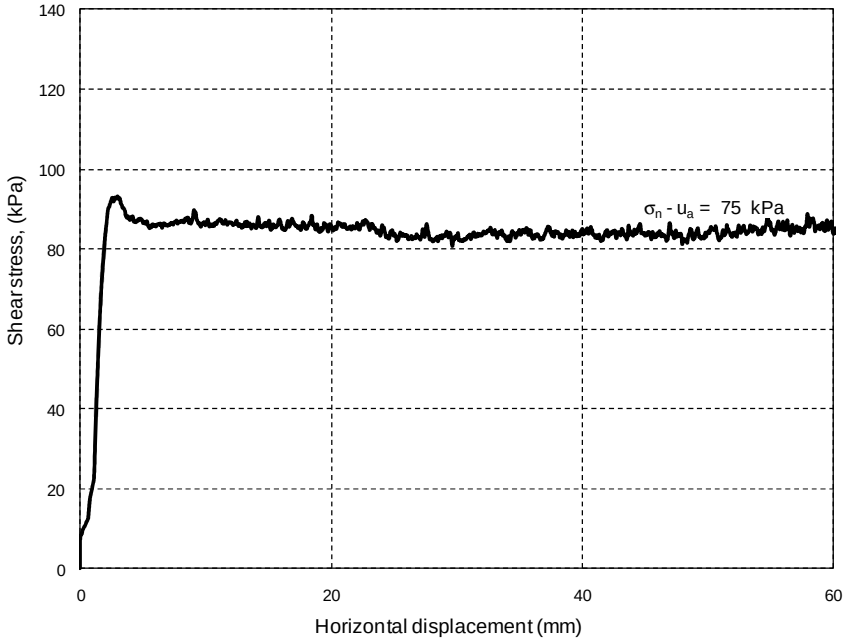

Figure 4-30 Results tests on SM soil for constant suction state, s = 25 kPa. From: (a) multi-stage RS, (b) and single-stage RS.

Next chapter describes the entire suction-controlled experimental program and test procedures followed in this research work, including a detailed list of all experimental variables. The chapter includes all the experimental results from this program.

CHAPTER 5

SUCTION-CONTROLLES EXPERIMENTAL PROGRAM AND TEST RESULTS

5.1 Introduction

In order to investigate several features of unsaturated soil behavior over a whole range of shear deformations a series of 22 suction-controlled ring shear tests were performed following completion of the novel suction-controlled ring shear test apparatus described in chapter 4. The series was comprised of nine ring shear tests for machine performance verification and thirteen suction-controlled RS tests for unsaturated residual shear strength assessment. Suction-controlled RS tests were performed following a multi-stage testing scheme, in which residual strength determinations were made at three or more net normal stresses. In view of the experimental novel nature of the apparatus, all test results, whether successful or inconclusive, are presented and discussed in this chapter. Three soils having widely varying properties were included in the test program, namely ,silty sand (SM), silty clayey sand (SC-SM) and silty clay (CL) soils. The basic engineering properties, compaction characteristics and SWCC curves are described in chapter 4. This chapter presents a comprehensive analysis of all these test results, focusing on the effect of matric suction and net normal stress on the unsaturated behavior of SM, SC-SM and CL soils over a whole range of shear deformations. To provide an orderly presentation of test results, tests performed on each type of soil are discussed in separate sections.

5.2 Experimental Variables

A summary of the experimental variables in the series of suction-controlled RS tests on compacted silty sand, silty clayey sand and silty clay is presented in Table 5-1, Table 5-2 and Table 5-3. The stress paths followed and the type of tests are also described.

Table 5-1 Experimental variables during suction-controlled RS testing for SM soil.

Soil	Test #	$\sigma_{vertical}$ (kPa)	u_a (kPa)	u_w (kPa)	$\sigma_v - u_a$ (kPa)	$u_a - u_w$ (kPa)	No. of stages	Comments
SM	1	50	0	0	50	0	3	ORIGINAL PLATEN Machine performance test (TOP CAP)
		100	0	0	100	0		
		200	0	0	200	0		
	2	50	25	0	25	25	2	Machine performance test (REPEATIBILITY-SUCTION CONTROL)
		75	25	0	50	25		
	3	25	0	0	25	0	3	Machine performance test (REPEATIBILITY-SAT)
		50	0	0	50	0		
		100	0	0	100	0		
	4	100	25	0	75	25	1	Machine performance test (SINGLE-STAGE)
	5	25	0	0	25	0	4	Machine performance test (CONVENTIONAL BROMHEAD RS)
		50	0	0	50	0		
		100	0	0	100	0		
		200	0	0	200	0		
	6	25	0	0	25	0	5	Load-unload net normal stress path at fully saturated conditions.
		50	0	0	50	0		
		100	0	0	100	0		
		200	0	0	200	0		
		50	0	0	50	0		
	7	50	25	0	25	25	4	Conventional multi-stage path
		75	25	0	50	25		
		100	25	0	75	25		
		125	25	0	100	25		
	8	75	50	0	25	50	3	Conventional multi-stage path
		100	50	0	50	50		
		150	50	0	100	50		
	9	100	75	0	25	75	6	Load-unload net normal stress path at matric suction constant, followed by a suction increase path at net normal stress constant
		125	75	0	50	75		
		150	75	0	75	75		
		125	75	0	50	75		
		100	75	0	25	75		
		125	100	0	25	100		
	10	125	100	0	25	100	1	multi-stage. Max capacity of torque sensor
	11	50	25	0	25	25	4	Suction increase path at net normal stress constant
		75	50	0	25	50		
		100	75	0	25	75		
		125	100	0	25	100		

Table 5-2 Experimental variables during suction-controlled RS testing for SC-SM soil.

Soil	Test #	$\sigma_{vertical}$ (kPa)	u_a (kPa)	u_w (kPa)	$\sigma_v - u_a$ (kPa)	$u_a - u_w$ (kPa)	No. of stages	Comments
SC-SM	12	25	0	0	25	0	4	ORIGINAL PLATEN Machine performance test (TOP CAP)
		50	0	0	50	0		
		100	0	0	100	0		
		200	0	0	200	0		
	13	25	0	0	25	0	4	Conventional multi-stage path
		50	0	0	50	0		
		100	0	0	100	0		
		200	0	0	200	0		
	14	50	25	0	25	25	4	Conventional multi-stage path
		75	25	0	50	25		
		100	25	0	75	25		
		125	25	0	100	25		
	15	75	50	0	25	50	5	Conventional multi-stage path
		100	50	0	50	50		
		125	50	0	75	50		
		150	50	0	100	50		
		250	50	0	200	50		
	16	125	100	0	25	100	4	Conventional multi-stage path
		150	100	0	50	100		
		175	100	0	75	100		
		200	100	0	100	100		

Table 5-3 Experimental variables during suction-controlled RS testing for CL soil.

Soil	Test #	$\sigma_{vertical}$ (kPa)	u_a (kPa)	u_w (kPa)	$\sigma_v - u_a$ (kPa)	$u-u_w$ (kPa)	No. of stages	Comments
CL	17	25	0	0	25	0	2	Machine performance test (REPEATIBILITY-SAT)
		50	0	0	50	0		
	18	25	0	0	25	0	2	Machine performance test (REPEATIBILITY-SAT)
		50	0	0	50	0		
	19	25	0	0	25	0	4	Machine performance test (CONVENTIONAL BROMHEAD RS)
		50	0	0	50	0		
		100	0	0	100	0		
		200	0	0	200	0		
	20	25	0	0	25	0	5	Conventional multi-stage path
		50	0	0	50	0		
		75	0	0	75	0		
		100	0	0	100	0		
		200	0	0	200	0		
	21	325	300	0	25	300	1	Shear strength higher than max capacity of load sensors
	22	25	0	0	25	0	2	Suction increase path at net normal stress constant. Shear strength higher than max capacity of load sensors
		325	300	0	25	300		

The selected range of matric suctions $(u_a - u_w)$ from 0 to 100 kPa for SM and SC-SM soils, and from 0 to 500 kPa for CL soil was intended to reproduce typical field suction values monitored in sandy and silty shallow formations, embankments, and skin landslides in the state of Texas. The suction ranges also included the saturated and transitional regimens of the SWCC where the main strength and volumetric changes of unsaturated soils take place, as explained in chapter 4. On the other hand, the selected range of normal stresses $(\sigma_n - u_a)$, from 25 to 200 kPa, is aimed at reproducing normal stress states typically encountered in first-time landslides in highway embankments (Stark and Eid 1997).

Soil samples were compacted directly into the lower annular platen using in-place static compaction following the procedure thoroughly explained in chapter 4. The upper platen was used to compress the loose soil-water mix until achieving a target density of 95% of maximum Proctor dry density. Samples were prepared with water contents equivalent to initial suction states of 25 kPa (five samples), 50 kPa (two samples), 75 kPa (one sample), 100 kPa (two samples) and 300 kPa (one sample), according to the soil-water characteristic curves (SWCC).

Eleven more samples were prepared with a moisture content that was 6% greater than Proctor optimum and subsequently soaked in distilled water in the main RS cell or in the conventional Bromhead RS for testing under zero suction state (s = 0).

5.3 Typical Suction-controlled RS Assembling Process

An orderly procedure has been established for the assembling of the new RS apparatus for suction-controlled testing. The main steps involved in the set-up process are described in this section. The whole set-up process takes approximately 120 min working in an organized manner and having previously prepared all the pieces to assemble the ring shear apparatus. The set-up procedure consists of the following steps:

- All actuators and the acquisition system are switched on to allow instruments to come into equilibrium and minimize the influence of temperature offsets (Figure 5-1).
- A small piece of wet filter paper is left over the top of each ceramic disk during the specimen setting up procedure to provide a better continuity between the water in the sample and the water in the ceramic disks (Figure 5-2a).
- The sample is statically compacted into the bottom plate following the procedure thoroughly explained in chapter 4 (Figure 5-2b).
- After being compacted into the bottom annular platen, the sample is quickly transferred to the ring shear frame in order to minimize evaporation or water loss from the sample. This assembly is fixed with six screws onto the bottom base plate of the ring shear frame, as shown in Figure 5-2(c).
- The load shaft is then brought up through the controller and the upper platen is fixed to the top of the piston shaft with six screws, as shown in Figure 5-2(d).
- All drainage lines are filled with deaired water and the whole system is flushed several times to avoid any trapped air in the system. The flushing and volume water indicator of the PCP-15U suction control panel are set in the appropriate positions before the test starts.
- A small vertical sitting load of 25 N is applied in order to bring the upper annular platen in contact to the sample (Figure 5-2e).
- The confining cell is installed and the top cover plate is fixed with three additional screws, as shown in Figure 5-2(f). The air pressure line is connected to the top cover plate and a thorough check is made to verify that the top and bottom seals are securely tightened. Readings of the load-torque transducer are

reset and the LVDT and angular deformation sensor are re-zeroed prior to testing.

- After full assembly of the RS apparatus the sample is subjected either to a single stage or multi-stage testing scheme depending on the sample being tested, following a procedure explained in chapter 4, and stress paths depicted in Table 5-1 to Table 5-3.
- When the test is finished, all pressures are gradually reduced back to atmospheric pressure. The cell chamber is opened and the failure surface of the soils specimen is thoroughly examined. A small part of the specimen is removed and quickly prepared for water content measurement and microscopic digital imaging.

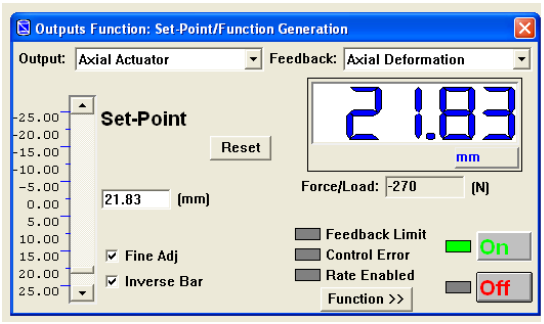

(a)

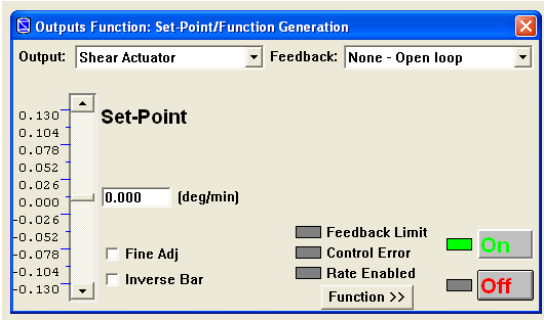

(b)

Figure 5-1 Output function on: (a) axial actuator; (b) shear actuator

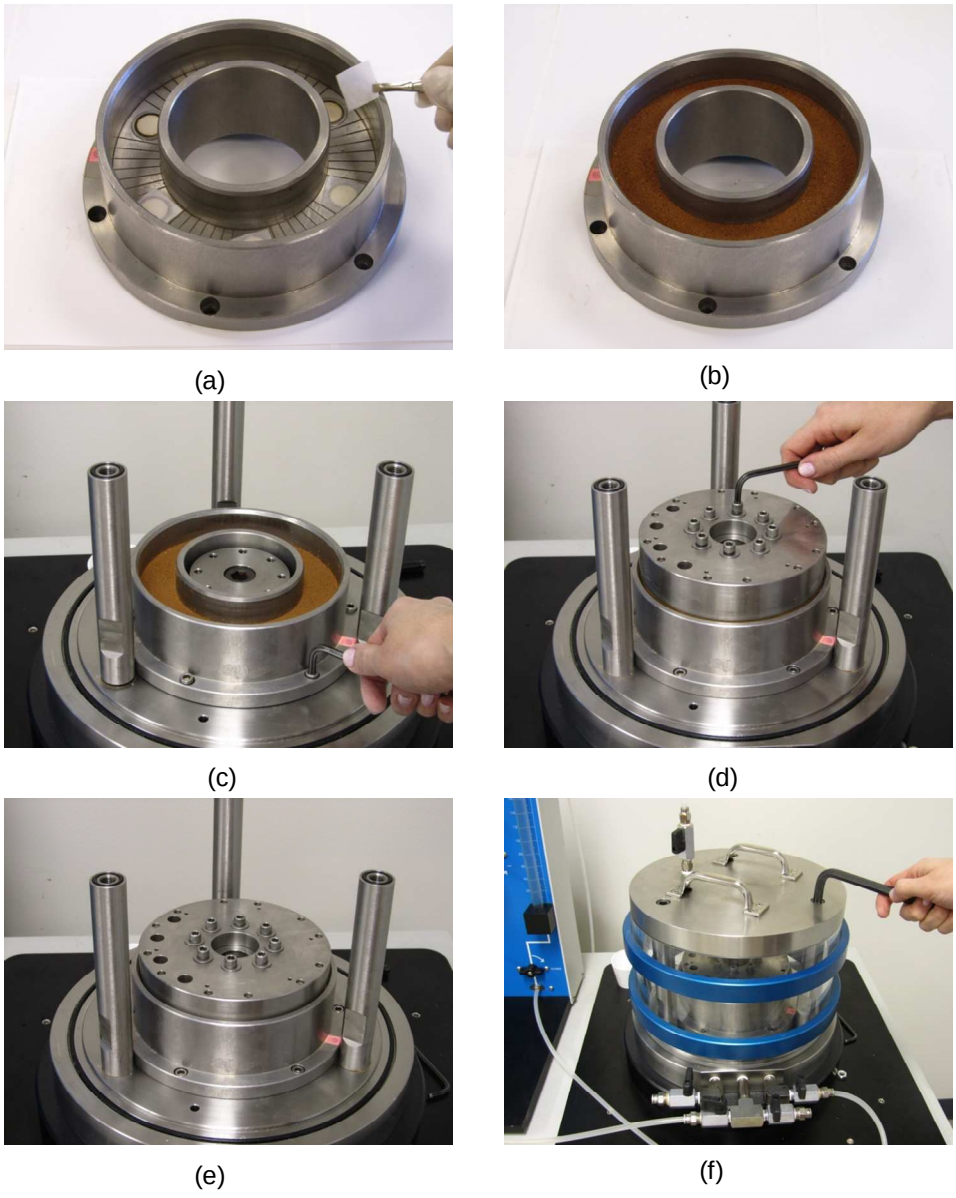

Figure 5-2 RS assembling: (a) filter paper interface; (b) exposed compacted sample; (c) instalation of bottom platen; (d) instalation of upper platen; (e) application of sitting load; (f) instalation of confining cell.

5.3.1 Equalization Stage

After setting up the soil specimen and completely assembling the RS device, the equipment is ready to perform the programmed test. The first stage of each multi-stage test requires bringing the sample to an initial net normal stress $(\sigma_n - u_a)$ of 25 kPa, and a corresponding matric suction of $(u_a - u_w)$ = 0, 25, 50, 75, 100 or 300 kPa. To accomplish this, a vertical load is monotonically applied via the upper annular platen to induce a normal stress 25 kPa greater than the corresponding value of suction. The soil is then allowed to consolidate under this load for at least 24 hours. Pore-air pressure u_a is then increased via compressed air in the main cell until achieving the desired suction state. The external normal stress is adjusted accordingly to keep a constant net normal stress, $(\sigma_n - u_a)$ = 25 kPa.

The equalization stage in every test specimen was considered accomplished when no further change in both water volume from within the sample (less than 0.035 ml/day) and vertical deformation of the sample was observed. The time required for the equalization ranged between 50 to 90 hours for SM soil and, 74 to 116 hours for SC-SM, depending of the selected value of suction and net normal stress.

Figure 5-3 shows the change in vertical displacement with time that occurred during a typical equalization stage for a suction value of 50 kPa and a net normal stress of 25 kPa for SM soil. The test starts with an immediate increase in vertical displacement due to the monotonic application of the vertical load. Once the vertical displacement reaches a constant value, air-pore pressure is increased to the target value, and an additional increase in vertical deformation could be observed. Then, because the initial suction of the sample was slightly lower than the target suction, thus following a drying path, a volumetric deformation of compression was observed during the equalization stage. All samples exhibited this typical behavior during the equalization stage.

A typical record for assessing the appropriate pore-fluid equalization time under a sustained suction state, s = u_a = 25, 50, 75 and 100 kPa, and net normal stress of 25 kPa for SM and SC-SM soils are shown in Figure 5-4 and Figure 5-5, respectively. All samples exhibited a water flow coming out from the sample during equalization, proving that the initial sample suction associated to the static compaction process and initial water content was below to the target matric suction.

In general, the volume of expelled water increased with suction for both soils, except for the SM sample stabilized to a suction equal to 75 kPa, which showed a lower volume of expelled water. That was associated to an initial compaction suction closer to the target suction compared with the other samples. As a result both vertical displacement and suction equilibrium showed a lower equalization time.

Finally, after initial consolidation and equalization of the pore fluids, the first shearing stage was initiated following the multi-stage testing scheme explained in chapter 4 and stress paths depicted in Table 5.1 to Table 5.2 and explained in detail later in this chapter.

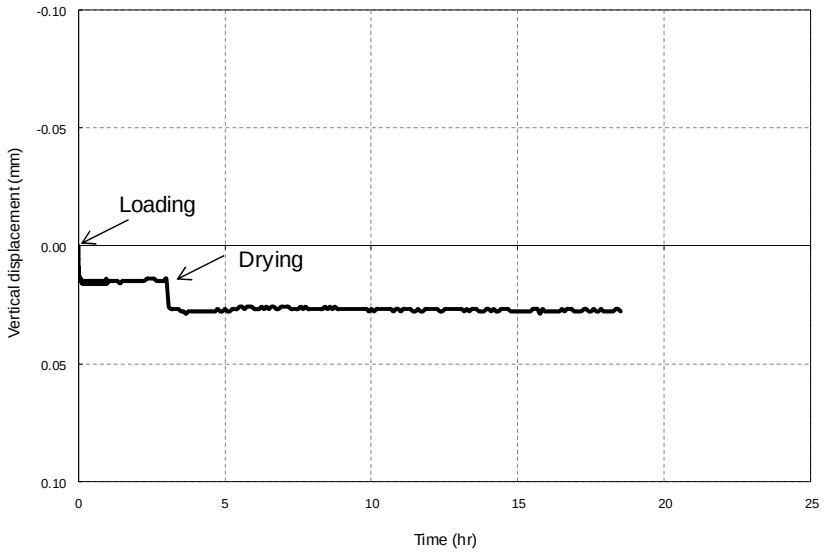

Figure 5-3 Typical change in vertical deformation with time during equalization stage for s = 50 kPa and $(\sigma_n - u_a)$ = 25 kPa for SM soil.

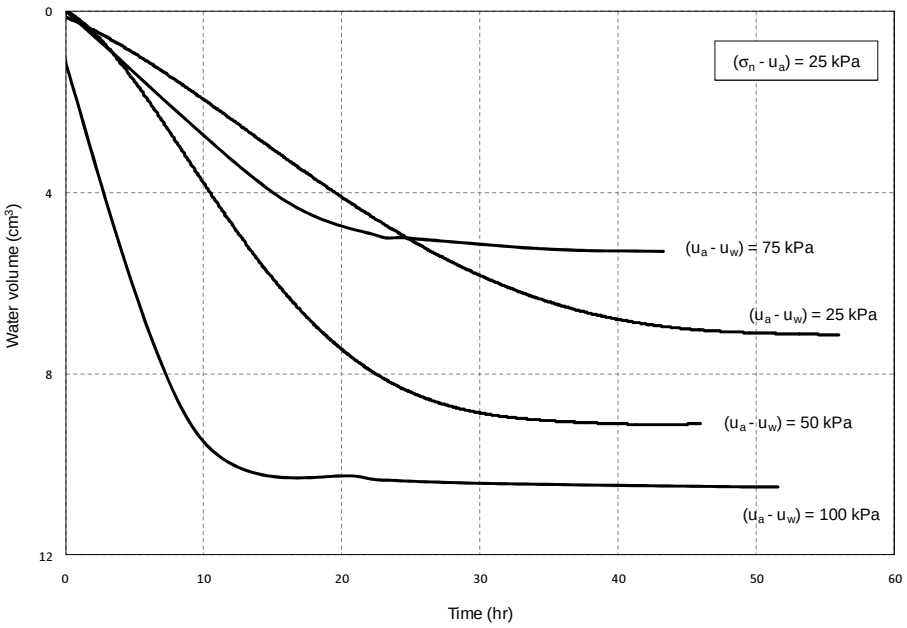

Figure 5-4 Volume of water expelled vs. time during equalization stage for SM soil

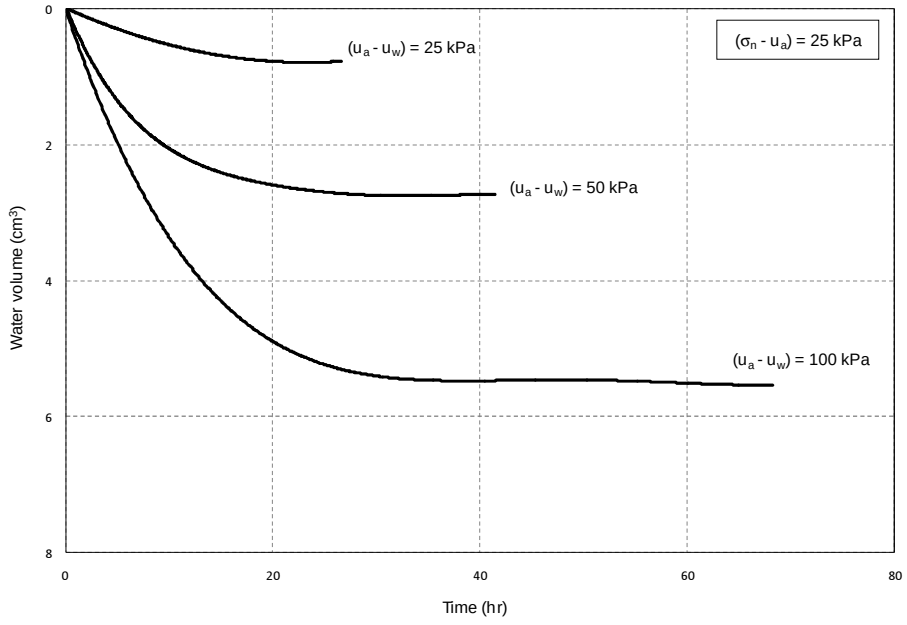

Figure 5-5 Volume of water expelled vs. time during equalization stage for SC-SM soil

5.3.2 Shearing Stage

The thirteen multi-stage suction-controlled RS tests for evaluation of residual strength were performed on a equal number of statically compacted samples of SM, SC-SM and CL soil under either fully saturated conditions or controlled suction states, s= 25, 50, 75, 100 or 300 kPa and for net normal stress, $(\sigma_n - u_a)$ = 25, 50, 75, 100 or 200 kPa.

The series was comprised of six tests on SM soil labeled: RS6, RS7, RS8, RS9, RS10 and RS11; four tests on SC-SC soil: RS13, RS14, RS15 and RS16, and three tests on CL soil: RS20, RS21 and RS22. The maximun shear deformation for these tets ranged between 30 mm and 100 mm. This range of maximun shear deformation was selected in order to allow residual shear strength and vertical deformation to reach the critical state on each stage. Critial state could be defined as the state reached in a soil when continuos shearing occurs at constant shear stress and constant volume (Budhu, 2007).

In this work, all ring shear tests were conducted at an equivalent horizontal displacement rate of 0.025 mm/min, which corresponds to a rotational speed of 0.023°/min. This rate is slightly lower than that recommended for conventional ring shear testing on saturated clayey soils, which is 0.024°/min (e.g. Meehan et al. 2007). Vaunat et al. (2006) also performed suction-controlled ring shear tests on Barcelona silty clay at two different rotational speeds, 0.024°/min and 0.12°/min: no significant differences were observed in the values of residual shear strength and, consequently, a rotational speed of 0.12°/min was adopted. In light of these observations, a rotational speed of 0.024°/min was adopted and considered more than suitable for the soils used in this research effort.

The GCTS software was programmed to take real-time readings of stress and soil displacement every 60 seconds throughout the entire test, which is a considerably high data-sampling rate compared to most work reported in the literature (e.g. Tiwari and Marui 2004, Infante Sedano 2006, Carrubba and Del Frabbo 2008). Therefore, the software was able to

capture phenomena as such particle re-accommodation or crushing during shearing. That explains the “noise” observed in some of the shear strength curves presented in this work. Nevertheless, closer inspection of all curves shows that the difference between the highest or lowest value of stress and the average residual value of stress is about 3 kPa, which corresponds to only a 5% difference on average – see, for instance, Figure 5-15 for net normal stress of 50 kPa.

On the other hand, Figure 5-6 shows a typical shear stress versus horizontal displacement curve. It can be readily observed that matric suction plays an important role over the shear strength developed by an unsaturated soil at large deformation. As shown in this figure, a gradual increase in shear strength was often observed as the specimen was sheared at large displacements. This phenomenon was also observed by other researchers testing clays in direct shear and conventional RS devices and is thougth to be caused by the combined effects of some soil extruction and wall friction (Bishop et al., 1971; Skempton, 1985, Meehan et al, 2007).

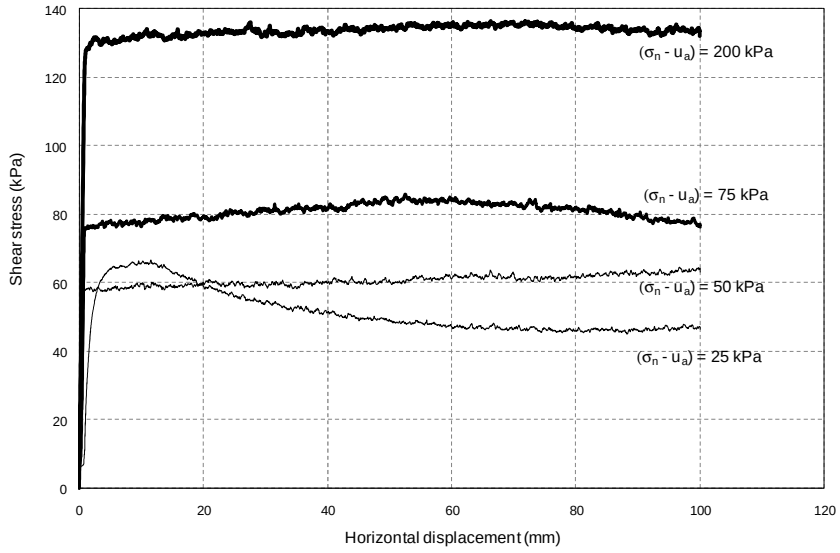

Figure 5-6 Shear stress vs. horizontal displacement from multi-stage RS test for SC-SM soil under s = 50 kPa, and $(\sigma_n - u_a)$ = 25, 50, 75, and 200 kPa.

Figure 5-7 shows a plot of the typical relationship between vertical and horizontal deformation. A positive volume change refers to a decrease in volume, whereas a negative volume change indicates a volume increase. This figure indicates that critical state has been achieved in most of the cases after a shear deformation approching to 80 mm for the first load increment and 60 mm for the rest of the stages.

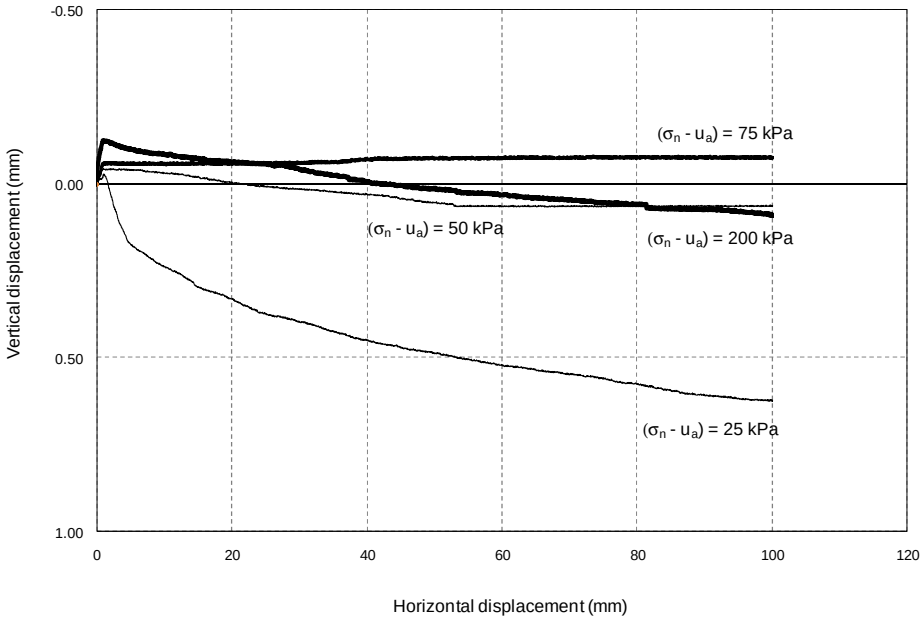

Figure 5-7 Relationship between vertical and horizontal displacement from multi-stage RS test for SC-SM soil under s = 50 kPa, and $(\sigma_n - u_a)$ = 25, 50, 75 and 200 kPa.

5.3.3 Stress paths

To study the behavior of compacted soil at large deformation, samples RS6, RS7, RS8, RS10, RS13, RS14, RS15, RS16, RS20, RS21 and RS22 were subjected to a typical multi-stage

testing scheme path that invloves shearing at different net normal stresses under constant matric suction. The stress path followed by these samples was schematically shown in Figure 4-29.

In addition, with the aim of studying the influence of pre-shearing and suction hystory over the value of unsaturated residual strength, sample RS9 was subjected to a load-unload net normal stress path at matric suction constant, followed by a suction increase path at net normal stress constant. Sample RS9 was initially sheared under a constant suction state, s = 75 kPa, involving a loading-unloading stress path of net normal stresses, $(\sigma_n - u_a)$ = 25, 50, 75, 50 and 25 kPa. Then the specimen was dried to a suction equal to 100 kPa and re-sheared under a constant net normal stress of 25 kPa. The multi-stage RS stress path folowed by sample RS9 is schematically shown in Figure 5-8.

Finally, sample RS11 was subject to a multi-stage path at constant net normal stress $(\sigma_n - u_a)$ = 25 kPa involving a range of matric suction s = 25, 50, 75 and 100 kPa. These results were comparded with the results from the first shearing stage from multi-stage RS tests decribed above for constant suction and differents values of net normal stress. They corresponds to samples with any stress or suction history and, hence they are equivalent to single-stage tests. This comparison was useful to determine the dependency of residual shear stress over the suction history of a compacted soil. The multi-stage testing scheme path at different controlled-suction states is shown schematically in Figure 5-9.

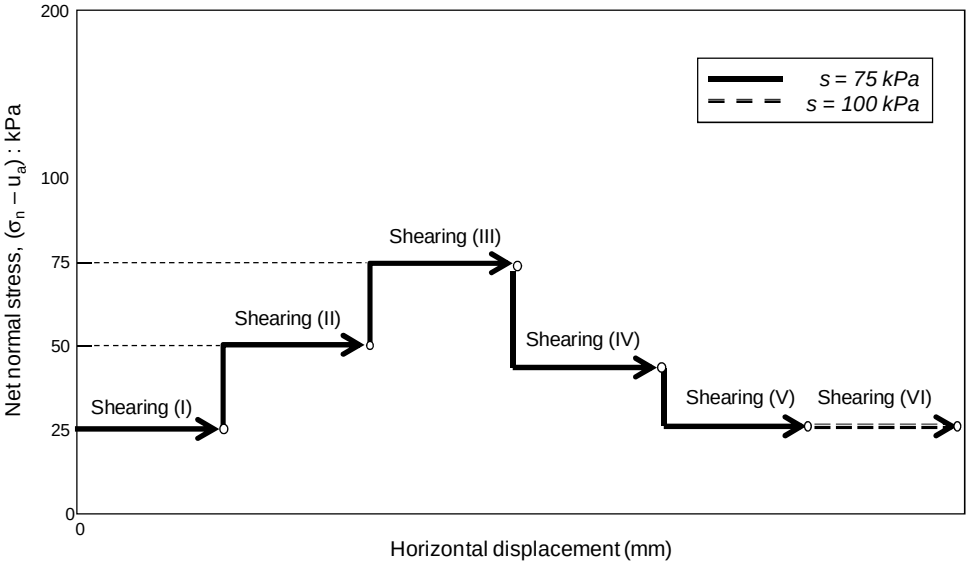

Figure 5-8 Load-unload net normal stress path at matric suction constant s = 75 kPa, followed by a suction increase path at net normal stress constant $(\sigma_n - u_a)$ = 25 kPa.

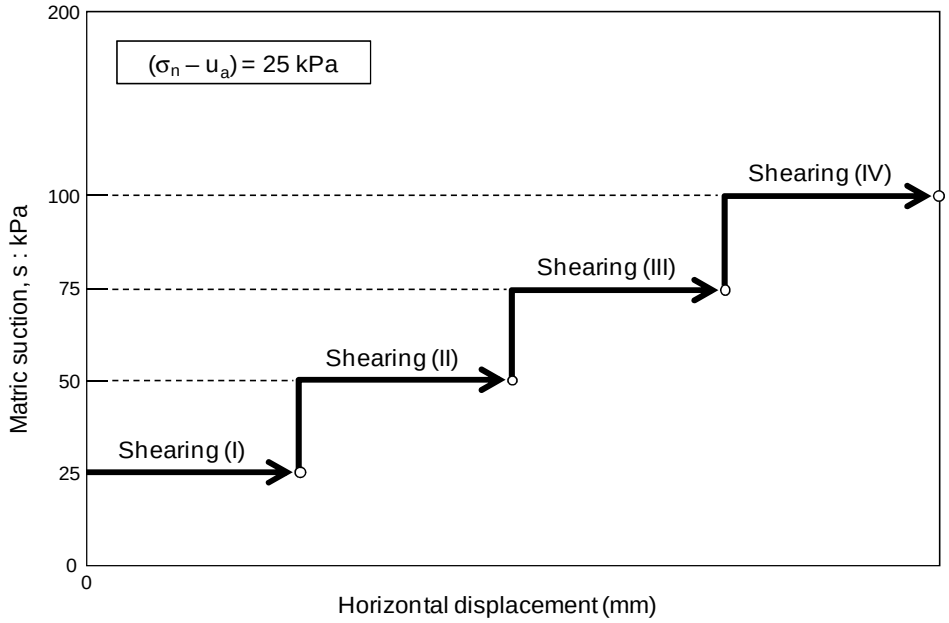

Figure 5-9 Multi-stage RS test paths for constant net normal stress $(\sigma_n - u_a)$ = 25 kPa and suction states, s = 25, 50, 75 or 100 kPa.

5.4 Test Results

5.4.1 Residual Strength of Fully Saturated Soil

In order to determine the saturated residual strength parameters for the test soils, three multi-stage RS tests were conducted under constant fully saturated conditions on SM, SC-SM and CL soils. RS tests are labeled as RS6, RS13 and RS20 in Table 5-1 to Table 5-3, respectively. The 15-mm (0.59-in) thick ring shear samples were all statically compacted to a target dry unit weight of 95% of the maximum Proctor dry unit weight, and with a moisture content of 6% more than the optimum, following the procedure described in chapter 4. The samples were then soaked in distilled water for at least 24 hours, attaining a final degree of saturation between 97% and 99% (calculated by using volume-weight relationships). The initial dry unit weight and initial water content values for each sample are presented in Table 5-4.

Table 5-4 Initial sample characteristics

Soil	Sample	Initial water content (%)	Initial dry density (kN/m^3)
SM	RS6	16.75	1.75
SC-SM	RS13	30.32	1.33
CL	RS20	24.08	1.68

Sample RS6 was initially subjected to a multi-stage stress path involving a range of net normal stresses of $(\sigma_n - u_a)$ = 25, 50, 100, and 200 kPa. Then, to study the effect of shearing history on saturated residual stress, RS6 sample was unloaded to a net normal stress of 50 kPa and re-sheared. Sample RS13 was subjected to a typical multi-stage stress path involving a range of net normal stresses of $(\sigma_n - u_a)$ = 25, 50, 100, and 200 kPa. Finally, sample RS20 was subjected to a multi-stage stress path involving a range of net normal stresses of $(\sigma_n - u_a)$ = 25,

50, 75, 100, and 200 kPa. A typical multi-stage test procedure was described in chapter 4. Results from RS6, RS13 and RS20 are shown in Figures 5-10, 5-11 and 5-12, respectively.

Saturated residual strength of SM soil:

From Figure 5-10 it can be noticed that SM soil shows a small peak at very low normal stress during first shearing, followed by a gradual decrease in shear resistance to the residual shear stress state. Soil presents an initial vertical compression due mainly to a particle adjustment and then dilates until an apparent stabilization of the vertical deformation is reached. The residual shear strength and dilatancy increase with normal stress(σ_n).

Results reveal that SM soil exhibits the typical "turbulent mode" of residual shear described by Lupini et al. (1981), in which the residual shear state involves shear at constant volume without particle reorientation. In this case the residual shear strength is that of the round particles alone due the low proportion of clayey particles presents in the soil (particle size < 2μ = 6.6%).

Figure 5-10 includes results of an additional shearing stage at net normal stress of 50 kPa (curve "A") after specimen had been sheared at net normal stresses of 25, 50, 100 and 200 kPa. It can be seen that the residual shear strength after unloading and a large shearing history is almost the same as the residual shear strength exhibited by the same sample with any previous stress history. This confirms that the saturated residual strength does not depend on the original soil structure or stress history experienced by the soil (Bishop et al. 1971; Lupini et al., 1981; Bromhead and Curtis 1983; Skempton, 1985). During the last shearing stage the soil became stiffer due to the unload stress path followed, then exhibiting a small peak stress and large dilatancy as the horizontal displacement increased (Figure 5-10).

Saturated residual strength response of SC-SM and CL soil:

Figure 5.11 and Figure 5-12 show that SC-SM and CL soils, respectively, exhibit a gradual increase in shear stress as the horizontal displacement increases until a constant residual shear stress is attained. For low normal effective stresses, samples show large deformations of compression after an initial expansion at low horizontal displacements. For larger normal stresses, the specimens show a rapid increase in shear stress reaching an apparent small peak value at low shear strains (compared with the response at 25 kPa) and then showing a decrease in shear stress with increasing shear displacement until the residual shear stress is attained. This can be attributed to the nature of the multi-stage testing scheme followed in this work, where a preexisting failure surface is induced on the sample before increasing the net normal stress to the next corresponding level. Thus, the apparent peak can be associated to the effort required initially to reorient the particles in the direction of shearing under the new net normal stress state, and the fall to residual strength is completed at smaller horizontal displacement. This small displacement suggests that the structure of the shear surface requires modification for the new residual strength to be established, and that the effect of normal stress on the residual friction angle is due to changes in structure between particles, rather than to changes in intrinsic friction between particles.

A closer look at the phenomenon is possible in Figure 5-13, which shows a typical shear strength response for CL soil during the first 10 mm of horizontal shear displacement. It can be noticed that peak stress is suppressed and the expansion decreases at large normal stress of 200 kPa. As it is expected, the residual strength increases and the amount of compression decreases with normal stress (σ_n), for both SC-SM and CL soils. The stress-displacement curve becomes brittle as the normal effective stress is increased.

Both SM-SC and CL soils exhibit the typical “sliding mode” of residual shear, in which the proportion of platy, low friction particles is sufficiently high for a well formed, polished sliding

surface of strongly oriented clayey particles. The post-peak drop in strength of CL soil with a larger clay fraction (particle size < 2μ = 32%) is due entirely to particle reorientation.

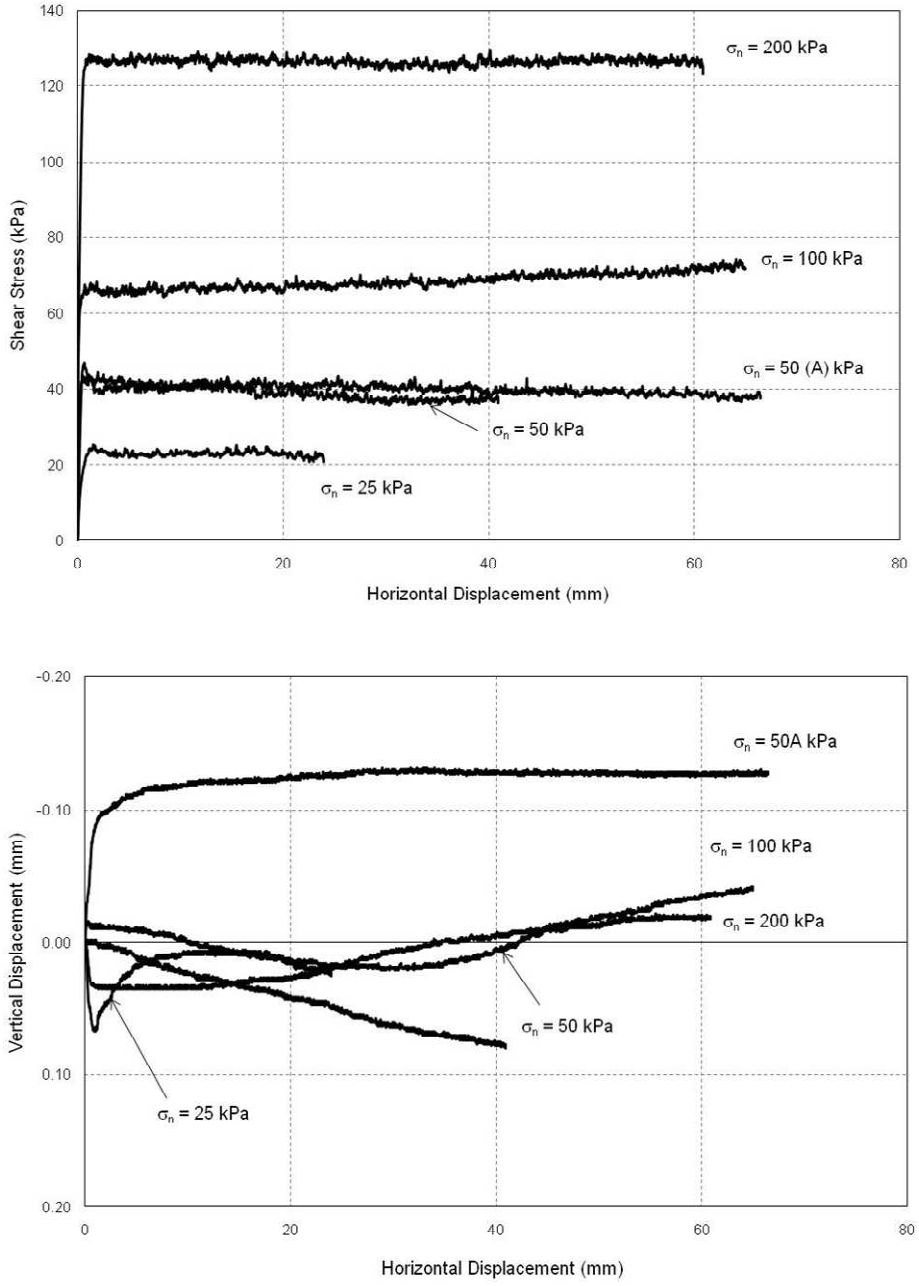

Figure 5-10 Results from multi-stage RS tests on SM soil under s = 0 kPa, and $(\sigma_n - u_a)$ = 25, 50, 100, 200 and 50 kPa.

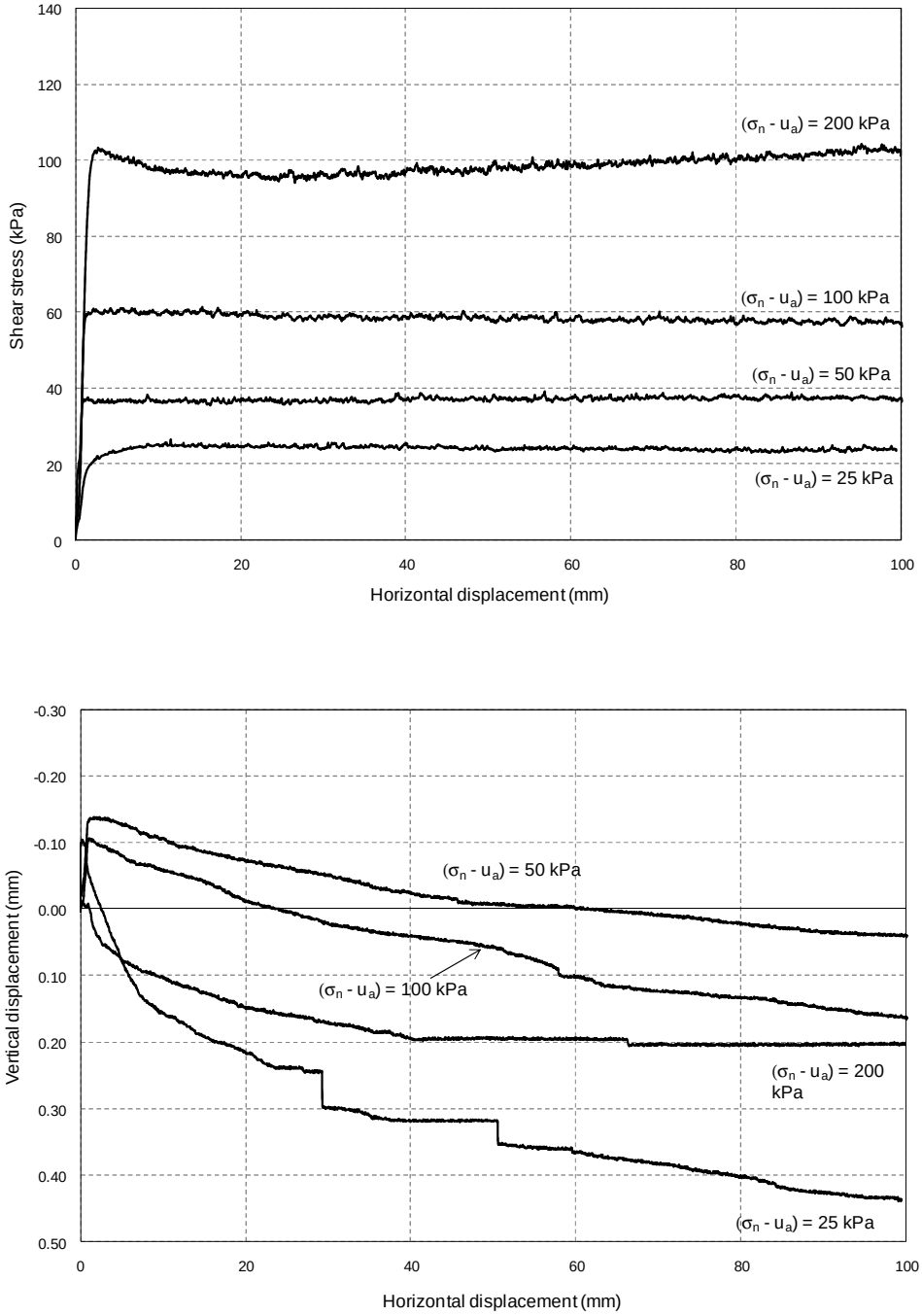

Figure 5-11 Results from multi-stage RS tests on SC-SM soil under s = 0 kPa, and $(\sigma_n - u_a)$ = 25, 50, 100 and 200 kPa.

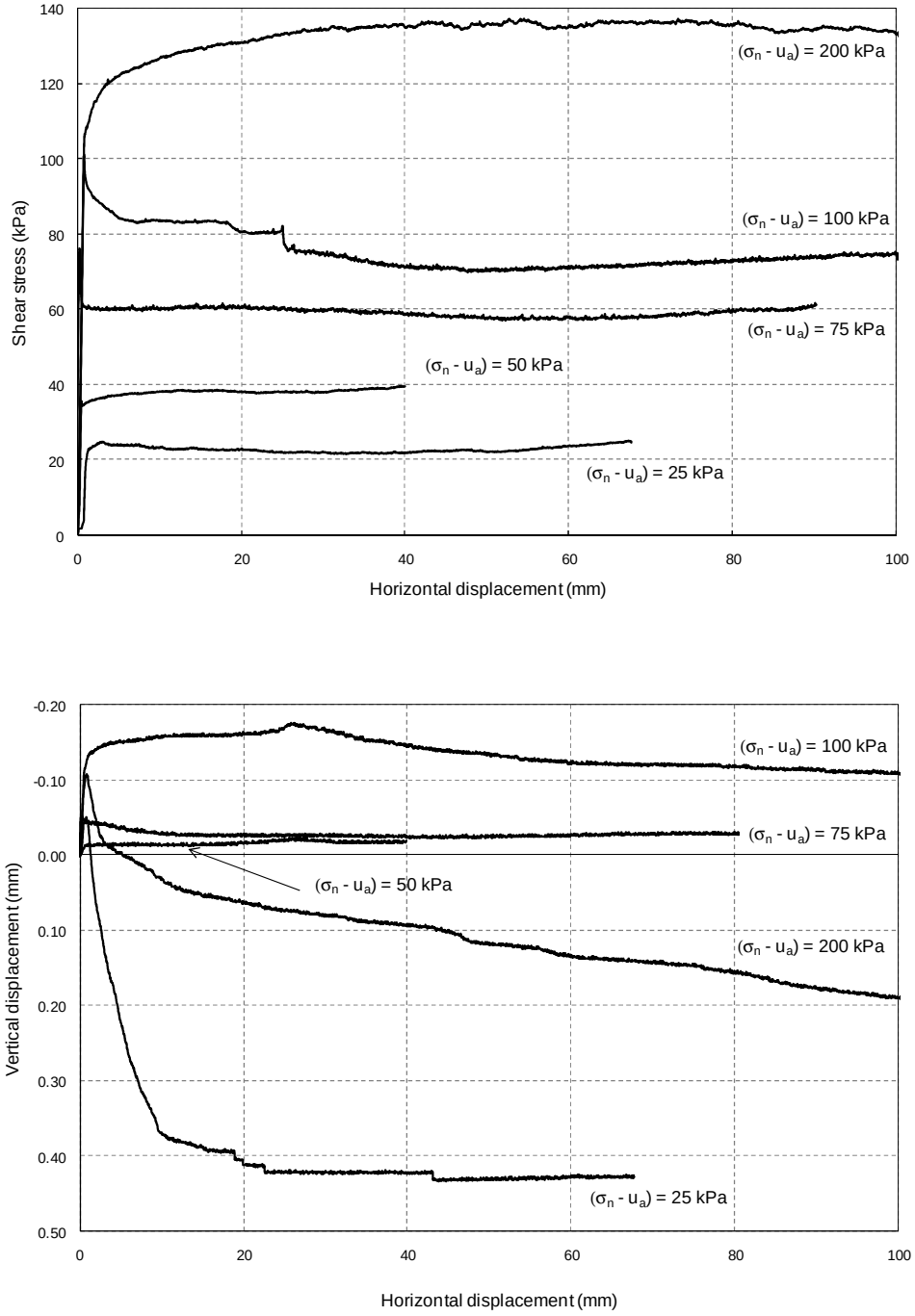

Figure 5-12 Results from multi-stage RS tests on CL soil under s = 0 kPa, and $(\sigma_n - u_a)$ = 25, 50, 75, 100 and 200 kPa.

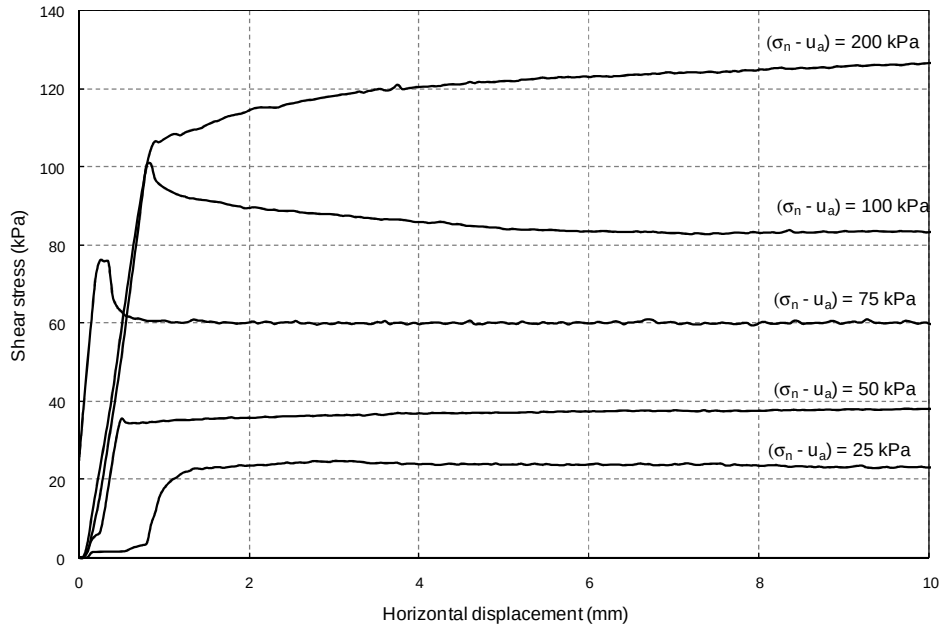

Figure 5-13 Shear stress at initial horizontal displacement from multi-stage RS tests on CL soil under s = 0 kPa, and $(\sigma_n - u_a)$ = 25, 50, 75, 100 and 200 kPa.

Saturated failure envelopes for SM, SC-SM and CL soil:

Figure 5-14 shows residual shear stress plotted against normal effective stress for the three soil testing SM, SC-SM and CL under fully saturated conditions. It has been recognized that for most clays the relation between residual strength and normal effective stress is nonlinear (Skempton 1985, Stark and Eid, 1997). However, for soils with low clay-size fraction (particle size <2μ = 45%), and soils with a liquid limit less than 60, the relatively spherical particles and/or stiff clay plates dominate the shear behavior (Stark and Eid, 1992). These particles are able to establish edge-to-face interaction even at the drained residual condition. Consequently, the initial contact area and the increase in contact area during shear are small, under any range of net normal stresses. This leads to an approximately linear drained residual failure envelope.

Therefore, considering that the test soils have a low clay-size fraction (CF less than 32%) the residual failure envelopes were approximated by a straight line, as shown in Figure 5.14. Saturated failure envelopes present R-squared values ranged between 0.9936 and 0.9999. As expected, SM shows the higher residual friction angle φ_r' = 30.28°. The residual friction angles for SC-SM and CL soils are 22.08° and 28.01°, respectively. The CL has a higher clay fraction and was initially expected to have a lower residual friction angle. Lupini et al. (1981) showed that the residual shear strength in the sliding mode of failure is strongly dependent on the mineralogy of the platy particles. In this case, SC-SM soil presents a large amount of platy mica, producing a more polished failure surface and, as a consequence, a lower residual friction angle.

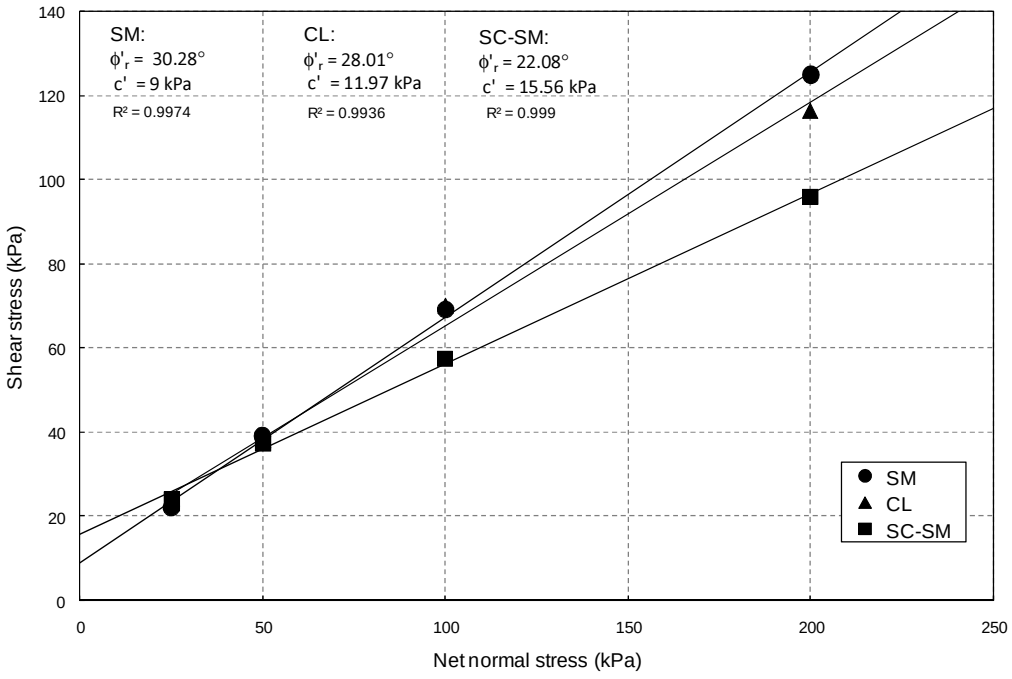

Figure 5-14 Residual failure envelopes for saturated SM, CL and SC-SM soils.

5.4.2 Residual Strength of Unsaturated SM Soil

Results from suction-controlled RS tests on SM soil at constant suction sates, s = 25, 50, 75 and 100 kPa, and net normal stress $(\sigma_n - u_a)$ = 25, 50, 75 or 100 kPa are shown in Figures 5-15, 5-16, 5-17 and 5-18, respectively. These results correspond to RS tests labeled as RS7, RS8, RS9 and RS10 in Table 5-1.

It can be readily observed that the residual shear strength increases with net normal stress, regardless of suction state. Also, matric suction exerts a significant effect on residual shear strength, with a considerable increase for s = 100 kPa. The relationship between vertical displacements as a function of horizontal displacement is also included in those figures.

Results were obtained following a multi-stage testing scheme, thus allowing determination of the peak shear strength only for the first shearing stage corresponding to a net normal stress of $(\sigma_n - u_a)$ = 25 kPa. Figure 5.19 shows the shear stress versus horizontal displacement for a net normal stress of $(\sigma_n - u_a)$ = 25 kPa at different levels of matric suction, s = 25, 50, 75 and 100 kPa (first shearing stage of multi-stage RS tests). The curves are plotted for the first 30 mm of horizontal displacement to better observe the behavior of the soil from peak to residual state. The sample volumetric change during shearing is also showed in that figure. It could be noticed that samples initially exhibit a peak shear stress, then reach a residual shear state and dilate toward a critical state after an initial compression at low horizontal displacements. Results evidence the enhancement of brittleness and dilatancy by suction increase during first shearing.It is worth noting that the term “peak shear strength” refers only to those peaks observed during the first shearing stage of a multi-stage RS test, like those observed in Figure 5-19. Any other “apparent” peak observed during a multi-stage RS test may be attributed to the effort required initially to reorient the particles in the direction of shearing altered by particle re-accommodation, particle crushing, and/or aging effects occurred during the first shearing, as suggested by Chandler (1977) and Carrubba and Del Frabbo (2008) for the

case of saturated materials. From Figures 5-15, 5-16, 5-17 and 5-18 it can be observed that the apparent peaks seem to be suppressed and the dilatancy reduced at larger net normal stresses and matric suction states.

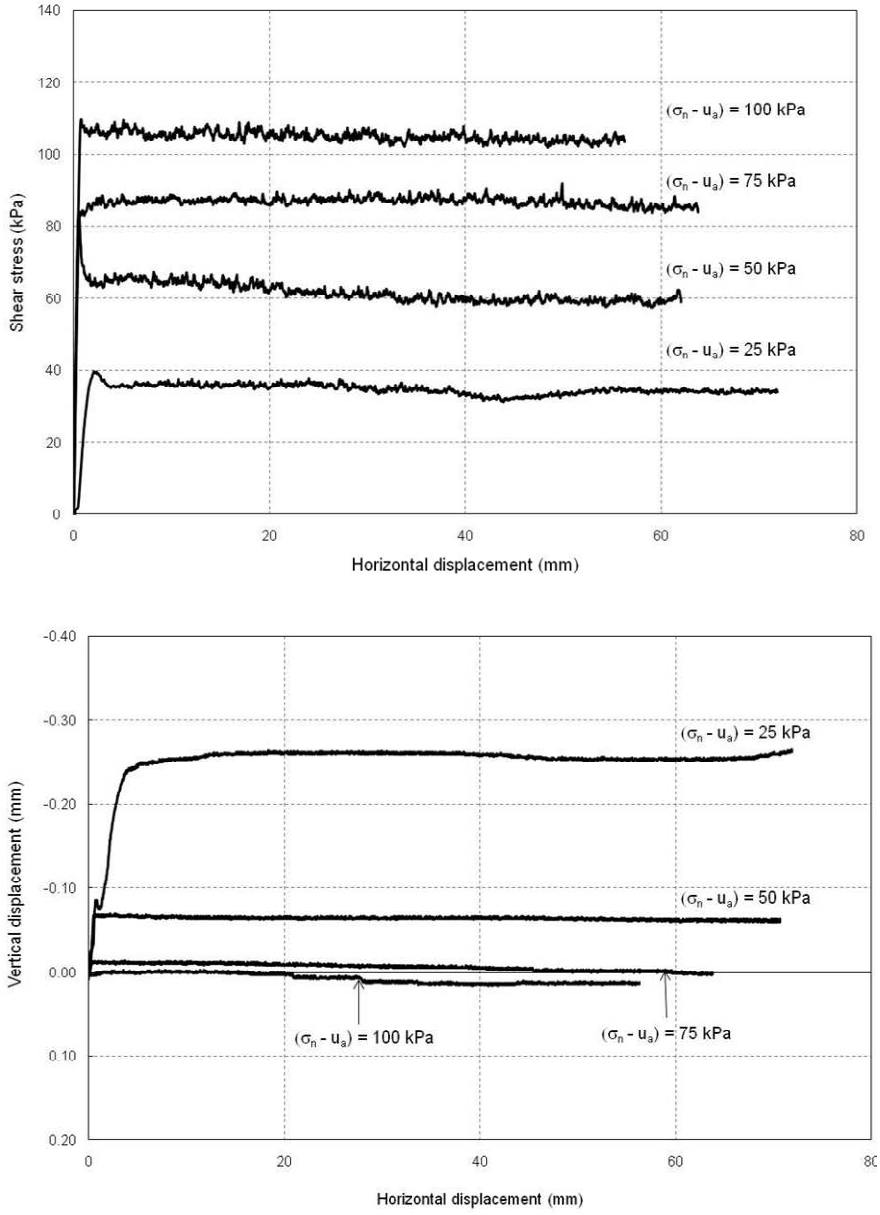

Figure 5-15 Results from multi-stage RS7 test on SM soil under s = 25 kPa, and $(\sigma_n - u_a)$ = 25, 50, 75, and 100kPa.

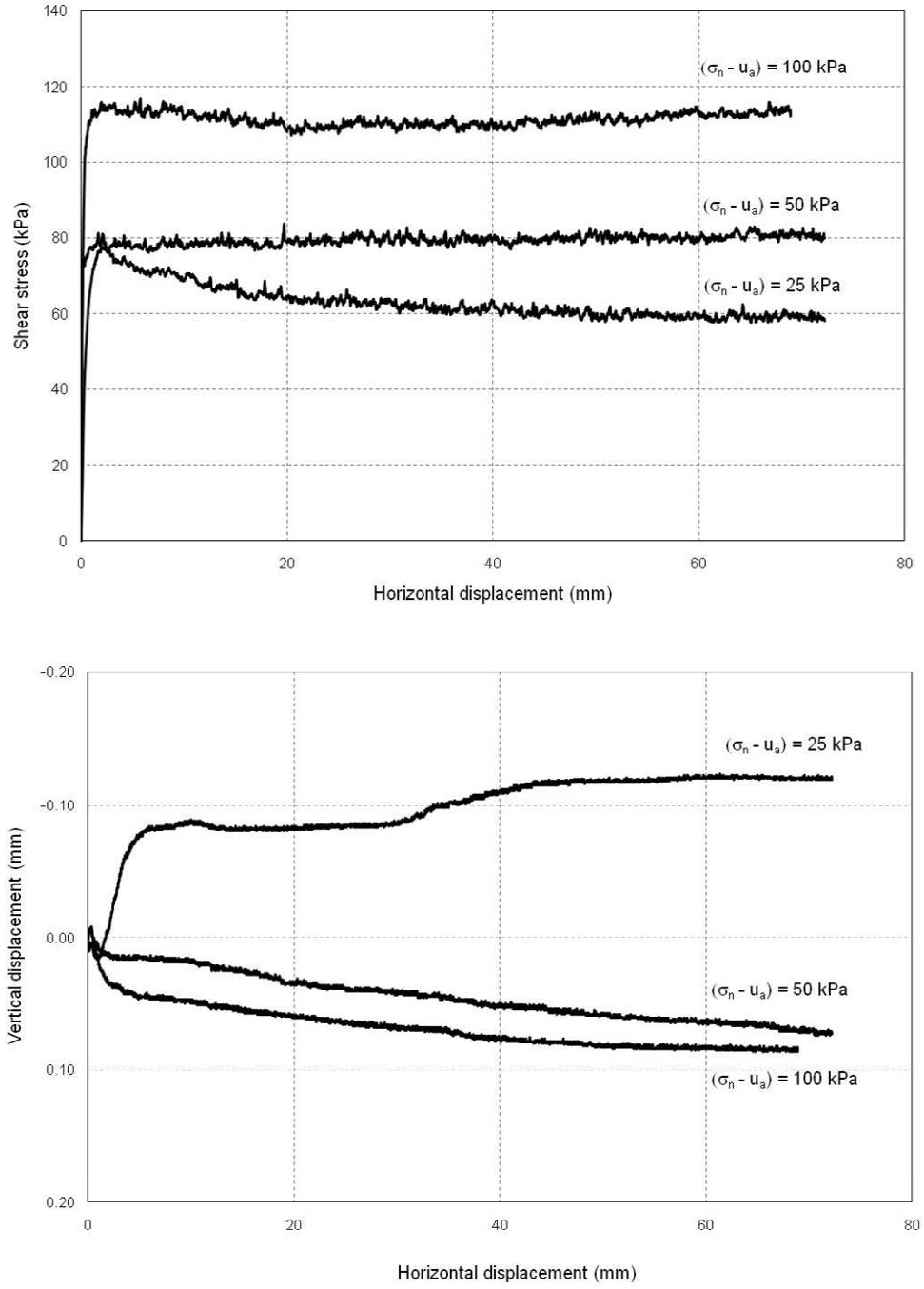

Figure 5-16 Results from multi-stage RS8 test on SM soil under s = 50 kPa, and $(\sigma_n - u_a)$ = 25, 50 and 100kPa.

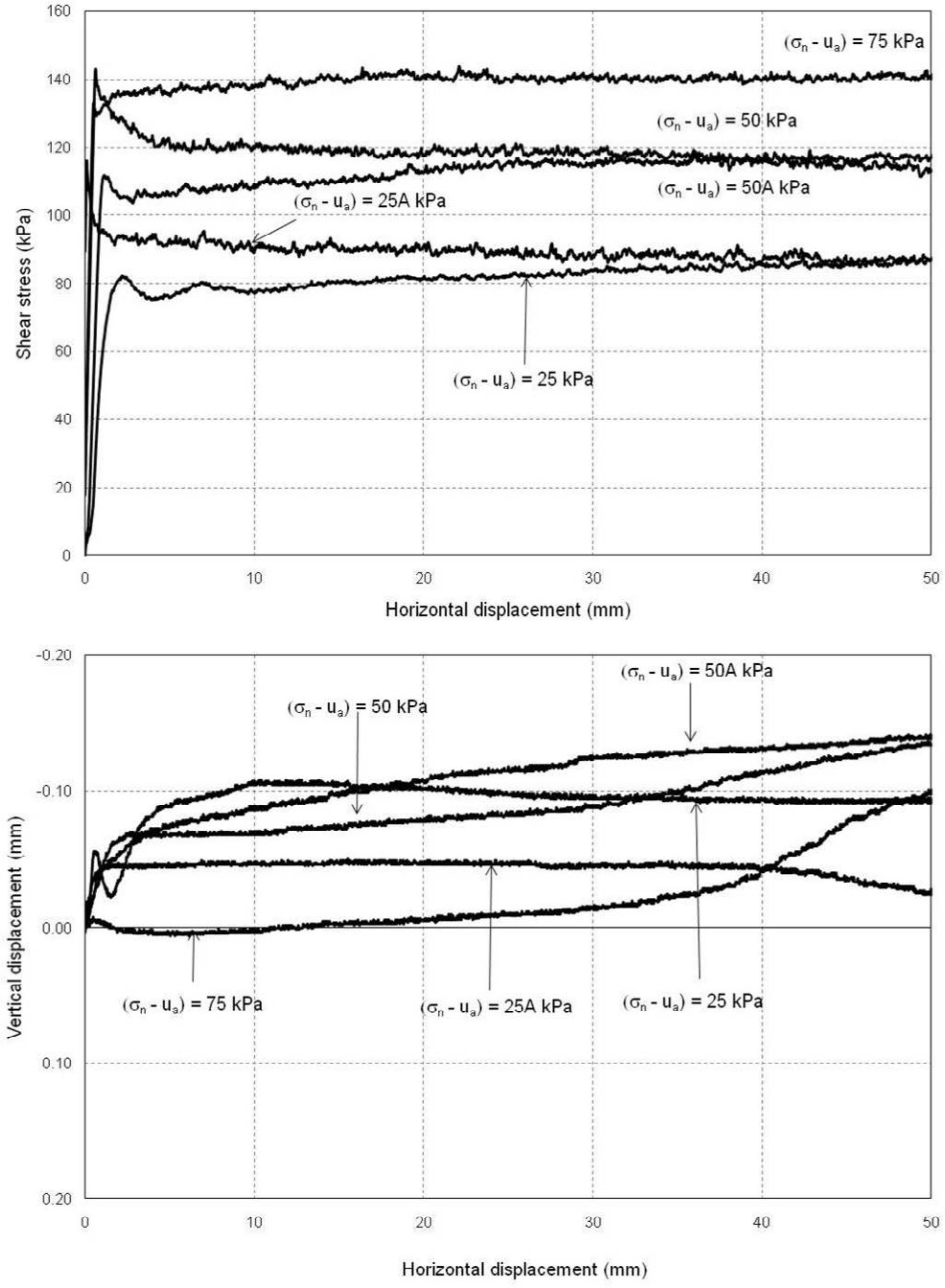

Figure 5-17 Results from multi-stage RS9 test on SM soil under s = 75 kPa, and $(\sigma_n - u_a)$ = 25, 50, 100, 50 and 25 kPa.

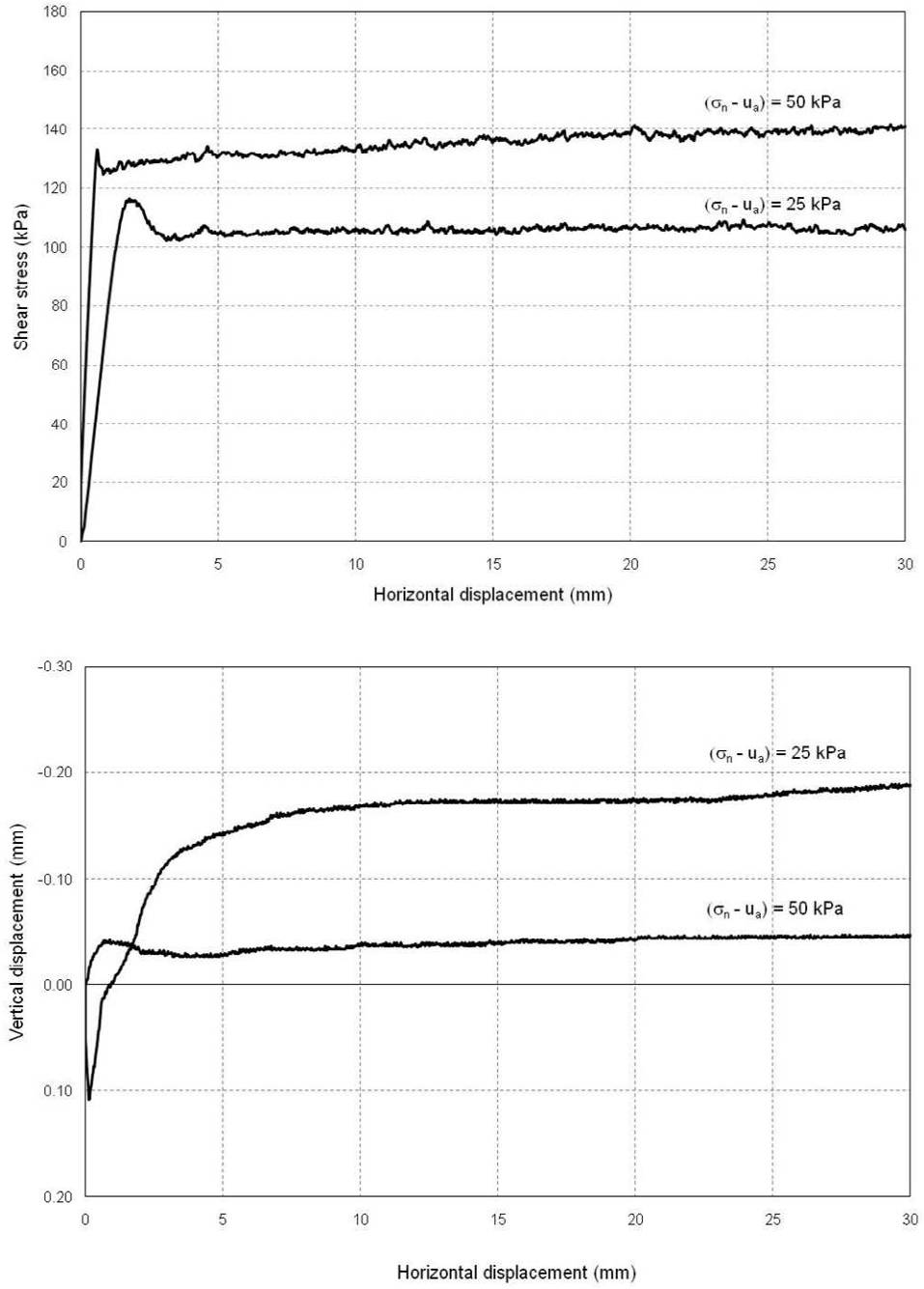

Figure 5-18 Results from multi-stage RS10 test on SM soil under s = 100 kPa, and $(\sigma_n - u_a)$ = 25 and 50 kPa.

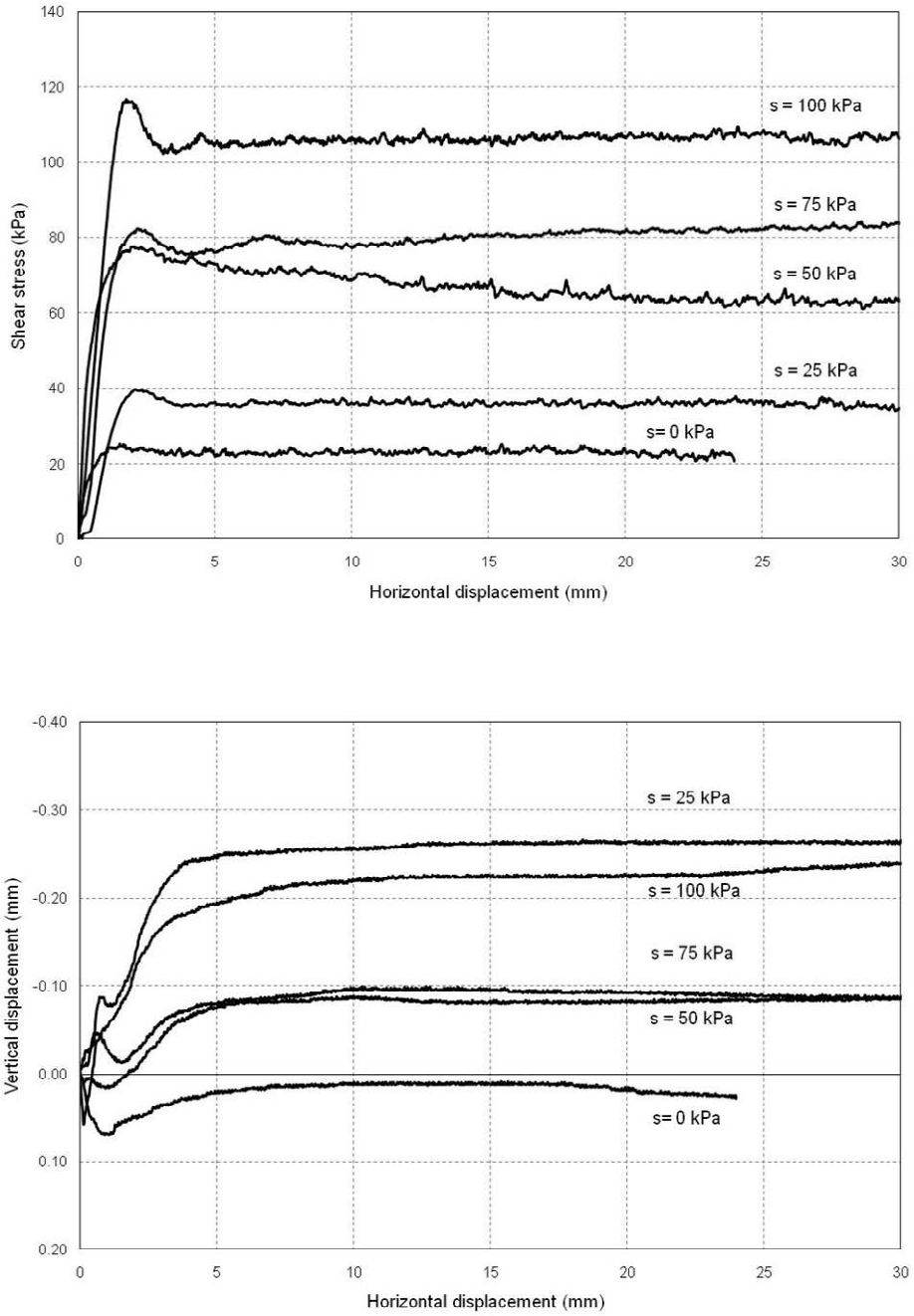

Figure 5-19 Results from single-stage RS6, RS7, RS8, RS9 and RS10 tests on SM soil under $(\sigma_n - u_a)$ = 25 kPa, and s = 0, 25, 50, 75 and 100 kPa.

As was observed previously for fully saturated samples, during multi-stage RS tests the fall to residual strength is also completed at smaller horizontal displacement after a first shearing stage. Figure 5-20 shows the initial shear strength response for SM at constant suction state s = 25 kPa under net normal stress $(\sigma_n - u_a)$ = 25, 50, 75 and 100 kPa during the first 10 mm of horizontal shear displacement. As it is expected, the residual strength increases with the net normal stress (σ_n).

Results, in general, show a noticeable influence of net normal stress and matric suction on the residual shear strength and volumetric behavior of statically compacted SM soil specimens.

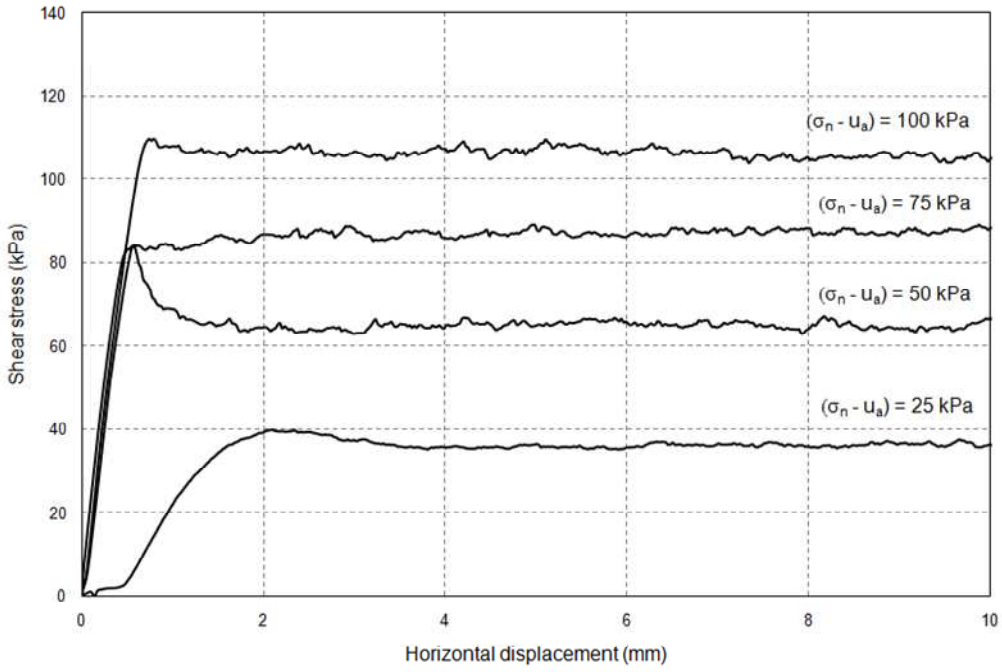

Figure 5-20 Shear stress at initial horizontal displacement from multi-stage RS tests on SM soil under s = 25 kPa, and $(\sigma_n - u_a)$ = 25, 50, 75, and 100 kPa.

Shearing stress history:

Figure 5-17 includes results of two additional shearing stages at normal effective stress $(\sigma_n - u_a)$ = 50 and 25 kPa after sample had been subjected to an unloading path at constant suction state s = 75 kPa. Results demonstrate that the unloading stress path yields residual strength results that are in reasonably good agreement with those from a sample with any or small shearing history. In the same way, results from multi-stage RS7 test at net normal stress of 75 kPa, were compared with those from a single-stage RS4 test (chapter 4) sheared under net normal stress, $(\sigma_n - u_a)$ = 75 kPa, and the same constant suction state, s = 25 kPa (Figure 5-21).

It can be noticed that when shearing is applied on a pre-sheared sample, the dilatant and peak shear strength response of the material disappear. However, the value of residual shear strength measured on pre-sheared sample is close to that obtained at the end of first shearing under the same net normal stress and matric suction. Results confirm the conclusions from other researchers that the unsaturated residual shear strength at a given suction depends only on the applied net normal stress and not on the initial structure or shearing history of the material (Vaunat et al., 2006).

The slightly higher values of residual strength from the sample sheared following a loading path can be attributed to possible wall-friction effects between the upper and bottom annular platens. It can be noticed that the wall friction reduces as the number of shearing stages increase. After an unloading stress path, the soil becomes stiffer, exhibiting a small peak stress and dilatancy as the horizontal displacement increases, even though the sample has been subjected to a large shearing history and a failure surface has already been developed.

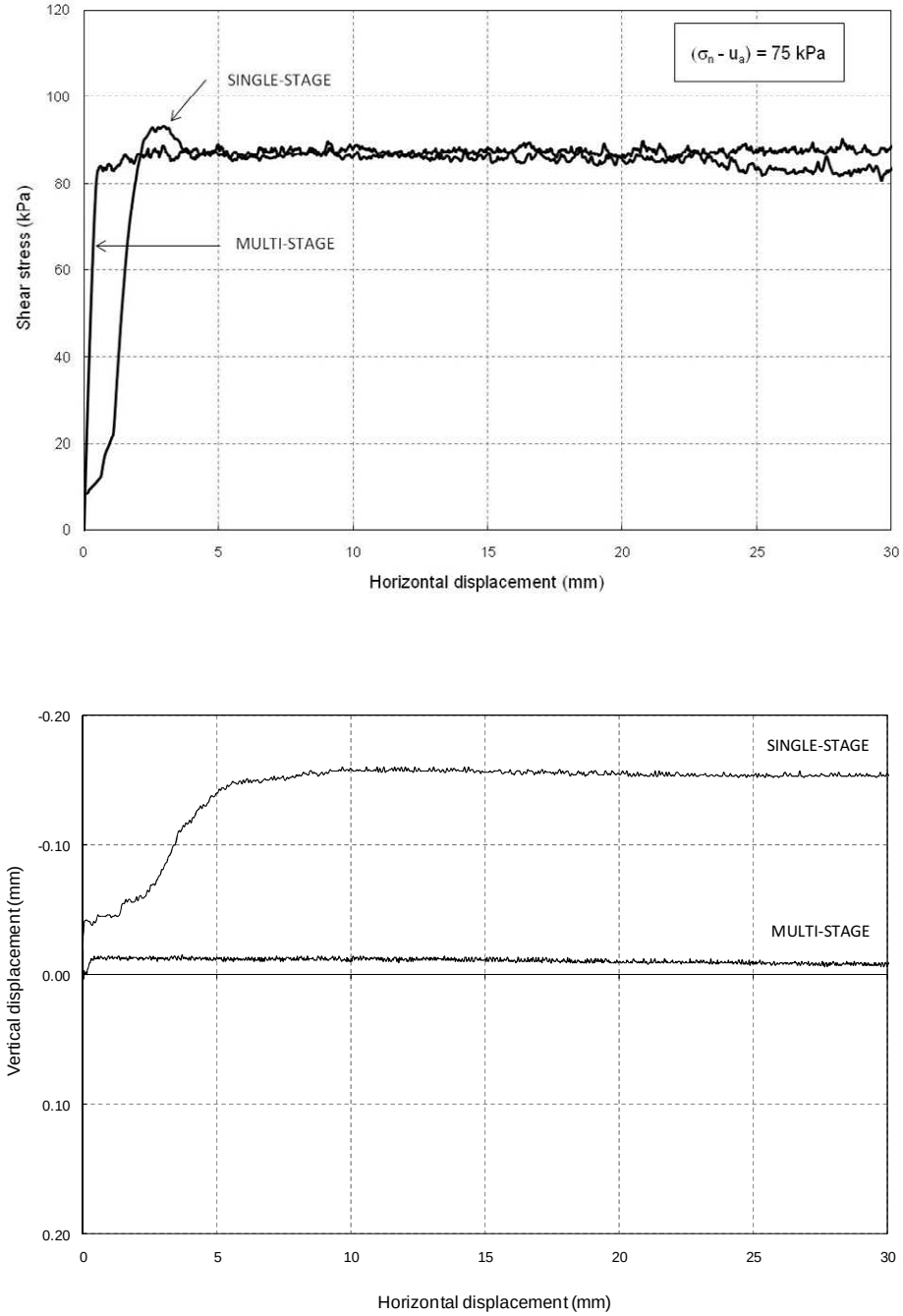

Figure 5-21 Results from single-stage RS4 and multi-stage RS7 tests on SM soil under $(\sigma_n - u_a)$ = 75 kPa, and s = 25 kPa.

Suction stress history:

Results from suction-controlled RS11 test under net normal stress, $(\sigma_n - u_a)$ = 25 kPa, and matric suction states, s = 25, 50, 75, and 100 kPa, are shown in Figure 5-22. As it is expected, both the apparent peak and residual shear strengths are significantly influenced by the level of matric suction, with a considerable increase in both values for s = 100 kPa. SM soil also seems to exhibit a more brittle-like behavior with increasing suction: at higher suction, there is a more appreciable difference between peak and residual shear strength.

As was explained, since all suction-controlled RS tests conducted in this research work were performed following a multi-stage testing scheme, results from the first shearing at a net normal stress of $(\sigma_n - u_a)$ = 25 kPa can be considered as single-stage tests. Therefore, in order to determine the effect of suction history on residual shear stress of SM soil, results from the first shearing stage of RS15, RS16, RS17 and RS18 tests conducted at net normal stress, $(\sigma_n - u_a)$ = 25 kPa, and constant matric suction states, s = 25, 50, 75, and 100 kPa (Figure 5.19) were compared with the results from the multi-stage RS11 previously described. Results are compared in Figure 5-23 in terms of residual shear stress at different matric suction values. It cab observed that when shearing is applied on a pre-sheared sample, the dilatant and peak shear strength responses of the material are reasonably the same.

These results confirm that residual strength is reasonably independent of the original soil structure or stress-suction history experienced by the soil, as reported by Vaunat et al. (2006, 2007) for unsaturated soils. Results also evidence that the drying process stiffens the pre-existing soil structure, which is also supported by the increase on dilatancy of the material. In addition, the effect of matric suction on the residual strength of compacted SM is larger than the effect of net normal stress given that the peak and dilatant behavior apparently are not deleted with the suction-stress history, as was observed for the effect of net normal stress. An increase in dilatancy with suction was also observed by Vaunat et al. (2006).

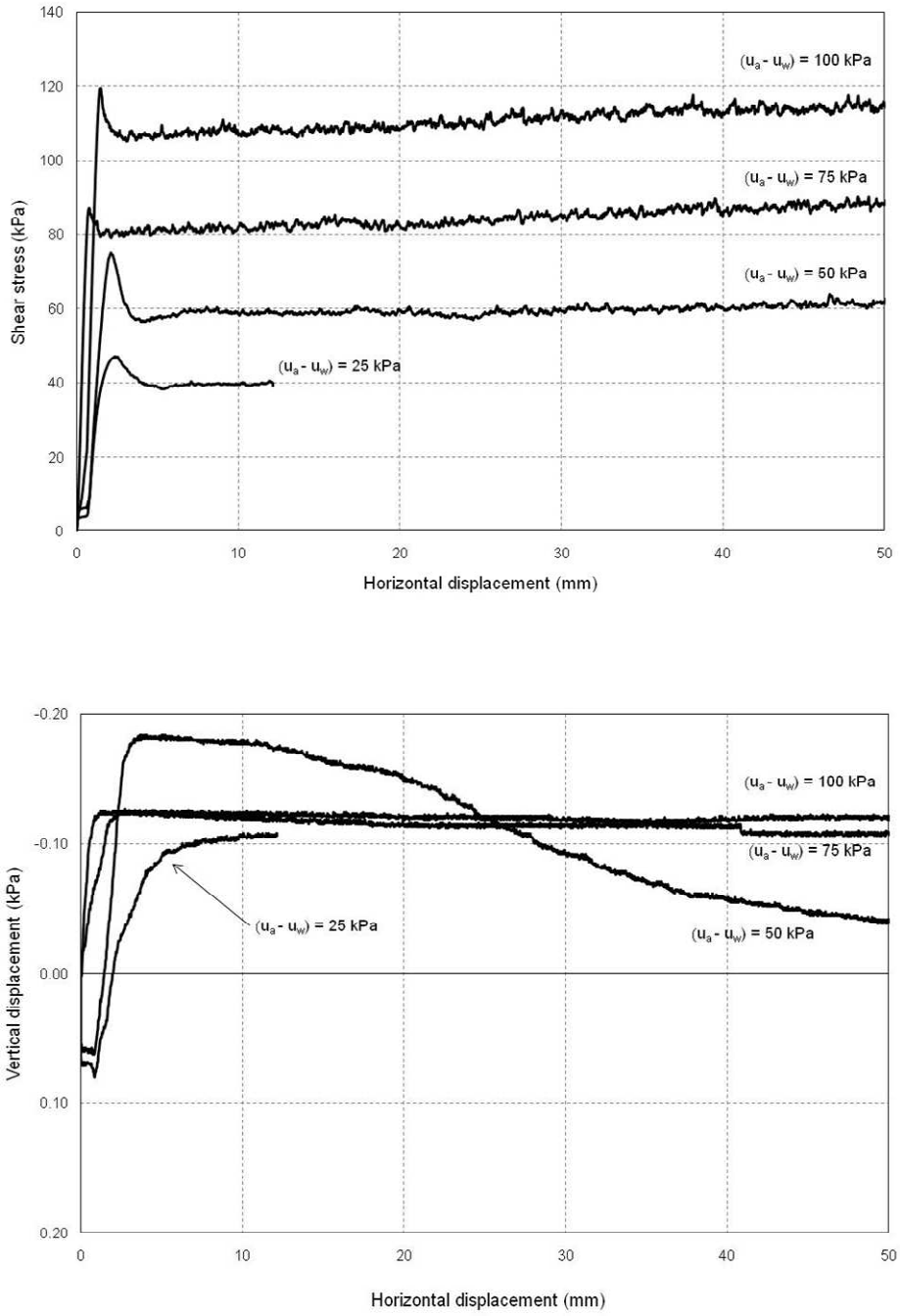

Figure 5-22 Results from multi-stage RS11 test on SM soil under $(\sigma_n - u_a)$ = 25 kPa, and s = 25, 50, 75 and 100 kPa.

Results from suction-controlled RS9 test at net normal stress, $(\sigma_n - u_a)$ = 25 kPa, and matric suction state, s = 100 kPa, correspond to a sample with a large stress and suction history. They are compared with results from RS10 test conducted under the same net normal stress and matric suction but following a single-stage testing scheme. They are represented in Figure 5-24 as rhombus symbols. Results show that residual shear strength following different testing schemes and suction history fall very close to a 45-degree line. Data lying on the 45 degree line would have perfect correlation. Results from Figure 5-23 are also shown as square symbols in this figure and confirm the conclusion previously drawn.

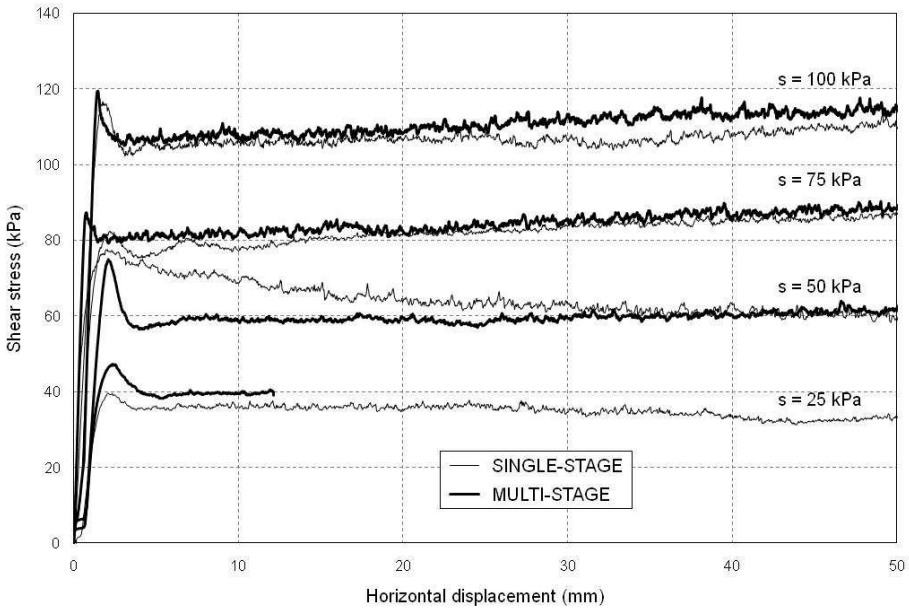

Figure 5-23 Comparison between single-stage and multi-stage tests on SM soil under $(\sigma_n - u_a)$ = 25 kPa, and s = 25, 50, 75 and 100 kPa.

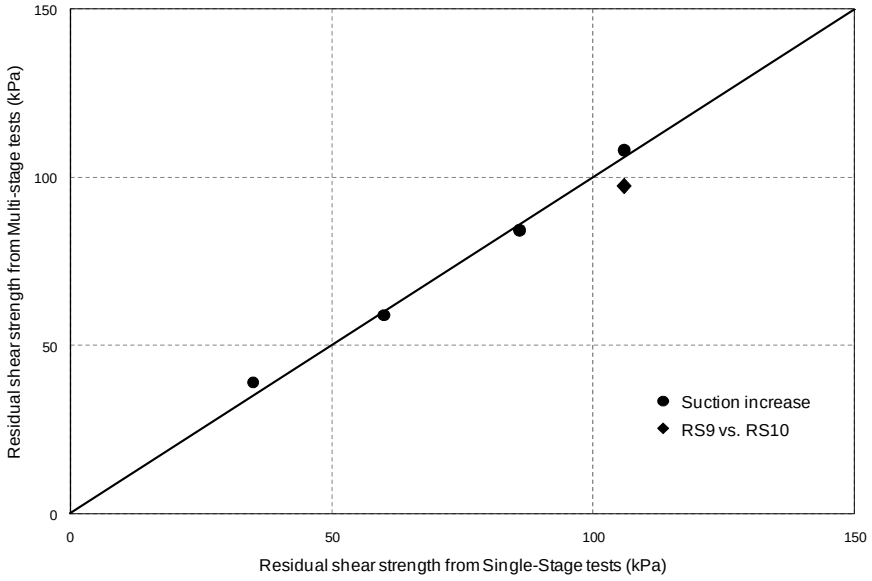

Figure 5-24 Comparison of residual shear strength from single-stage and multi-stage schemes for SM soil.

5.4.3 Residual Strength of Unsaturated SC-SM Soil

Results from suction-controlled RS tests on SC-SM soil at constant suction sates, s = 25, 50 and 100 kPa, are shown in Figures 5-25, 5-26 and 5-27, respectively. These results correspond to the RS tests labeled as RS14, RS15 and RS16 in Table 5-2. It can be readily observed that the residual shear strength increases with net normal stress, regardless of suction state. Also, matric suction exerts a significant effect on residual shear strength, with a considerable increase for s = 100 kPa. Figures also include the relationship between vertical deformations as a function of horizontal displacement during shearing.

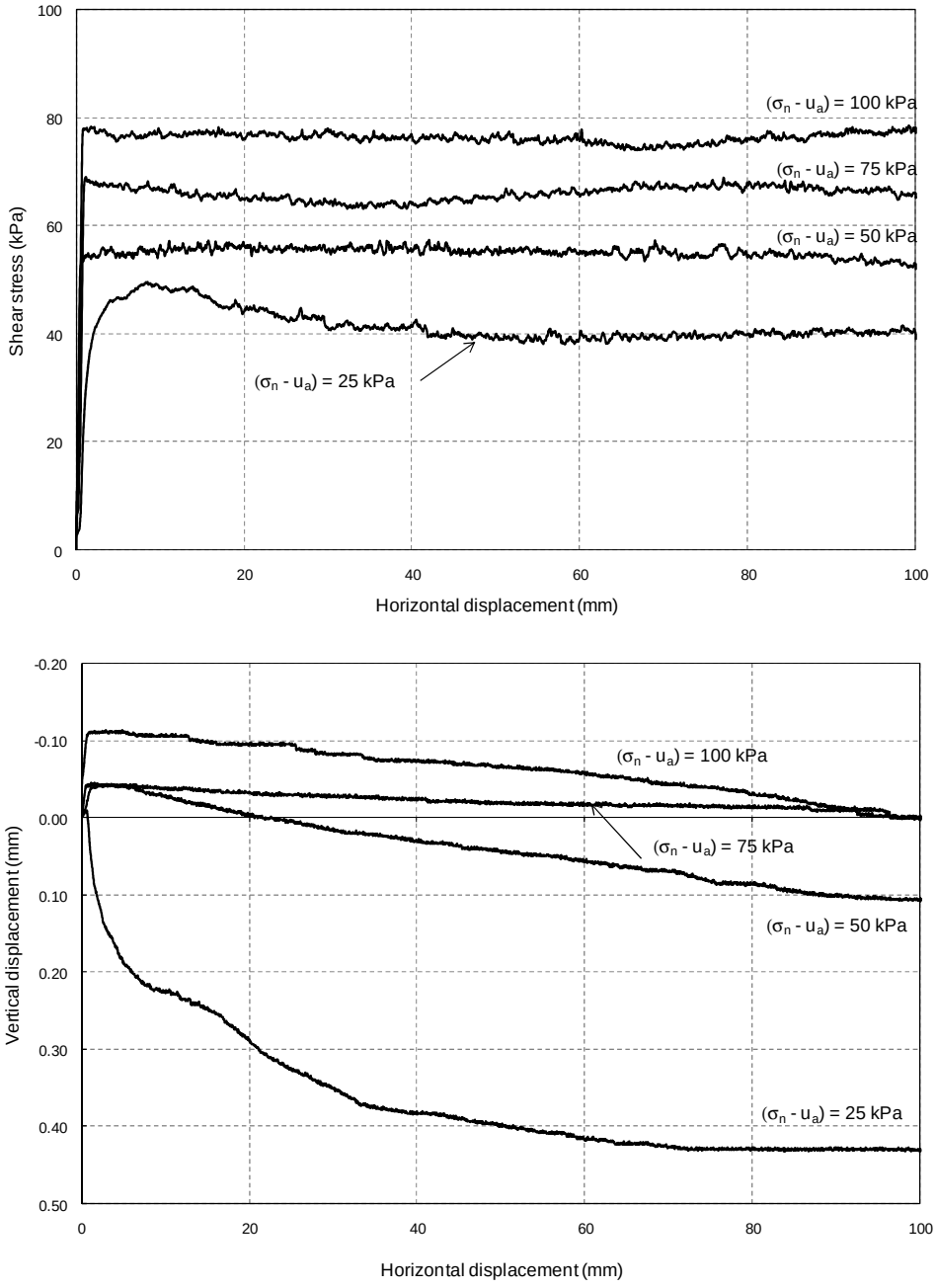

Figure 5-25 Results from multi-stage RS14 test on SC-SM soil under s = 25 kPa, and $(\sigma_n - u_a)$ = 25, 50, 75 and 100 kPa.

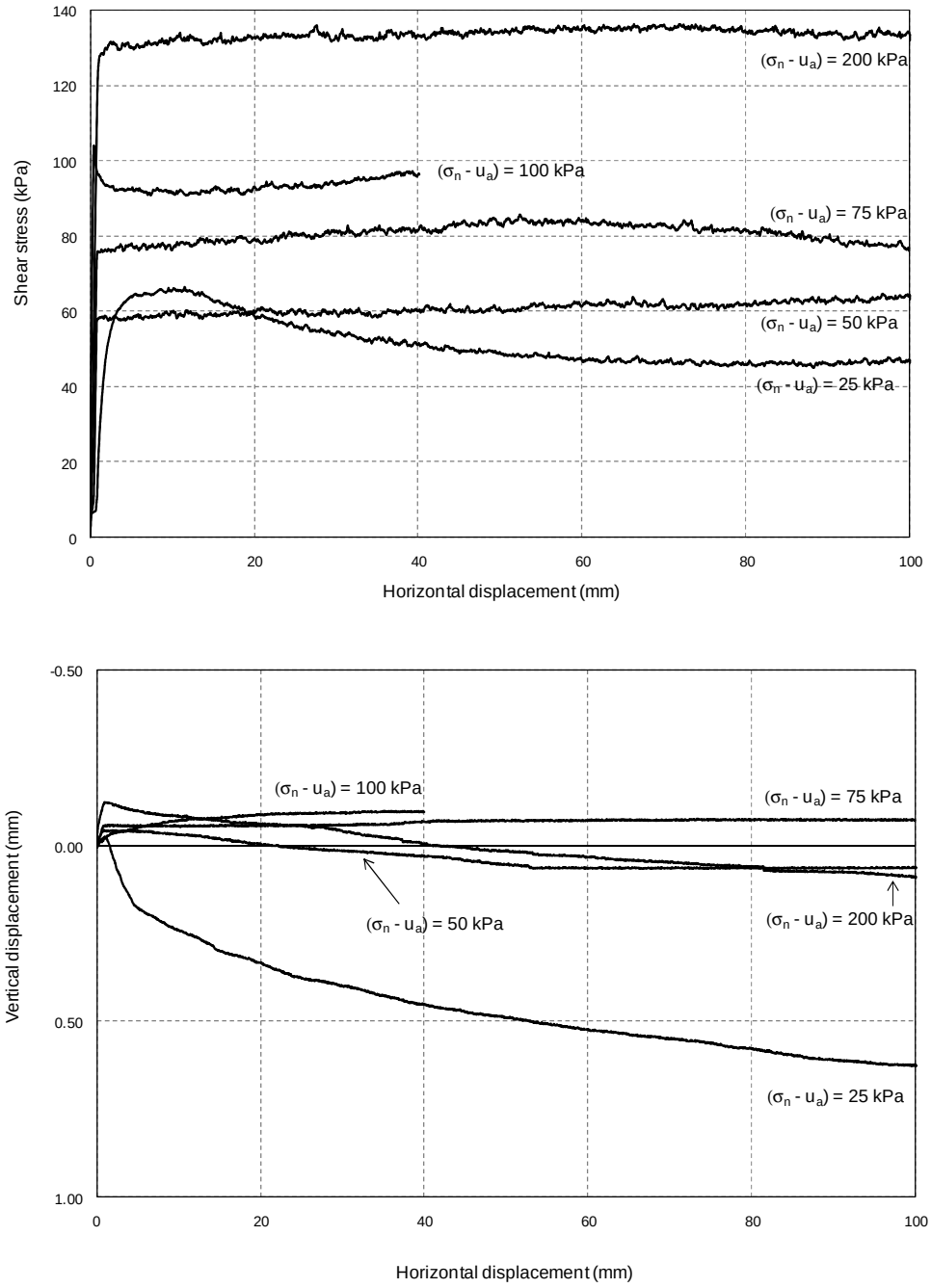

Figure 5-26 Results from multi-stage RS15 test on SC-SM soil under s = 50 kPa, and $(\sigma_n - u_a)$ = 25, 50, 75, 100 and 200 kPa.

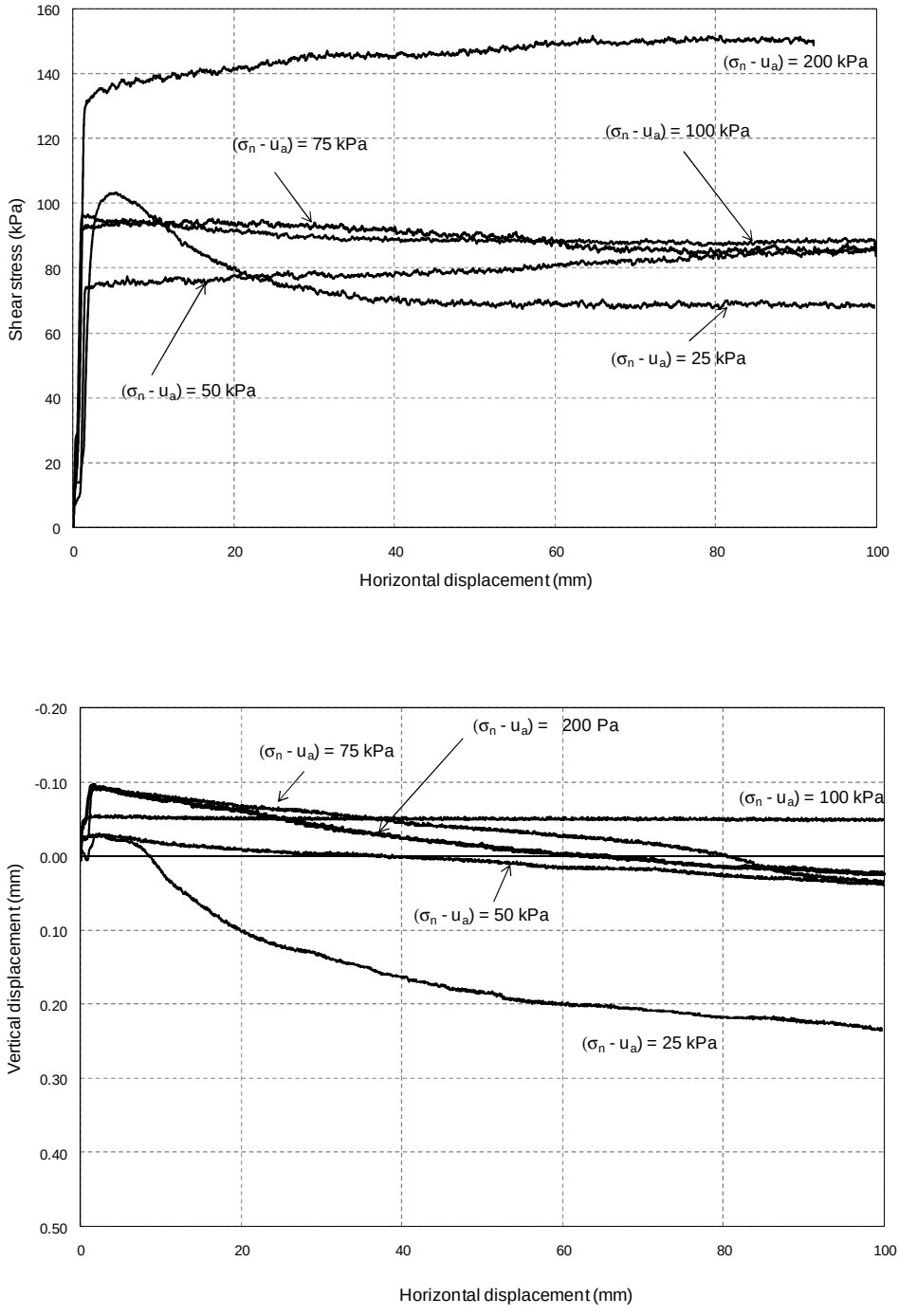

Figure 5-27 Results from multi-stage RS16 test on SC-SM soil under s = 100 kPa, and $(\sigma_n - u_a)$ = 25, 50, 75 and 100 kPa.

The shear stress versus horizontal displacement curves for the first shearing stage from multi-stage RS tests are shown in Figure 5.28. Samples show an increase in shear stress reaching a peak value and then show a gradual decrease in shear stress with increasing horizontal displacement until the residual shear state is attained. As is expected, the maximum residual shear stress increases with suction. The critical state is reached at horizontal displacement nearly to 60 mm for lower matric suctions and beyond to 100 mm for higher suctions. It can be noticed that as suction increases, samples with any suction or shearing history initially exhibit vertical deformations of dilatancy followed by compression. Compression is reduced at a higher net normal stress of 100 kPa.

The peak and residual failure envelopes projected onto the residual shear stress versus matric suction plane for the first shearing at net normal stress of 25 kPa are shown in Figure 5.29. It can be noticed that the peak shear strength and the difference with residual shear strength increase with suction. Such an increase is interpreted as being due to a process of particle aggregation during drying, which makes the material essentially more granular at higher suctions. This interpretation has been reinforced by observations about the increase of dilatancy of the material for a suction of 100 kPa, indicating that suction has a significant effect of increasing the dilatation of SC-SM soil. This behavior was also observed for unsaturated peak strength states by Zhan and Ng (2006), and Hossain and Yin (2010).

From Figures 5-25, 5-26 and 5-27, it can be noticed, that, in most cases, the amount of dilatancy increases with suction and net normal stress after the first shearing stage. At large net normal stresses the peak shear stress is suppressed and the amount of dilatancy reduced. Overall, residual shear stress and volumetric behavior of compacted SM-SC soil depend on the magnitude of suction and net normal stress.

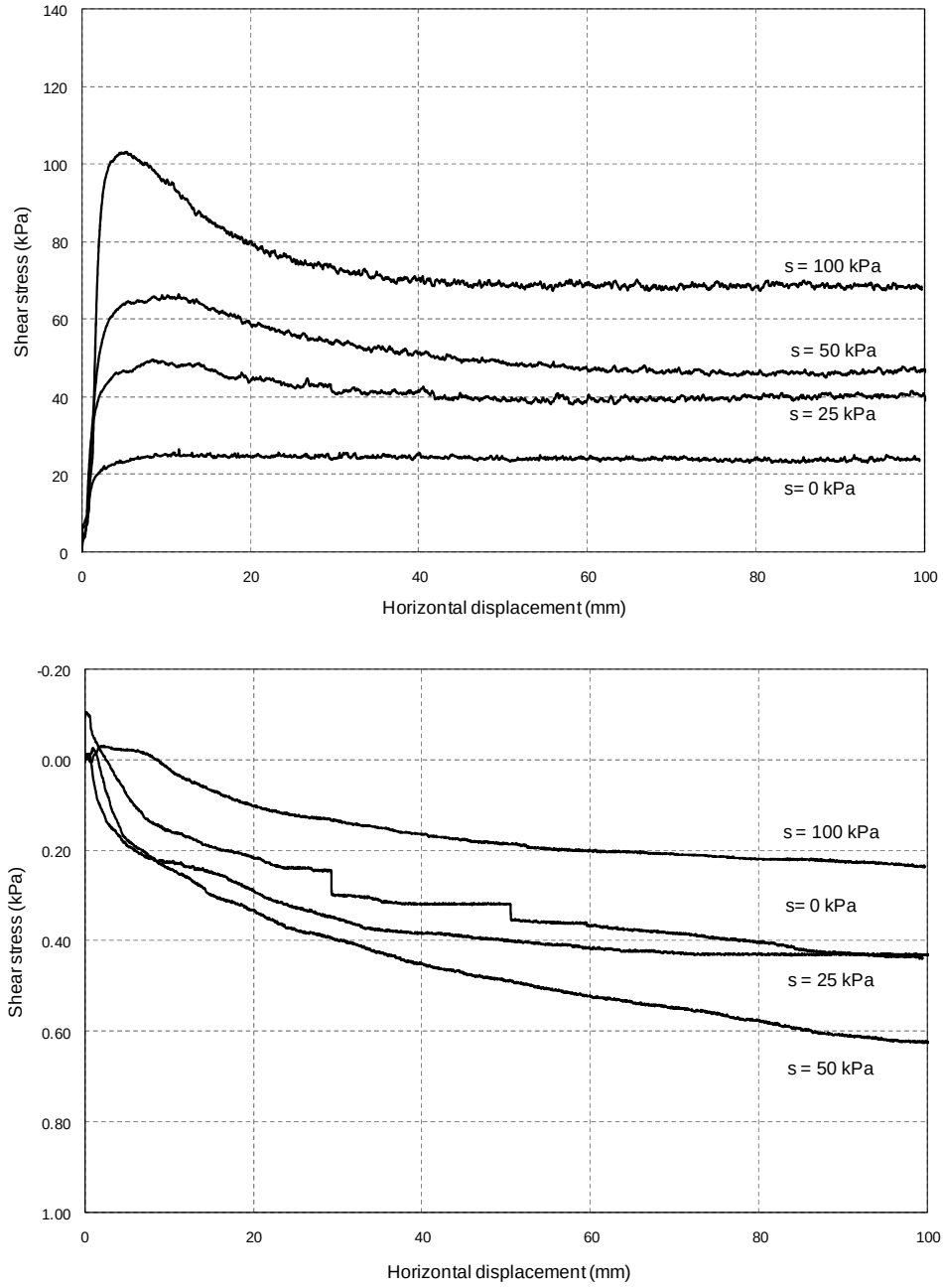

Figure 5-28 Results from single-stage RS13, RS14, RS15 and RS16 tests on SC-SM soil under $(\sigma_n - u_a)$ = 25 kPa, and s = 0, 25, 50, and 100 kPa.

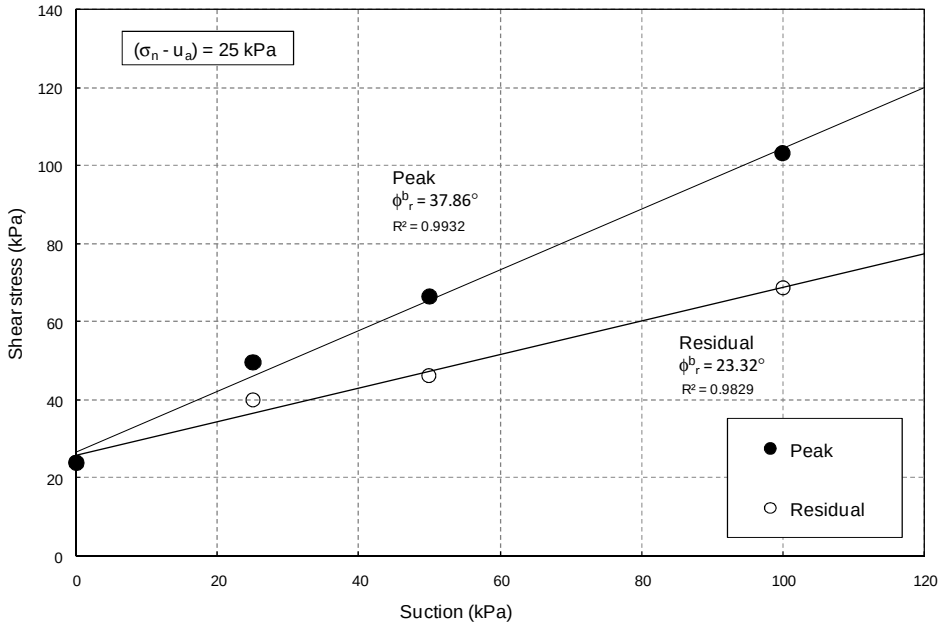

Figure 5-29 Peak and residual failure envelopes for compacted SC-SM soil under $(\sigma_n - u_a)$ = 25 kPa.

5.4.4 Residual Strength of Unsaturated CL Soil

The unsaturated soil behavior of CL soil over a large range of shear deformations could not be studied in this research work since the capacity of the torque sensor of the novel RS was not enough to capture the peak and residual shear stress of the soil under suction-controlled states. Two suction-controlled RS tests, RS21 and RS22, were conducted on CL soil at matric suction of s = 300 kPa and net normal stress of $(\sigma_n - u_a)$ 25 kPa. Although the results were inconclusive the data will be presented and discussed.

RS21 corresponds to a sample prepared with a water content equivalent to an initial suction state of 300 kPa according to the soil-water characteristic curve (SWCC) shown in Figure 4-13. Sample was compacted and sheared following the procedure described in Chapter 4. After complete equalization of pore fluids under a constant pore-air pressure, the shearing stage was initiated. Shear stress showed a rapid increase exceeding the maximum capacity of the torque sensor before allowing the sample to reach a peak value and, as a consequence, a residual shear state. Hence, RS21 test could not be finished.

A second sample RS22 was then prepared, but this time the sample was first soaked in distilled water in the main RS cell and sheared under fully saturated conditions at a constant normal stress $(\sigma_n - u_a)$ = 25 kPa. Once the residual shear state was reached under fully saturated conditions, shearing was stopped and pore-air pressure (u_a) was then increased until achieving a matric suction of 300 kPa. The external normal stress was adjusted accordingly to keep a constant net normal stress, $(\sigma_n - u_a)$ = 25 kPa. After initial consolidation and equalization of the pore fluids a second shearing stage was initiated.

Results from RS22 test are shown in Figure 5-30. It can be noticed that the shear stress of CL under a constant s = 300 kPa increases again beyond the maximum capacity of the sensor and any peak or residual stress data could not be registered. The expectation was to be able to

measure a peak and residual shear stress value because a failure surface was previously developed under saturated conditions.

Results show a clear influence of matric suction on the shear resistance of compacted CL even though the increase on suction was just slightly higher than the air-entry value of this material.

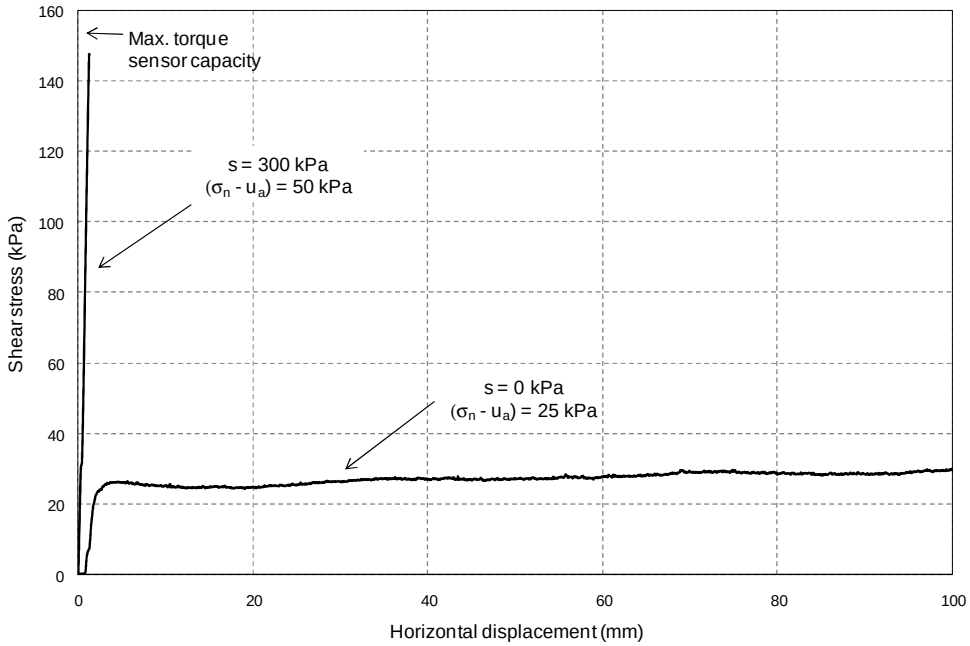

Figure 5-30 Results from multi-stage RS22 test on CL soil under $(\sigma_n - u_a)$ = 25 kPa and, s = 0 and 300 kPa.

Next chapter presents a thorough regression analysis and discussion of experimental results from all suction-controlled ring shear tests performed on silty sand and silty clayey sand soils. Results from this work are also compared to those previously reported for similar soils.

CHAPTER 6

ANALYSIS OF TEST RESULTS

6.1 Introduction

Assessment of residual strength parameters of unsaturated soils at relatively low net normal stresses and matric suction states is of critical importance since most rainfall induced slope failures are shallow and occur at relatively high degrees of saturation.

In this chapter the results from suction-controlled RS tests are discussed in detail. The influence of matric suction and net normal stress on the residual strength of unsaturated SM and SC-SM are analyzed. A three-dimensional, non-linear regression analysis is used to describe the variation of the residual shear strength with matric suction and net normal stress. Based on the results, the stress-strain behavior of SM and SC-SM soils are shown in terms of net normal stress and suction. Results from this work are compared to those previously reported in the literature.

6.2 Residual Failure Envelopes

Unsaturated Silty Sand (SM):

Figure 6-1 shows the effect of matric suction on both the position and slope of unsaturated residual failure envelopes for compacted SM soil. In this figure, experimental data points represent residual strength values obtained from multi-stage suction-controlled RS tests as described in chapter 5. It can be observed that matric suction exerts a critical influence on the final position of the residual failure envelope, with a considerably higher position for s = 100 kPa.

Likewise, suction shows a significant influence on the residual apparent cohesion, with a value of close to 9 kPa in the saturated state (s = 0).

For the range of matric suction measured in the suction-controlled RS tests, the increase in residual strength with increasing net normal stress appears to be linear. In the present work, the average coefficient of determination, R^2, for the linear envelopes shown in Figures 6-1, including s = 0 kPa, ranged between 0.994 and 1.0. It can be observed that the residual failure envelopes are essentially parallel. However, both the residual apparent cohesion, c'_r and the residual friction angle, φ'_r , increase with suction.

Figure 6-2 shows the variation of residual friction angle as well as residual cohesion intercept with suction. The non-linear variation of residual friction angle with suction is evident. Most of the increase in friction angle occurs between suction 0 and 25 kPa. Afterwards, the effect of suction on φ'_r becomes significantly smaller and tends to an asymptotic value for suction close to 75 kPa, very close to the residual suction state according to the SWCC. Such increase can be associated to an increase in stiffness of the material during drying. This explanation is reinforced by observations about the dilatancy of the material during the first shearing, as shown in Figure 5-19. This is also verified by the difference in peak and residual failure envelopes shown in Figure 6-3 for a net normal stress of 25 kPa.

On the other hand, the variations of the residual cohesion intercept with suction exhibit a different behavior. It can be noticed that the residual cohesion intercept does not increase significantly so much in the range of 0 to 25 kPa, but drastically increases with higher suctions, as shown in Figure 6-2. The increase in the cohesion intercept indicates an increase in residual strength as matric suction increases. The variation of residual cohesion intercept with suction appears to be linear for suctions greater than 25 kPa, having a coefficient of determination of 0.984.

This suggests that the increase in residual shear stress with suction is mainly due to an increase in capillary cohesion rather than to an increase in the residual friction angle, which appears to be constant at larger matric suctions.

Evidence of an increase in friction angle with increasing suction has been reported by other authors, including Salman (1975), via triaxial testing; Feuerharmel et al. (2006), Zhan and Ng (2006), Hossain and Yin (2010) via direct shear testing; and on the residual friction angle by Vaunat et al. (2007) via ring shear testing.

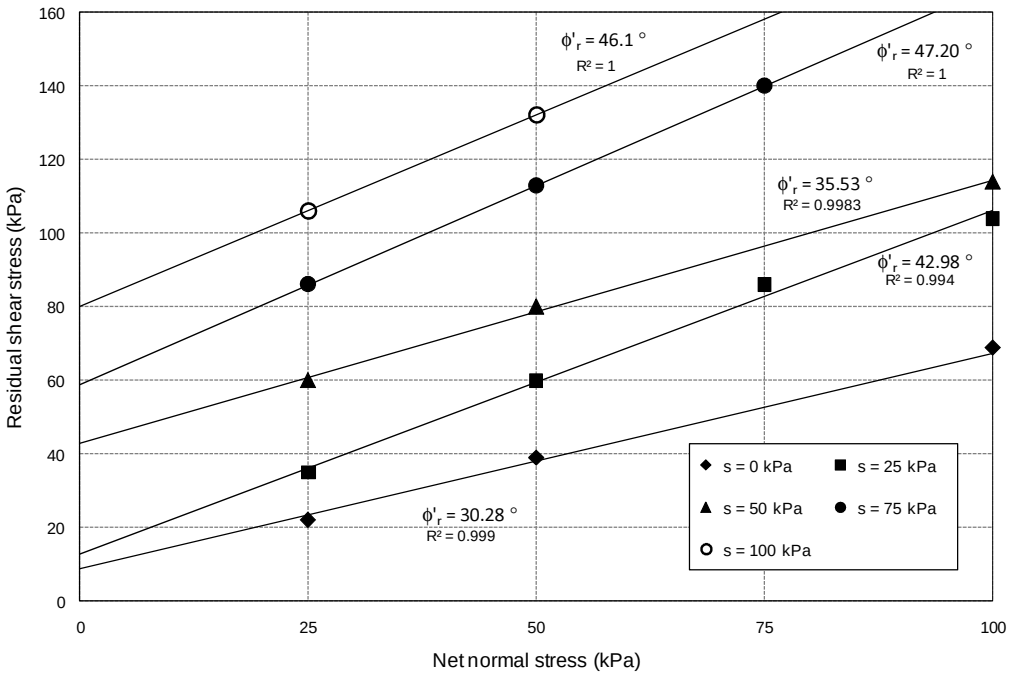

Figure 6-1 Effect of matric suction state on residual failure envelopes of compacted SM soil.

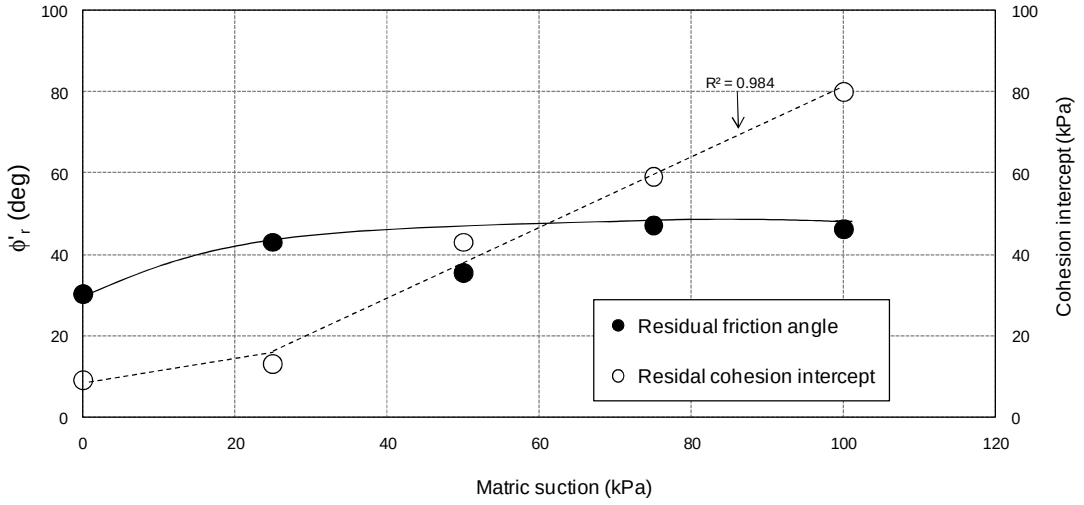

Figure 6-2 Variation of the residual friction angle and residual cohesion intercept with suction of compacted SM soil.

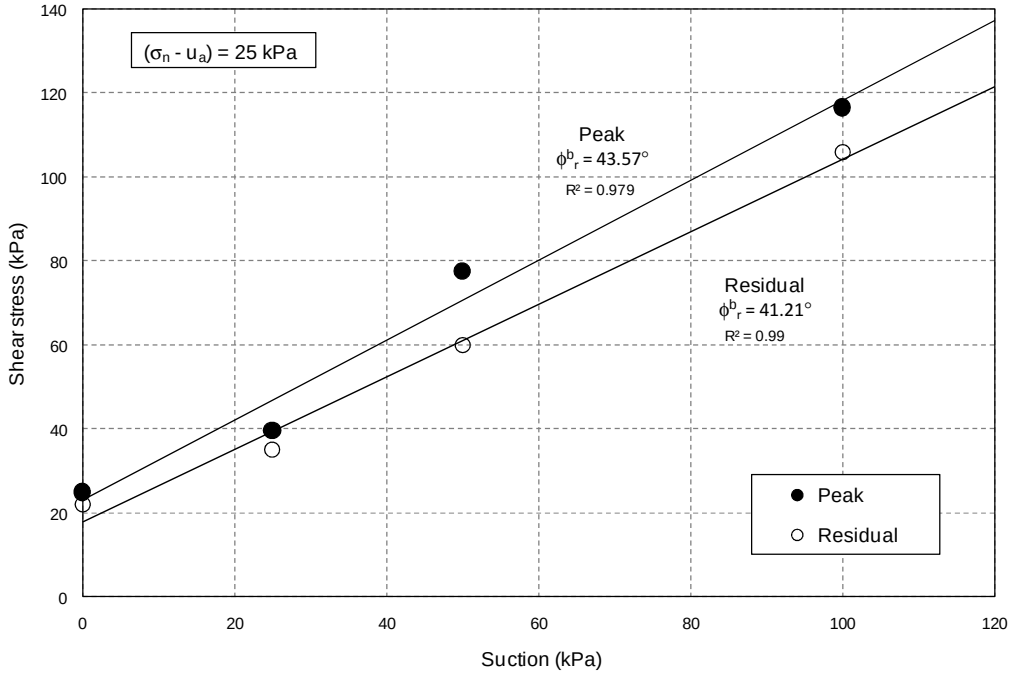

Figure 6-3 Effect of matric suction state on peak and residual failure envelopes at net normal stress constant of 25 kPa of compacted SM soil.

Figure 6-4 shows the effect of net normal stress on both the position and slope of residual failure envelopes projected onto the residual shear stress versus matric suction plane for compacted SM soil. For the range of matric suction measured in the suction-controlled RS tests, the increase in residual strength with increasing suction appears to be linear. Residual failure envelopes present R-squared values ranged between 0.906 and 1.00. It can be observed that the residual failure envelopes are also essentially parallel and that φ_r^b tends to increase with net normal stress. However, further RS tests at higher suctions are recommended to more fully characterize the entire failure envelope, and verify if φ_r^b really yields a linear function with respect to matric suction.

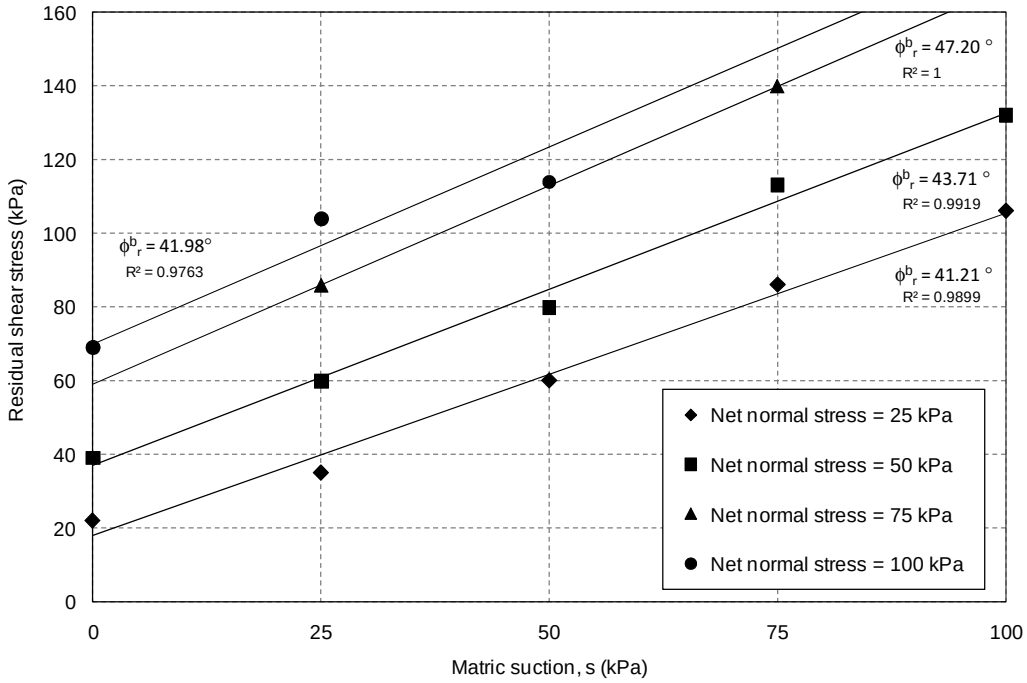

Figure 6-4 Effect of net normal stress on residual failure envelopes of compacted SM.

The variation of φ_r^b with net normal stress is shown in Figure 6-5. It can be noticed that φ_r^b increases with net normal stress and then becomes smaller for net normal stress close to

100 kPa. It is worth nothing that φ_r^b increases with suction as shown in Figure 6-4. This trend was also observed for the variation of residual friction angle φ_r' when it is compared with φ_r^b , but this time as a function of suction (Figure 6.6). Data are represented as circular symbols in that figure.

Data show that for the range of suction and net normal stresses used in this work, φ_r' is slightly larger than φ_r^b. It suggests that the effect of suction and net normal stress on the residual strength of compacted SM is practically equivalent for the range of stresses analyzed. In other words, an increase in suction at a given net normal stress is equivalent to a decrease of the same magnitude on the net normal stress. Likewise, a decrease in suction at a given net normal stress is equivalent to an increase of the same magnitude in the net normal stress. For example, the residual shear stress of a sample having a suction = 25 kPa and net normal stress = 100 kPa is equivalent to the residual shear stress of a sample with a suction = 100 kPa and a net normal stress of 25 kPa (see Figure 5-15 and Figure 5-18). More experimental evidence, however, on compacted SM soil at larger suction and net normal stresses is necessary in order to validate this interpretation.

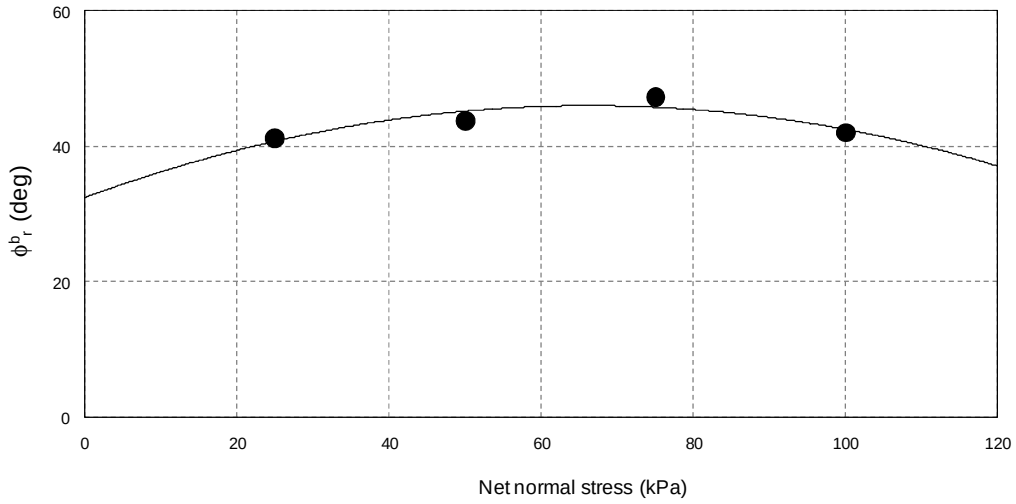

Figure 6-5 Variation of φ_r^b with net normal stress of compacted SM soil.

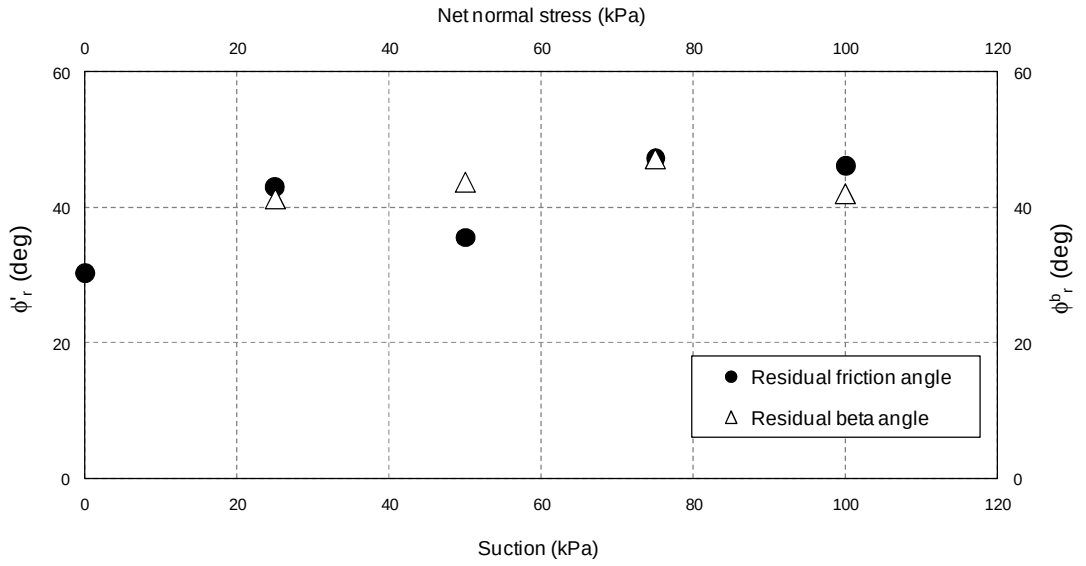

Figure 6-6 Variation of φ_r' and φ_r^b with suction and net normal stress for SM soil.

All of these preliminary observations suggest that a residual shear strength framework, similar to that postulated for peak shear strength (Fredlund and Rahardjo 1993) could eventually be devised for the range of suction states measured in this research work for unsaturated SM soil. Therefore an essentially planar failure envelope can be plotted when the residual shear strength is plotted with respect to the independent stress state variables, namely, matric suction and net normal stress.

The residual failure surface in three-dimensional stress space is shown in Figure 6.7. The computational software program Mathematica.6 was utilized to model the pattern of residual shear strength change with net normal stress and matric suction by producing a best-fitting surface to the experimental data. Then, using a multiple linear regression model, the best fitted regression equation of the generated surface was obtained as follows:

$$\tau_r = -3.61612 + 0.8262(\sigma - u_a) + 0.9174(u_a - u_w) \qquad (6.1)$$

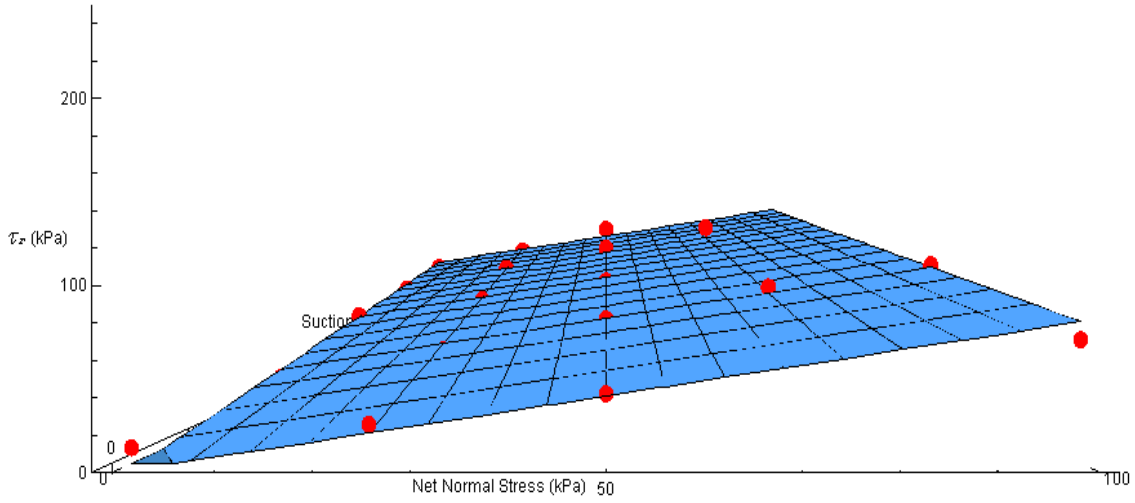

Figure 6-7 Residual failure surface for compacted SM.

The proposed fitted regression equation provided an excellent fit to the experimental data, with a coefficient of correlation of about 0.951. Experimental data are shown in Figure 6.7 as dots, highlighting the good agreement between them and the proposed surface.

Unsaturated Clayey Silty Sand (SC-SM):

A plot of the residual shear stress versus net normal stress for clayey silty sand (SC-SM) at different levels of matric suction is shown in Figure 6-8. The data were obtained from multi-

stage suction-controlled RS tests described in chapter 5. It can be observed that the residual shear strength increases as applied matric suction increases. For the range of matric suction and net normal stresses measured in the RS testing series, the parallel trend of the failure envelopes at various levels of matric suction is more evident, suggesting that the increase in strength with increasing suction also appears to be linear.

Figure 6-9 shows the variation of residual friction angle as well as residual cohesion intercept with suction for SC-SM soil. The non-linear variation of residual friction angle with suction, as was observed for compacted SM, is slightly perceptible. The increase in friction angle occurs gradually between 0 and 50 kPa. Afterwards, the effect of suction on φ_r' becomes smaller. The increase in φ_r' with suction seems to be related to an increase in the dilatancy of the material with suction.

The non-linearity of the variation of φ_r' with suction is confirmed by the shear-horizontal displacement curves shown in Figure 5-28, and peak and residual failure envelopes shown in Figure 6-10 for the first shear of samples sheared at a constant net normal stress = 25 kPa and matric states of 0, 25, 50 and 100 kPa. The difference between the failure shear stress and residual shear stress envelopes increases with suction.

In contrast, the residual cohesion intercept appears to increase linearly with suction having a coefficient of determination of 0.9864. The variation of the residual cohesion intercept for SC-SM (Figure 6-9) shows similar behavior to that of the compacted SM (Figure 6-2). However, a non-linear behavior of the residual cohesion intercept could be expected at higher suction, as was observed by other researchers for peak states (Futai and Almeida, 2005). Therefore, more experimental data are necessary at higher suction to validate the linearity or non-linearity of residual cohesion intercept under different suction states.

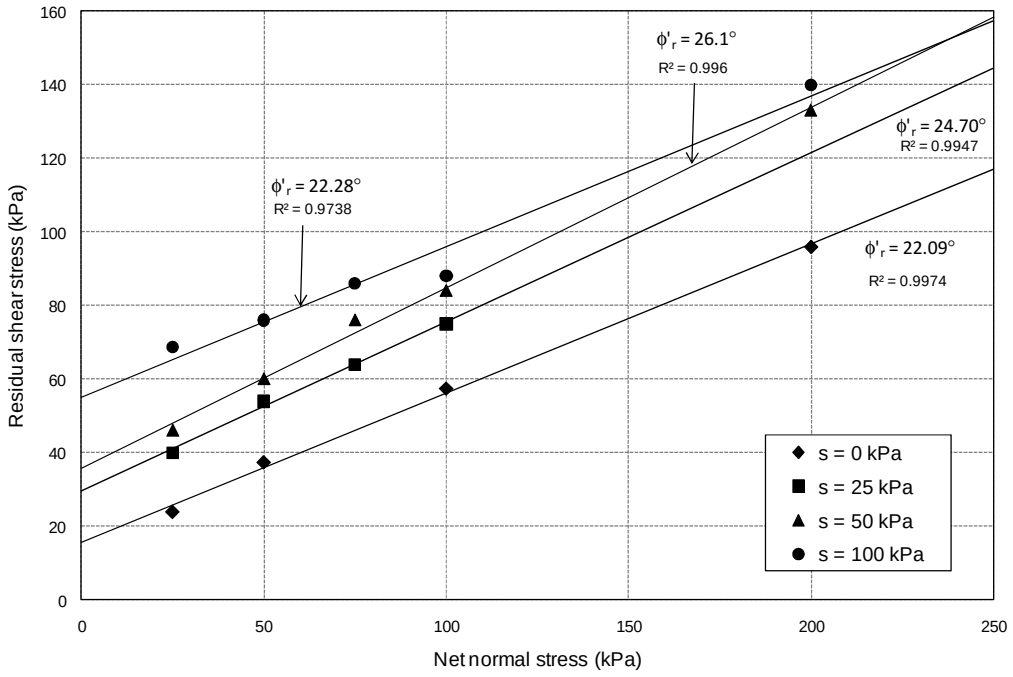

Figure 6-8 Effect of matric suction state on residual failure envelopes of compacted SC-SM soil.

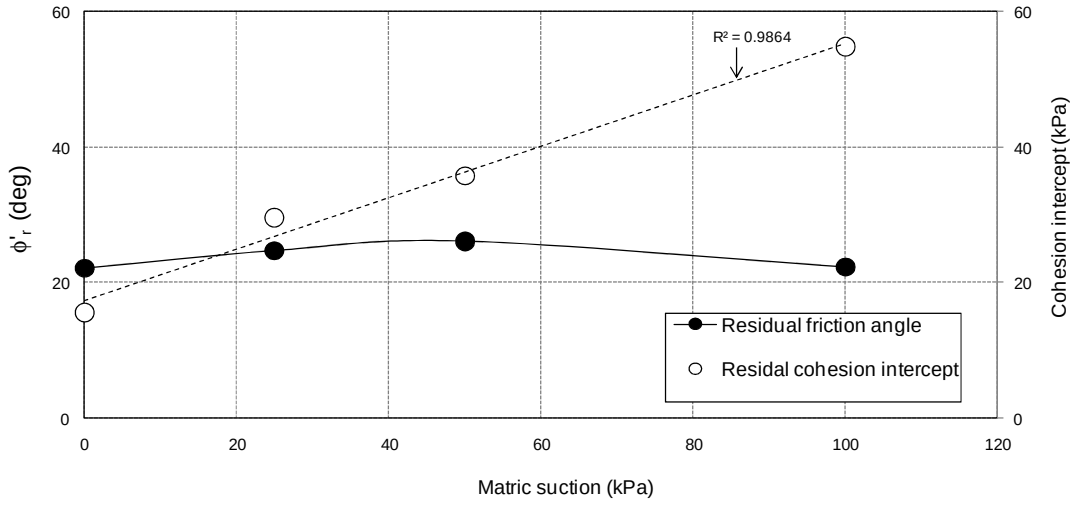

Figure 6-9 Variation of the residual friction angle and residual apparent cohesion with suction of compacted SC-SM soil.

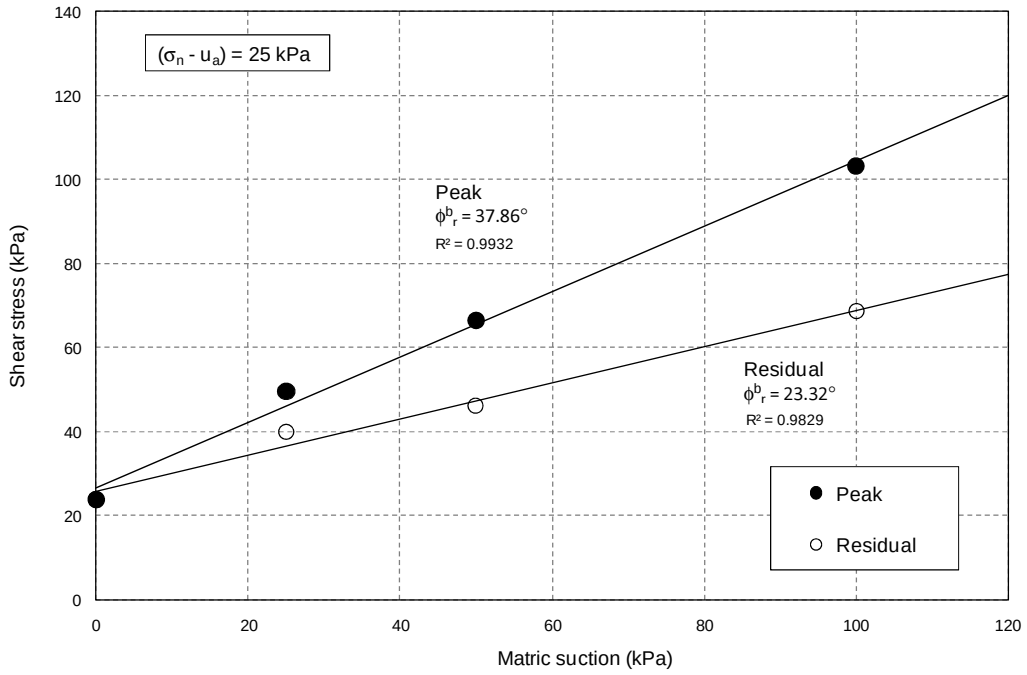

Figure 6-10 Effect of matric suction on peak and residual failure envelopes at net normal stress constant of 25 kPa of compacted SC-SM soil.

Figure 6-11 shows the effect of net normal stress on both the position and slope of residual failure envelopes projected onto the residual shear stress versus matric suction plane for SC-SM. Results show a high nonlinearity for the residual failure envelopes with respect to matric suction. The experimental data were approximated by a second degree polynomial having R-squared values ranged between 0.9845 and 1.00.

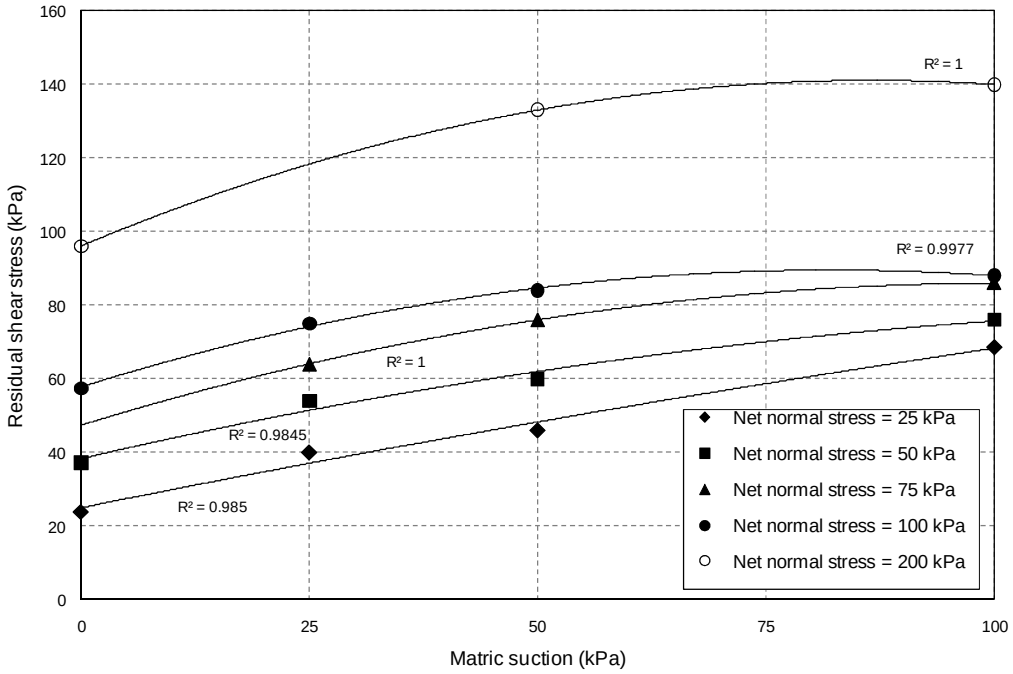

Figure 6-11 Effect of net normal stress on residual failure envelopes of compacted SC-SM soil.

In order to appreciate the effect of matric suction on the residual shear strength, values of angle φ_r^b are plotted in Figure 6-12 with respect to matric suction at different levels of net normal stress. The variation of φ_r' with net normal stress is also included. As shown in this figure, φ_r^b angles start at a value of 22.09° at matric suctions close to saturation ($\varphi_r^b = \varphi_r'$), then increase until suction values close to the air entry value ($\varphi_r^b > \varphi_r'$), and finally decrease significantly to as low as 0° or even negative values for higher suction values ($\varphi_r^b < \varphi_r'$). The decrease in φ_r^b is more drastic for high levels of net normal stress.

From this figure it can also be noticed that for low net normal stress values (i.e., $\sigma_n - u_a$ < 50 kPa) the contribution of matric suction to the residual shear strength represented by φ_r^b is partially reduced as the matric suction increase. On the other hand, for higher net normal

stresses (i.e., $\sigma_n - u_a$ > 75 kPa) the contribution that matric suction has toward the increase of the residual shear strength is almost completely reduced, while values of φ_r^b close to zero and even negative are observed as matric suction increase. The reduction of φ_r^b with suction is larger as the net normal stress increases.

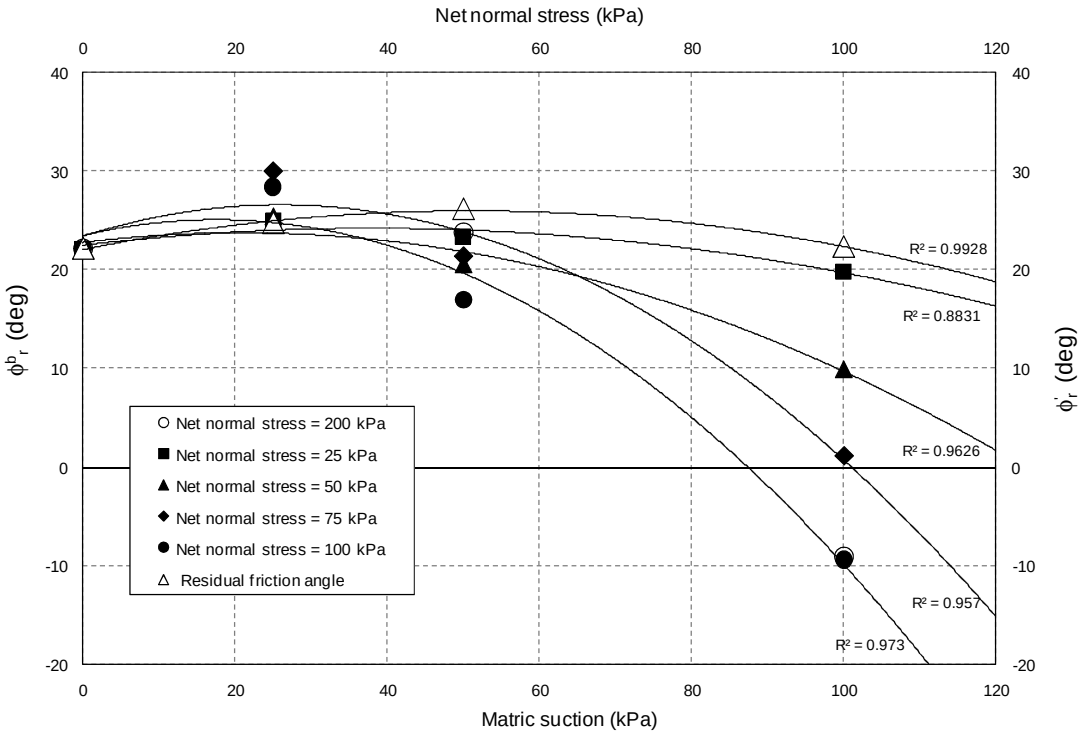

Figure 6-12 Variation of φ_r' and φ_r^b with suction and net normal stress for SC-SM soil.

Vanapalli et al. (2006) and Lu and Likos (2004) consider that there is a direct correspondence between the nonlinear nature of the peak shear strength envelope with respect to increasing matric suction and the behavior of the SWCC. Figure 6-13 shows a conceptualized SWCC along a drained path, as the one followed in this research work, and the corresponding shear strength envelope with respect to increasing matric suction for a typical soil. Within the

regime of relatively low matric suction, and prior to the air-entry pressure, the soil pores remain essentially saturated, the shear strength envelope is approximately linear, and $\varphi^b$is effectively equal to the angle of internal friction φ'. As the soil becomes unsaturated, the geometries of the interparticle pore water menisci dramatically change, thus affecting the resultant interparticle forces that contribute to effective stress on the soil skeleton and, ultimately, to shear strength. The reduction in the volume of pore water within this regime effectively reduces the contribution that matric suction has toward increasing shear strength. This effect is more noticeable as the net normal stress increases, that is, as the stress history of soil increases. This relationship between the nonlinear nature of the peak shear strength envelope and the behavior of the SWCC can be extrapolated to the analysis of residual shear strength at large deformations.

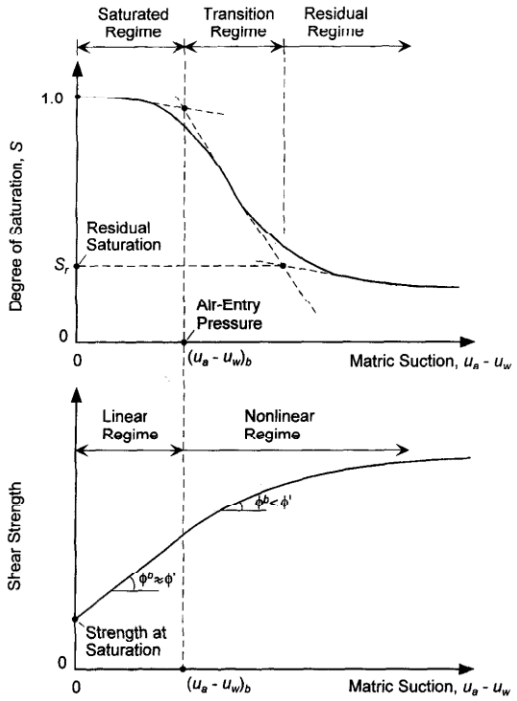

Figure 6-13 Conceptual relationship between soil-water characteristic curve and unsaturated shear strength envelope (modified from Vanapalli et al., 1996).

It has been widely recognized that SWCC curves differ depending on the applied total stress path and stress history (Fredlund, 2002; Fredlund and Pham 2006; Fredlund and Pham 2008). Therefore, the significant effect of net normal stress on the behavior of φ_r^b with respect to suction appears to be related with changes in the geometry and distribution of the water in the liquid phase and therefore in the SWCC curve at large deformations.

At high net normal stresses the volume of pore water in the soil is reduced due to the effect of the initial consolidation process, which leads to a reduction in void ratio, forcing changes in the water and air phases in the soil. Changes of this nature are also induced by the shearing process. At large deformations the initial structure developed by the compaction process is completely destroyed and a thorough particle reorientation is produced at the end of the process. As a consequence, the geometry and distribution of the water in the liquid phase is again modified. Then, in order to maintain a condition of constant suction, a new menisci state has to be developed thus affecting the resultant interparticle forces that contribute to effective stress on the soil skeleton. For that reason, at constant matric suction, soils sheared at low normal stresses will present a higher volume of water contributing to shear strength, compared with those sheared under greater net normal stresses.

As a result, the contribution of matric suction on residual shear stress is reduced as matric suction increases, and this contribution is more drastically lost as the magnitude of the net normal stress on the soil increases. This allows concluding that the nonlinearity of the residual shear strength with suction can be associated to a different relationship between suction and the pore water phase in the soil when this is subjected to large deformations. In other words, a new SWCC is developed, compared with the initial SWCC obtained under zero confinement stress and no previously induced stress history.

This suggests that the SWCC determined at zero confinement stress and with any stress history may not be representative of the relation between suction and pore-water in the soil once it is subjected to large deformations.

During shearing of SC-SM samples at constant net normal stress and matric suction, a water movement from within the specimen was typically observed. A reduction in soil water content measured on the failure surface at the end of the multi-stage suction-controlled tests allowed verifying that drastic changes occurred in the air and water phases during shearing, indicating that the target suction was reached at relatively low water content with respect to the initial SWCC.

Finally, with the aim to fully describe the residual shear strength behavior of compacted SC-SM soil over a realistically wide range, while taking into account the non-linear nature of the relationship between residual shear strength and suction, a non-planar residual failure surface in three-dimensional space was developed.

Similar to the residual failure surface assessed for SM soil, a 3D residual failure surface for SC-SM soil was obtained using the software Mathematica.6. The best-fitting surface to the experimental data is shown in Figure 6-14. The best fitted regression equation for the generated surface obtained via multiple regression model can be described as follows:

$$\tau_r = 17.54 + 0.395(\sigma - u_a) + 0.377(u_a - u_w) + 0.0037(\sigma - u_a)(u_a - u_w) - 0.000036(\sigma - u_a)(u_a - u_w)^2 \quad (6.2)$$

The proposed fitted regression equation provided an excellent fit to the experimental data, with a coefficient of correlation of about 0.985. Experimental data are showed in Figure 6.14 as dots. In summary, the nonlinear interpretation of the residual shear strength tests data for unsaturated soils appears to provide a good estimation.

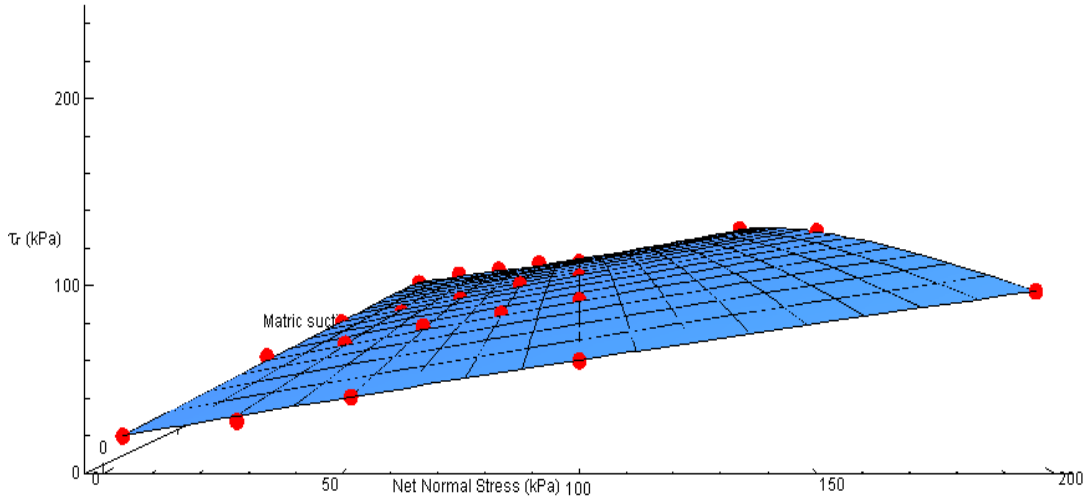

Figure 6-14 Residual failure surface for compacted SC-SM soil.

6.3 Residual Shear Strength for Unsaturated Soils: State of the Art

A review of the literature on residual strength of unsaturated soils via suction-controlled RS testing was conducted, including a review of dissertations, conference articles and journals to establish an art-state of publish results. Results on the effect of suction and net normal stress on the residual strength parameters for different soils were compared with the obtained results in this research. It was found that there was not sufficient data to develop a truly comprehensive database. However, they are summarized and analyzed and some conclusions are addressed on the behavior of unsaturated soils at large deformations under low and high suction states and different net normal stress states.

The data found on the literature are summarized in Table 6-1 including the main index properties of the soils used. Due to the significantly difference on the range of matric suction used by different researchers and with the aim to provide and organized presentation of them, results at low suction states (between 0 to 400 kPa) and results at high suction states (s > 32 MPa) are discussed in separated sections.

Table 6-1 Summary of works on residual strength of unsaturated soils

Reference	Soil type	Gs	LL (%)	PL (%)	PI (%)	Sand (%)	Silt (%)	Clay (%)	Pass 200 (%)	Suction range
This research	SM	2.68	NL	NP	-	83.6	9.8	6.6	16.4	0 - 100 kPa
This research	SC-SM	2.71	26.4	20.2	6.2	60	34.05	5.95	40	0 - 100 kPa
Infante Sedano (2006)	Indian Head till	2.71	32.5	17	15.5	22.5	47.5	30	77.5	0 - 400 kPa
Merchan et al. (2008)	FEBEX bentonite	2.7	102	53	49	-	-	68	100	0 kPa and s > 32 MPa
Vaunat et al. (2007)	Boom clay	2.7	55	28	27	-	-	40	-	0 kPa and s > 37.5 MPa
Vaunat et al. (2006)	Barcelona silty clay	2.66	30	16	14	-	-	15	-	0 kPa and s > 18 MPa

Effect of High Matric Suction on Unsaturated Residual Shear Strength:

One of the first works reported in the literature on the behavior of unsaturated soils at large deformations is the presented by Vaunat et al. (2006). They conducted suction-controlled ring shear tests via a modified Bromhead type ring shear adapted to allow for application of high suctions during shear via the vapor transfer technique. A series of four single-stage RS tests and two multi-stage RS tests were conducted on a low plasticity silty clay known as Barcelona silty clay. The main index properties of this low plasticity clay are presented in Table 6-1. RS tests were conducted under matric suctions of 0, 32, 75 and 277 MPa and net normal stress between 50 and 300 kPa.

They found that suction do not create a cohesive-like increase but cause an increase of the residual friction angle. The residual failure envelopes in the residual shear strength and net normal stress space appears to be almost linear. For the tested material, φ_r' passes from 19.6° in saturated conditions to 24.5° in the dry state (s = 277 MPa). The variation of the residual friction angle with suction is presented in Figure 6-15 for the range of suctions used in that work.

Although the authors do not report residual failure envelopes in the space residual shear strength with suction, data presented in Figure 6-12 for a net normal stress of 50 and 300 kPa are now plotted in Figure 6-13 as a function of suction. Results show that the variation of

residual shear strength of Barcelona silty clay with suction is non-linear. This indicates that φ_r^b is not constant and as can be observed φ_r^b reduces with suction until values close to zero at very high suction (dry condition). Values of φ_r^b close to zero or even negatives were also observed on SM and SC-SM soils at suctions close to the residual state. Later on, Vaunat et al. (2007) using the same modified Bromhead RS reported residual shear strength of a plastic clay (Boom clay) under high suctions. Two multi-stage suction-controlled RS tests were conducted under constant suction of 0 and 70 MPa and net normal stress between 37.5 kPa and 300 kPa. They display evidence of a huge increase in the residual friction angle whose value is 15° greater that that measured in saturated conditions. The variation of φ_r' with suction for the range of suctions used in that work is also presented in Figure 6-15. To determine the effect of plasticity on behavior of φ_r^b the variation of residual shear strength with suction for Boom clay under a net normal stress of 37.5 and 300 kPa is also showed in Figure 6-16. Finally, as part of the previous work realized in the range of high suctions, Merchan et al (2008) report results on the effect of high suctions on the residual shear strength of high plasticity clay (FEBEX bentonite). Once again a significant increment of φ_r' with suction was observed. Suction-controlled RS were conducted at constant suction s = 0, 18 and 75 MPa and net normal stress between 100 and 450 kPa. The variation of φ_r' and residual shear strength with suction is shown in Figure 6-15 and 6-16 respectively.From Figures 6-12 and 6-16 the significant effect of matric suction on φ_r' and φ_r^b can be noticed. The non-linearity of both, φ_r' and φ_r^b with suction is also apparent. For these materials, most of the increase in both residual angles occurs between 0 and 100 MPa. For the high plasticity clay, the effect of suction on φ_r' and φ_r^b becomes smaller beyond this suction and tends to an asymptotic value for a suction close to 300 MPa. Moreover, the increase in residual friction angle increases with the plasticity of the clay presenting an increment from saturated to dry conditions of about 2.5° for low plasticity silty clay, 15° for the medium plasticity clay and 21° for the high plasticity clay as shown in Figure 6-17. The authors suggested that increase in friction angle φ_r' is

associated to a process of clay aggregation or aggregation stiffening during strong drying that makes the material behave in a more granular way.

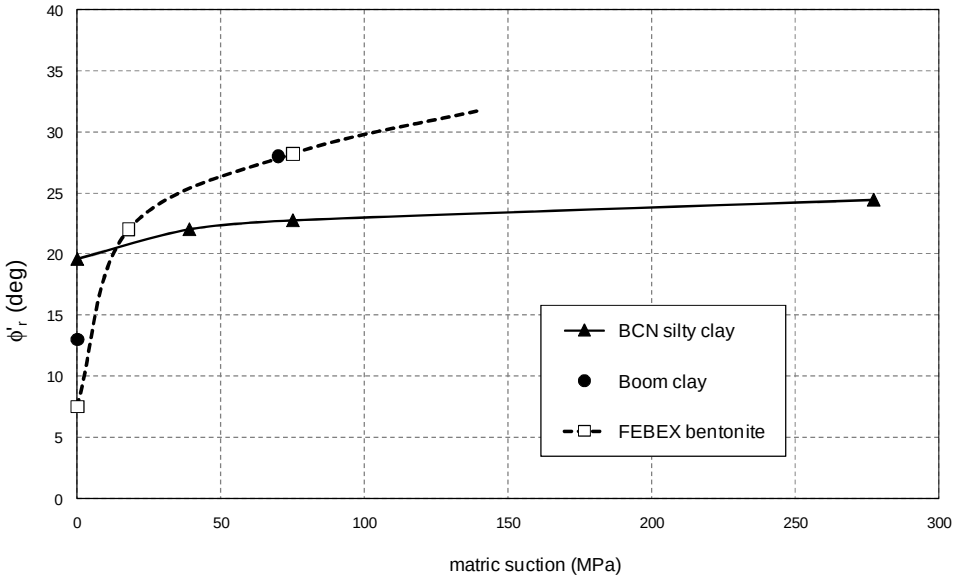

Figure 6-15 Variation of φ_r' with suction.

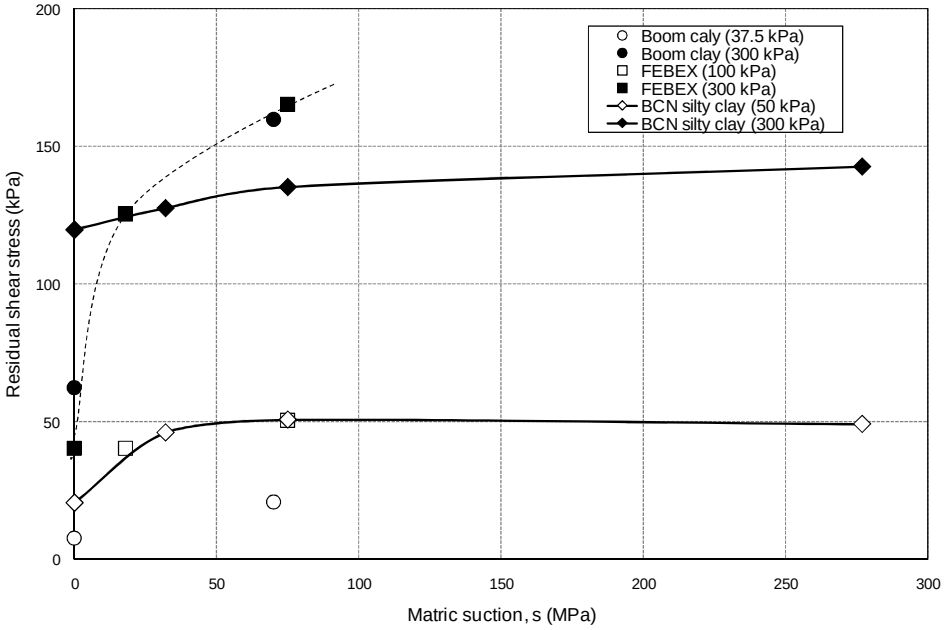

Figure 6-16 Effect of net normal stress on residual failure envelopes.

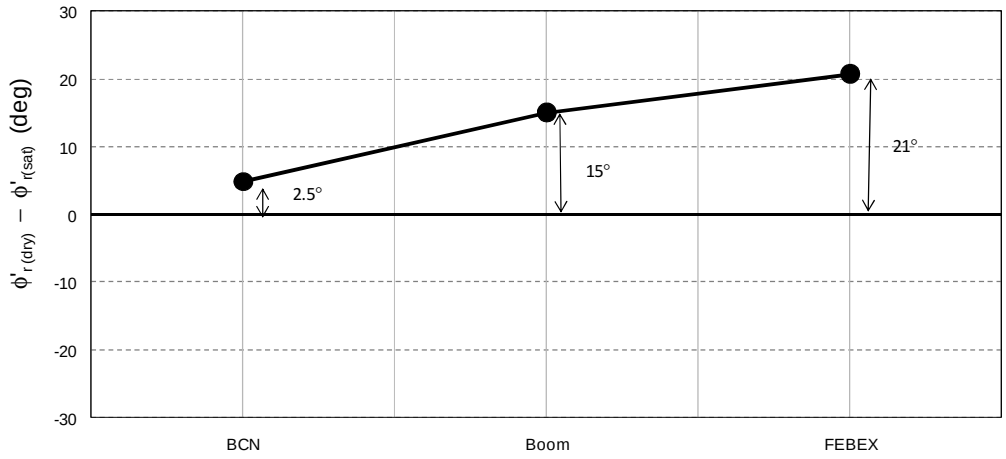

Figure 6-17 Variation of φ'_r with clay plasticity.

Effect of Low Matric Suction on Residual Shear Strength:

Infante Sedano (2006) report data of residual shear strength on unsaturated Indian Head till using a modified Bromhead type RS apparatus for controlling suction via the axis translation technique. Only data of residual shear strength for a net normal stress of 150 kPa under different low suction states between 0 and 400 kPa are reported. Consequently the variation of the residual friction angle with suction could not be analyzed or compared with the data obtained in the present work. However, it was possible to determine the variation of residual shear strength with suction for a net normal stress of 150 kPa as shown in Figure 6-18. The non linearity of the residual failure envelope is noticeable. The variation of φ_r^b with suction at a net normal stress of 150 kPa for Indian Head till is shown in Figure 6-19. This Figure includes φ_r^b values obtained in the present work for SC-SM at different net normal stress. Likewise to the trend observed for SC-SM soil, φ_r^b for Indian Head till decreases with suction reaching values close to zero and even negative values at suctions close to 250 kPa. It is apparent that the higher the plasticity of

the soil (the more fine grained), the higher the contribution of suction on the residual shear stress for a given net normal stress.

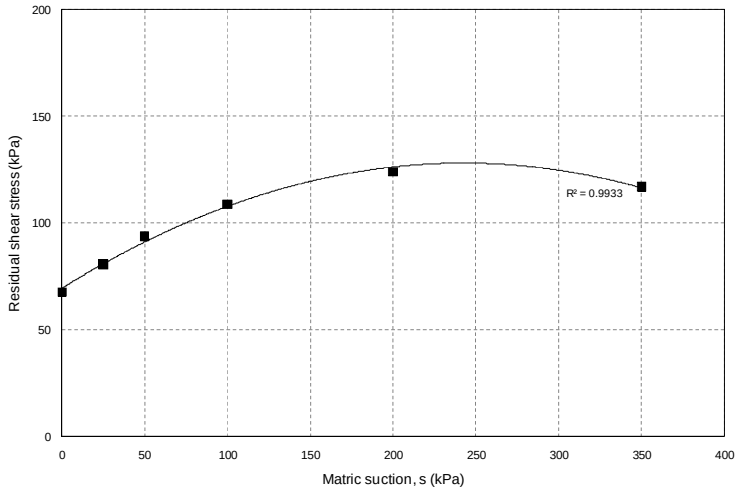

Figure 6-18 Variation of residual shear strength with suction at net normal stress of 150 kPa for Indian Head till.

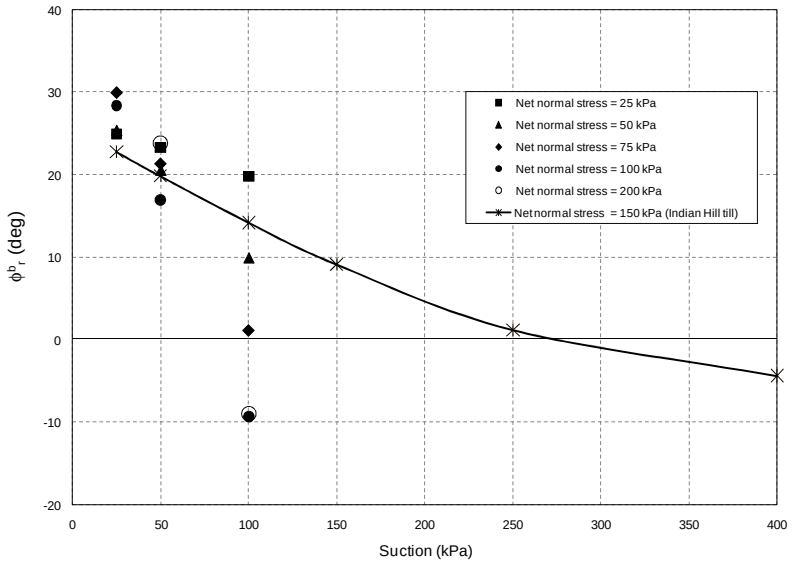

Figure 6-19 Variation of φ_r^b whit suction.

6.4 Studies on Soil Fabric on the Failure Surface

There are strong reasons to believe that, in most cases, the induced horizontal failure plane was within the thickness of the sheared specimen of SM and SC-SM soils. First of all, the rough-surfaced disk adapted to the top annular platen (Figure 4-15) is a custom-made, sintered-bronze porous disk designed and manufactured by Geotest Instrument Corp. Although the actual "roughness" index of the custom-made disk was never provided by the manufacturer, its roughness was made considerably higher than that of the top porous disk used in the conventional Bromhead apparatus (as per request).

On the other hand, visual inspection of tests on saturated and partially saturated SM samples showed a distinct failure surface where the organization of the particles were slightly loose, presumably due to the crushing of the particles in the shear zone.

Thus, to verify the presence of a failure plane, the SM was removed in layers upon completion of the test. Digital images using a scanning electron microscope (SEM) were taken on the samples in order to identify the degree of particle crushing due to RS shearing precisely. The images were compared with images taken on SM without any RS shearing history.

Sample preparation is an important aspect of conventional SEM studies. SEM and other optical and electron microscopy techniques require the pore fluid to be removed, replaced, or frozen, since the instrument is operated under high vacuum 10^{-5} to 10^{-6} Torr (10^{-6} to 10^{-10} atm). The extraction of the pore water without causing disturbance to the original soil fabric is a very difficult process. In addition, normally there is no way to establish how much disturbance has occurred.

However, although it is possible to remove the water from soil samples without causing too much disturbance and shrinkage, as is caused by using air and oven drying, via freeze-drying and critical point drying; these methods were not available at the University of Texas at

Arlington. Therefore, regular drying process under atmospheric conditions was chosen to extract the pore water before SEM testing on SM samples. As a consequence, only a qualitative analysis on the shape and size of the soil particles could be undertaken.

Typical SEM micrographs from a SM sample before being subjected to a shearing process are shown in Figure 6-20 to Figure 6-23. Figure 6-20 and Figure 6-21 show images of compacted SM after being statically compacted. Figure 6-22 and Figure 6-23 show images of the material from the first layer taken after a RS tests. The magnification used in all images was 500X.

Close examination of the SEM micrographs prior to shearing indicates that the sandy particles seem to be generally sub-angular in shape, with a relatively homogeneous particle size. After shearing, the sandy particles seem to be generally angular in shape, exhibiting a wider range of particle sizes. This phenomenon is associated to the possible breaking of sand particles during shearing and, in some cases, could explain the slight reduction in shear strength, from peak to residual, when the material is subject to relatively large angular deformations.

Therefore, the changes observed in the size and shape of the sand particles provided a strong evidence of the presence of a horizontal failure plane within the SM specimen.

Garga and Infante Sedano (2002), also related the particle crushing observed at the end of RS tests to the existence of a failure surface within the annular RS sample. In that work a conventional Bromhead apparatus was modified to undertake constant-volume ring shear testing on 20-mm (0.78-in) thick specimens of poorly-graded sand. In their work, the fines distribution curves for shear displacements of 500 mm and 250 mm indicated that considerable crushing occurred near the middle of the specimen, thus providing a strong evidence of the presence of a horizontal failure plane well within the specimen. It is also worth noting that the SM soil used in the present work has 16.4% of fine-grained material.

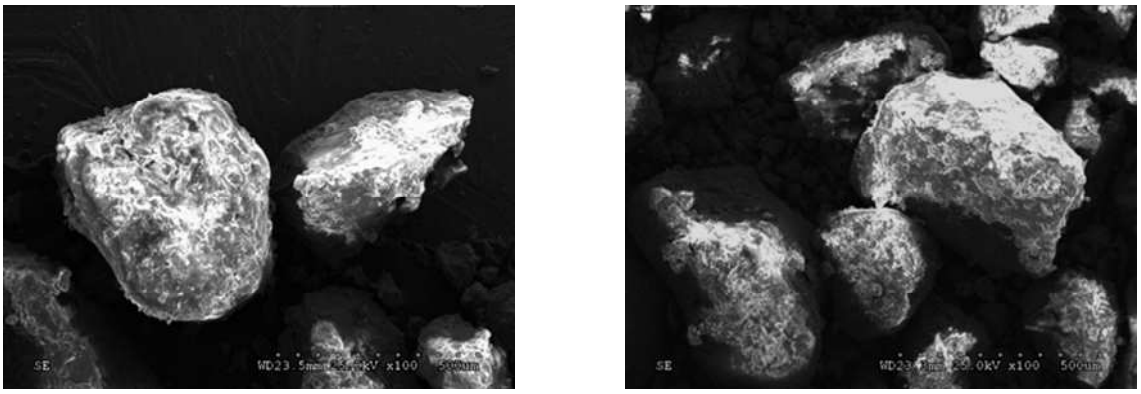

Figure 6-20 SM soil before RS shearing. Magnification 100X.

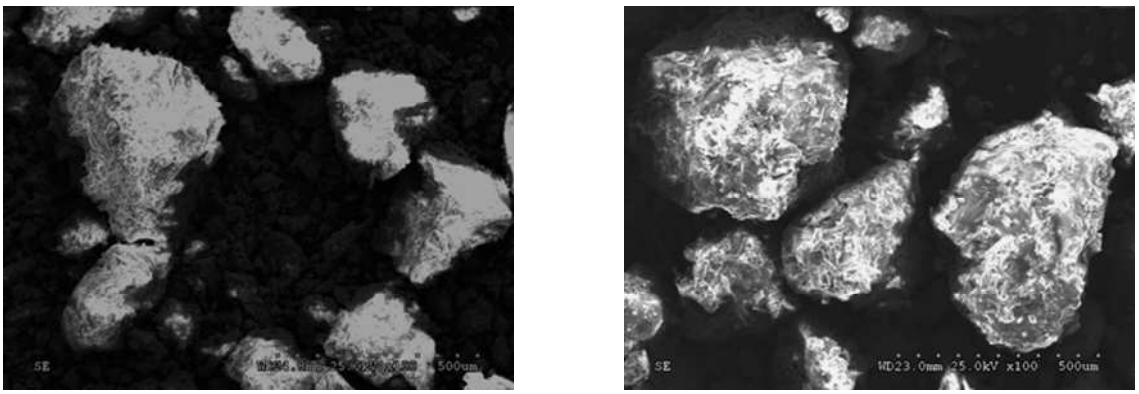

Figure 6-21 SM soil before RS shearing. Magnification 100X.

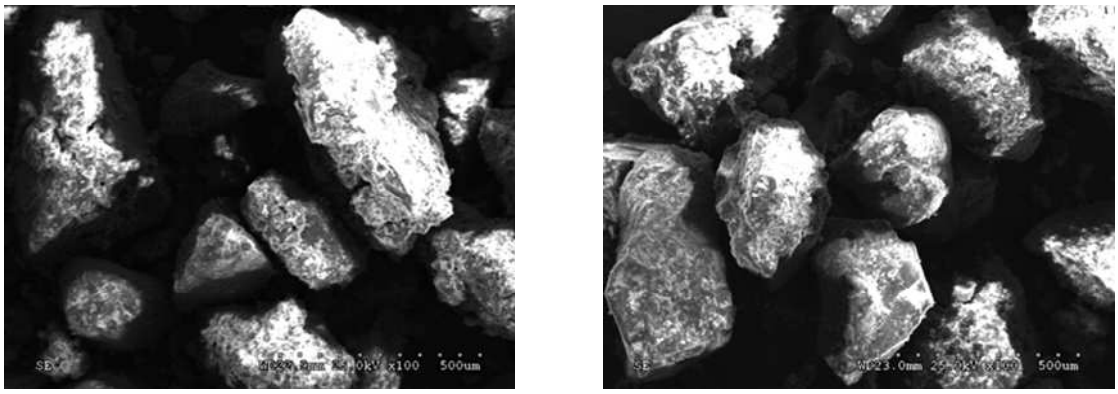

Figure 6-22 SM soil after RS shearing. Magnification 100X.

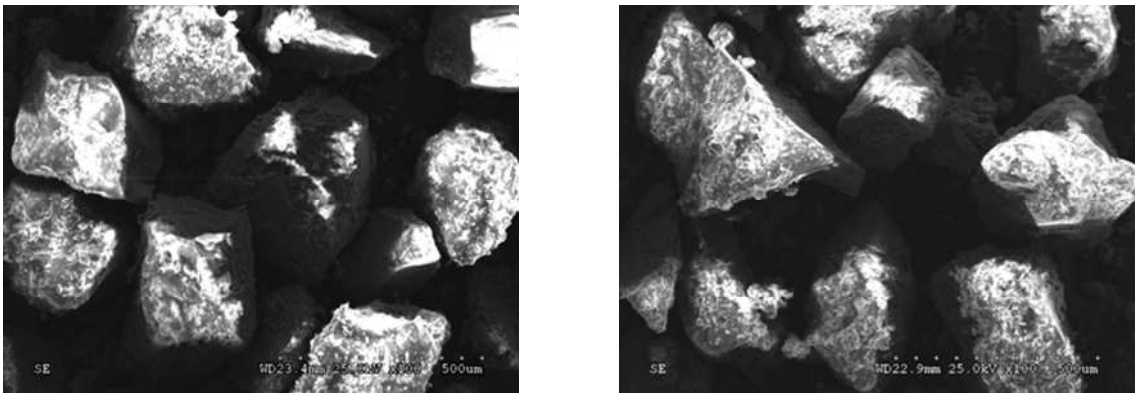

Figure 6-23 SM soil after RS shearing. Magnification 100X.

On the other hand, for the reasons previously explained about the limitations of the SEM device on the requirement of the extract of any pore water from samples, digital images using an optical microscope were taken on the failure surface of SC-SM soils samples. SC-SM is a soil having a relatively high percentage of clay particles (particle with size < 2μ = 32%). Therefore inducing an air drying process on the samples for taking the SEM images could provoke drastic changes on the original structure and organization of the particles, and produce possible false interpretation of the effect of shearing on the structure at large deformations.

In addition of a close analysis of the digital images, a detailed visual inspection of the surface of the sample, as well as the top cap after shearing, allowed verifying the formation of a failure surface within of the SC-SM sample after RS shearing. As shown in Figure 6-24, failure occurs by rupture of the soil specimen along its upper surface, where a layer of clay particles that adhere to the roughened upper annular platen are displaced relative to clay particles below (Fig. 6-24a). Continued shearing resulted in an orientation of the plately particles along the failure plane, and the development of slickensides along which residual strength is measured (Figure 6-24b).

Figure 6-25, 6-26 and 6-27 show digital pictures of the surface of the sample right after the static compaction and prior shearing for samples RS14, RS15 and RS16. In the figures, digital pictures of the failure surface at the end of tests are also showed. Failure surface of SC-SM is characterized by a polished and bright surface, which indicates a clear reorientation of the plately clayey minerals (e.g., mica). This kind of failure surface is typical of soils exhibiting “sliding mode” of residual shearing described by Lupini (1981). The large particle reorientation observed explain the drop from peak to residual stages observed in all the first shearing stages and the subsequent ductile behavior exhibited by the residual shear stress after several shearing stages.

Thus, the post-peak drop in strength observed in all first shear stage on SC-SM is due entirely to particle reorientation. After this first shearing, as all plately particles have been oriented an additional shearing under a higher net normal stress is going to be reflected just in an increase on the residual strength value and not in changes in the stress-displacement behavior (ductile/brittle). In others words compacted SC-SM soil is going to exhibit a typical ductile behavior.

Figure 6-24 Failure plane of SM soil: (a) Top annular platen after shearing and detail of the material adhered to the roughened sintered-bronze porous disk; (b) Bottom annular and detail of the polished, striated failure plane.

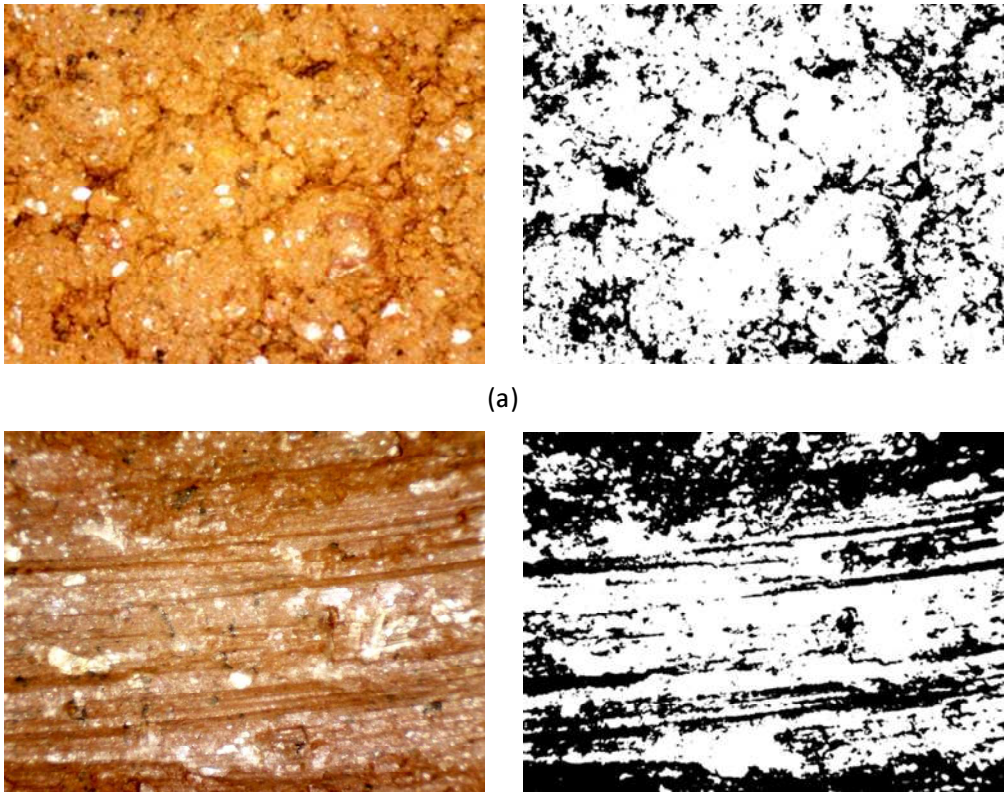

Figure 6-25 RS14 test on SC-SM: (a) before RS shearing; (b) after RS shearing. Magnification 50X.

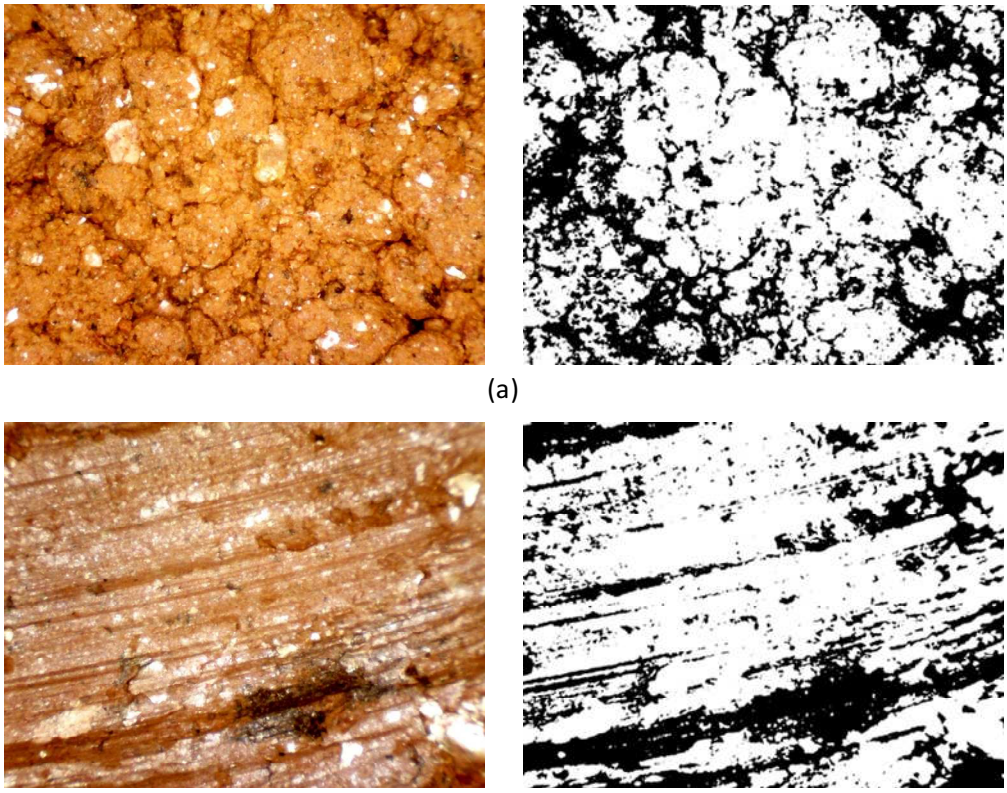

Figure 6-26 RS15 test on SC-SM: (a) before RS shearing; (b) after RS shearing. Magnification 50X.

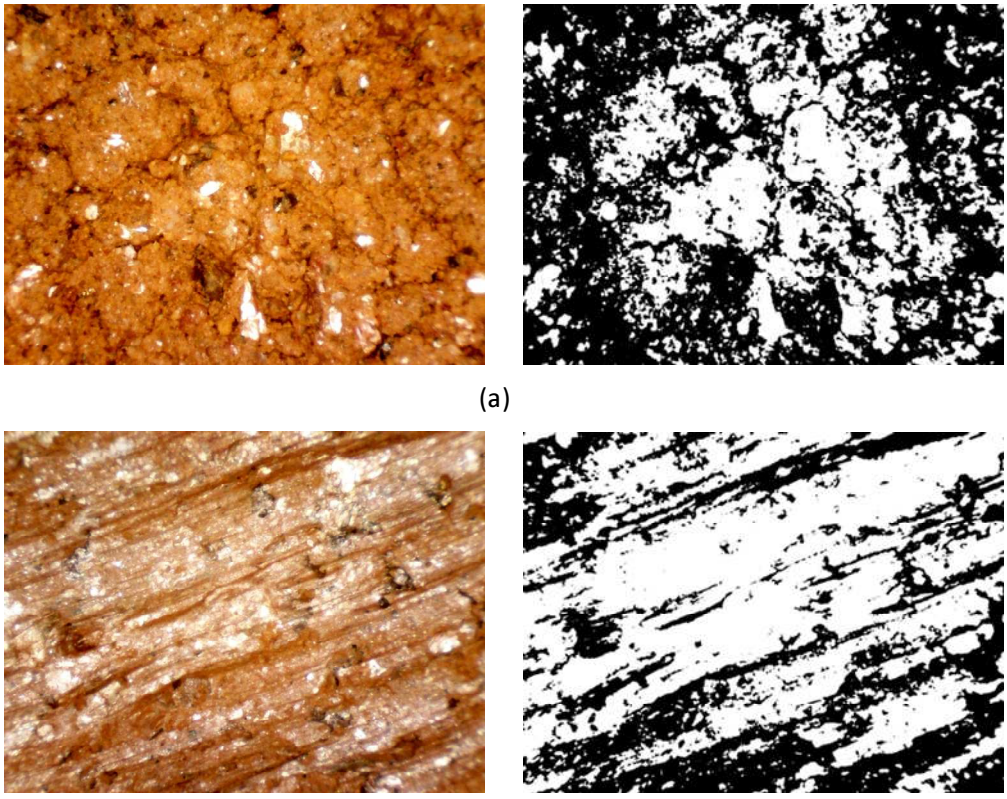

Figure 6-27 RS16 test on SC-SM: (a) before RS shearing; (b) after RS shearing. Magnification 50X.

CHAPTER 7

CONCLUSIONS AND RECOMENDATIONS

7.1 Summary

In recent years, the key hypotheses of most constitutive frameworks postulated for unsaturated soils have been validated via suction-controlled oedometer, triaxial, and direct shear testing. These techniques, however, allow for the application of loads along limited modes and levels of soil deformation. Today, it is well known that most of the geotechnical infrastructure resting on unsaturated ground involves a wide range of deformations. Calculation of foundation settlement, for instance, requires a good estimation of soil stiffness at relatively small strains. Analysis of slopes, embankments, and soil bearing capacity, on the other hand, requires an adequate estimation of shear strength, from peak to residual. To date, however, there is very limited experimental evidence of unsaturated soil response under mid-to-large strain levels under controlled-suction states. This research work introduces a novel suction-controlled ring shear apparatus that has been made suitable for testing unsaturated soils over a whole range of deformations using axis translation technique. The research work outlined the full development of the apparatus, including details of its main components and the corresponding performance and verification testing through comparisons with the conventional Bromhead ring shear apparatus. Results from a series of suction-controlled ring shear tests on statically compacted silty sand and silty clayey soils were presented. Results reflect the important role played by matric suction on residual shear strength response of unsaturated soils. The following sections summarize the main conclusions drawn from this investigation and recommendations for future work.

7.2 Main Conclusions

Performance of Servo Suction-Controlled RS Apparatus:

The principal conclusions regarding the new apparatus are as follows:

- The original disk adapted to the top annular platen was successfully modified to suit the particular material requirements of SM soil. In order to induce a horizontal failure plane within the thickness of the sheared specimen, it was necessary to adapt to the top annular platen a custom-made, sintered-bronze porous disk with a roughness considerably higher than that of the top porous disk used in the conventional Bromhead apparatus. The localization of the failure plane within the sample was verified through the analysis of digital images of the failure zone using an optical microscope and scanning electron microscope (SEM).
- The new RS apparatus can be reliably used for the assessment of residual strength parameters under fully saturated conditions, yielding a similar degree of accuracy compared to the conventional Bromhead type RS device.
- Repeatability of tests results from suction-controlled RS testing on compacted SM and SC-SM soils shows that the newly developed RS apparatus is suitable for testing unsaturated soils under constant suction states via the axis-translation technique.
- The single-stage testing scheme allows for the determination of both peak ad residual shear strength in statically compacted samples of SM and SC-SM soils.
- The data acquisition and process control (DA/PC) system exhibited continuous stability during long-term RS testing, with steady real-time monitoring of applied torque, induced shear and normal stresses, and, angular and vertical deformation in the sample.

Suction-Controlled Ring Shear Testing on Compacted SM and SC-SM soils:

- Residual strength has been shown to be reasonably independent of the original soil structure or the stress-suction history experienced by the soil.
- Results corroborate that the net normal stress has a remarkable influence on the residual shear strength. Matric suction also plays a significant role on the residual shear strength characteristics of compacted SM and SM-SC soils. Residual shear strength increases with matric suction and net normal stress. Both soils exhibit a gradually transition from hardening behavior (showing no peak shear stress) to hardening-softening behavior (showing a peak shear stress) as matric suction increase at lower net normal stress. Hardening-softening is more notorious in the SC-SM soil.
- In general, soil dilatancy associated with shearing increases with suction. This behavior is more significant on SM soil.
- Residual failure envelopes in the $\tau:(\sigma_n - \sigma_a)$ plane were found to be reasonably linear for both SM and SC-SM soils. The residual friction angle φ_r' increases with matric suction and trend to be constant at higher suctions (close to residual suction sates). On the other hand, the residual cohesion intercept increases linearly with suction.
- For the range of suction and net normal stress states investigated in this research work, the increase in residual strength with increasing suction in the $\tau:(u_a - u_w)$ plane appears to be linear for SM soil, but significantly non-linear for SC-SM soil.
- For SC-SM soil, φ_r^b angle, which represents the change in shear strength with suction, tends to decrease with an increase in suction, reaching negative values at

high suction levels. This effect is less significant as the net normal stress and the plasticity of the tests soil increase.

- The findings from this research work are consistent with results previously reported in the literature at low net normal and suction states, and further substantiate some of the reported at high suction states in highly plastic materials.
- A conceptual, three-dimensional residual strength framework for unsaturated soils, similar to that postulated for the peak strength (Fredlund and Rahardjo 1996), was tentatively formulated with the experimental data from RS testing on SM and SC-SM soils.
- SEM and optical microscopic imaging confirmed the development of a well-defined failure surface within the first half of the sample thickness in both soils. SEM and optical microscopic imaging also confirmed particle crushing in SM soil and particle reorientation in SC-SM soil on the respective failure surfaces.

7.3 Future Research Work

Performance of Servo Suction-Controlled RS Apparatus:

- In the suction-controlled RS apparatus, an amount of wall friction (not measured in this research work) is developed specially when sandy material are tested, due to extrusion and entrapment of particles between the top annular platen and the side walls of the specimen container. Therefore, it is necessary to investigate the effect of wall friction on the residual shear strength measured, and modify either the top annular platen or the bottom annular platen in order to minimize this effect and improve the accuracy of the measurements.

- Although a good characterization of the behavior of SM and SM-SC soils in the range of low suction and net normal stresses was achieved, it is necessary to modify the load-torque sensor system to increase the range of residual strength measured, and embrace the range of high suction and net normal stress states.
- The development of a suction control system for suctions higher than 800 kPa is necessary. For short term testing, possible options are using the axis translation technique combined with vapor transfer technique taking into account the advantage that it already has a closed cell chamber on the sample.
- The main drawback of several ring shear devices developed so far to measure the undrained shear strength testing is their inability to measure the pore pressure at the shearing plane. The measurement of average pore pressure or matric suction at the end may not represent the exact pore pressure or suction at the sliding plane. It is necessary to adapt a direct suction measurement system on the failure plane. An option is the installation of high capacity tensiometers as the developed by the Imperial College of London (Ridley and Burland, 1993) which allow the direct assessment in real time of matric suction up to 1500 kPa.

Suction-Controlled Ring Shear Testing on Compacted SM and SC-SM soils:

- It is important to follow a similar testing program to the one followed in this investigation testing plastic soils and embracing a more larger range of suction and net normal stress states to obtain a comprehensive understanding of the behavior of unsaturated soils at large deformations, and to postulate a conceptual residual strength framework.
- Most of the rainfall-induced slope failures are shallow and occur at high degree of saturation (low matric suction). It has been recognized that an unsaturated soil behaves

differently at wetting and drying. Therefore, studies of the effect of wetting and drying on the unsaturated residual behavior of soils under different net normal stresses are recommended.

- When an unsaturated soil is subjected to shear, menisci are strained and may eventually break, causing a reduction in matric suction effect. When the strain in a soil exceeds the strain that menisci can sustain, both soil strength and stiffness are affected. Therefore, uncontrolled-suction tests to assess the rate of loss/gain of suction (menisci failure or rupture) over a large range of shear deformations are recommended.
- Fabric studies of undisturbed samples at natural water content from the failure zone prepared by using freeze drying are necessary to produce reliable results when using SEM in materials with an important component of highly plastic clay.
- It has been widely recognized that SWCC curves differ depending on the applied total stress path and stress history. Studies to determine changes of the SWCC during large shearing and hydraulic hysteresis phenomenon are recommended.

REFERENCES

Alonso, E.E., Gens, A., and Hight, D.W. (1987). “Special problem soils. General report.” Proceedings of the 9th European Conference on Soil Mechanics. Dublin, 3, 1087-1146.

Alonso, E.E., A. Gens & Josa (1990). “A constitutive model for partially saturated soils.” Geotechnique, 40(3), 405-430.

Anayi, J. T., Boyce, J. R., and Rogers, C. D. (1988). "Comparison of alternative methods of measuring the residual strength of a clay." Transportation Research Record, 1192, 16-26.

Anayi, J. T., Boyce, J. R., and Rogers, C. D. F. (1989). "Modified Bromhead ring shear apparatus." Geotechnical Testing Journal, ASTM, 12(2), 171-173.

Anderson, W. F., and Hammoud, F. (1988). "Effect of testing procedure in ring shear tests." Geotechnical Testing Journal, ASTM, 11(3), 204-207.

Anderson, W.F., Yong, K.Y., and Sulaiman, J.I. (1985). “Shaft adhesion of bored and Cast-In-Situ piles” Proceedings of 11th International Conference on Soils Mechanics and Foundation Engineering, 3, 1333-1336.

ASTM (2000). "Designation: D 6467-99, Standard Test Method for Torsional Ring Shear Test to Determine Drained Residual Shear Strength of Cohesive Soils." Annual Book of Standards, Volume 04.08, Soil and Rock; Dimension Stone; Geosynthetics, ASTM, Philadelphia, PA.

Bishop, A.W. (1959). “The principle of effective stress.” Teknisk Ukeblad I Samarbeide Med Teknikk, Oslo, Norway, 106(39), 859-863.

Bishop, A. W., Alpan, I., Blight, G. E., and Donald, I. B. (1960). ‘‘Factors controlling the hear strength of partly saturated cohesive soils,’’ in ASCE Research Conference on the Shear Strength of Cohesive Soils, University of Colorado, Boulder, 503–532.

Bishop, A.W., Green, G.E., Garga, V.K., Andresen, A., and Brown, J.D. (1971). “A new ring shear apparatus and its application to the measurement of residual strength.” Géotechnique, 21(2), 273-328.

Bocking, K, A., Fredlund, D.G. (1980). Limitations of the axis translation technique. In Proceedings of the 4th International Conference on Expansive Soils, Denver, CO, pp. 117-135.

Bromhead, E.N. (1979). “A simple ring shear apparatus.” Ground Engineering, 12(5), 40-44

Bromhead, E.N., and Curtis, R.D (1983) “A comparison of alternative methods of measuring the residual strength of London clay” Ground Engineering, 16(4), 39-41

Bromhead, E.N and Dixon, N (1986) “The field residual strength of London clay and its correlations with laboratory measurements, especially ring shear test” Geotechnique, 36(4), 449-452

Brooks, R. H., and Corey, A. T. (1964). ‘‘Hydraulic properties of porous media,’’ Colorado State University, Hydrology Paper No. 3, March.

Burland, J. B., and Ridley, A.M. (1996). The importance of suction in soil mechanics. Proceedings of the 12th Southeast Asian Geotechnical Conf., Kuala Lumpu, 2, 27-49.

Budhu, M. (2007). Soil mechanics and foundations. John Wiley & Sons, Inc.

Carrubba, P., and Del Fabbro, M. (2008). “Laboratory investigation on reactivated residual strength.” Journal of Geotechnical and Geoenvironmental Engineering, ASCE, 143(3), 302-315.

Chandler, R.J. (1977). “Back analysis techniques for slope stabilization works: a case record.” Géotechnique, 27(4), 479-495.

Coleman, J. D. (1962) “Stress/strain relations for partly saturated soils.” Geotechnique, 12(4), 348-350.

Cui, Y.J, and Delage, P. (1996). “Yielding and plastic behavior of an unsaturated compacted silt.” Géotechnique, 46 (2), 291-311.

DeCampos, T. M. P., and Carrillo, C. W. (1995). ‘‘Direct shear testing on an unsaturated soil from Rio de Janeiro,’’ Proceedings of the 1st International Conference on Unsaturated Soils, Paris, 31–38.

Dineen, K. (1997). The influence of soil suction on Compressibility and Swelling. PhD Thesis, University of London.

Escario, V. (1980). “Suction-controlled penetration and shear tests.” In Proceedings of 4th International Conference on Expansive Soils, Denver, CO, 781-787.

Escario, V., Juca, J., and Coppe, M.S. (1989). “Strength and deformation of partly saturated soils.” In Proceedings of the 12th International Conference on Soil Mechanics and Foundation Engineering, Rio de Janeiro, 3, 43-46.

Escario, V., and Saez, J. (1986). ‘‘The shear strength of partly saturated soils,’’ Geotechnique, 36(3), 453–456.

Feuerharmel, C., Pereira, A., Gehling, W.Y.Y., and Bica, A. V. D (2006) “Determination of the shear strength parameters of two unsaturated colluvium soils using the direct shear test”. Proc. 4st International Conference on Unsaturated Soils, v1: 189-193 Carefree, Arizona. Pg: 1181-1190.

Fredlund, D. G. (1989) ‘‘Soil suction monitoring for roads and airfields,’’ Symposium on the State-of-the-Art of Pavement Response Monitoring Systems for Roads and Airfields, sponsored by the U.S. Army Corps of Engineers, Hanover, NH, March. 6–9.

Fredlund D. G. (1998). “Bringing unsaturated soil mechanics into engineering practice.” II International Conference on Unsaturated Soils, UNSAT ’98, Beijing 2, 1-36.

Fredlund, D.G. (2006). “Unsaturated soil mechanics in engineering practice.” Journal of Geotechnical and Geoenviromental Engineering, 132(3), 286-321.

Fredlund, M. D., Fredlund, D. G., and Wilson, G. W. (2000). “An equation to represent grain-size distribution.” Canadian Geotechnical Journal., 37(4), 817-827.

Fredlund, D.G., and Morgenstern, N.R. (1977). “Stress state variables for unsaturated soils.” Journal of Geotechnical Engineering Division, 103, 447-466.

Fredlund, D.G., Morgenstern, N.R., Wider, R.A. (1978). “Shear strength of unsaturated soils” Canadian Geotechnical Journal, 15(3), 313-321.

Fredlund, D. G. and Rahardjo, H. (1993). "Soil mechanics for unsaturated soils." John Wiley and Sons, Inc., New York.

Fredlund, D. G., and Xing, A. (1994). “Equation for the soil-water characteristic curve.” Canadian Geotechnical Journal, 31(4), 521-532.

Fredlund, D. G., Xing, A., Huang, S., (1994). “Predicting the permeability functions for unsaturated soils using the soil-water characteristic curve.” Canadian Geotechnical Journal, 31, 533-546.

Fredlund, M. D., Wilson, G. W., and Fredlund, D. G., (1997). “Prediction of the soil-water characteristic curve from the grain-size distribution curve.” Proceedings of the 3rd Symposium on Unsaturated Soil, Rio de Janeiro, Brazil, 13-23.

Feuerharmel, C., Pereira, A., Gehling, W.Y.Y., and Bica, A.V.D. (2006). “Determination of the shear strength parameters of two unsaturated colluvium soils using the direct shear test.” Proceedings of the Fourth International Conference of Unsaturated Soils, Carefree, Arizona, 1, 1181-1190.

Gan, J. K., Fredlund, D. G., and Rahardjo, H. (1988). ‘‘Determination of the shear strength parameters of an unsaturated soil using the direct shear test,’’ Canadian Geotechnical Journal, 25(3), 500–510.

Garga, V.K., and Infante, J.A. (2002). “Steady state of sands in a constant volume ring shear apparatus.” Geotechnical Testing Journal, 25(4), 1-8.

Geotechnical Consulting and Testing System (2009). CATS Ring Shear Apparatus 1.8: User guide and reference. GCTS, Tempe, AZ.

Haefeli, R. (1951). “Investigation and measurements of the shear strength of saturated cohesive soils” Geotechnique 2, No. 3, 186-207.

Hilf, J. W. (1956).‘‘An investigation of pore water pressure in compacted cohesive soils,’’ Technical Memorandum No. 654, United States Department of the Interior, Bureau of Reclamation, Design and Construction Division, Denver, CO.

Hossain, Md. A., and Yin, J.H. (2010). “Behavior of a compacted completely decomposed granite soil from suction controlled direct shear tests.” Journal of Geotechnical and Geoenviromental Engineering, 136(1), 189-198.

Hoyos, L.R. (1998). Experimental and computational modeling of unsaturated soil behavior under true triaxial stress states. Ph.D. dissertation, Georgia Institute of Technology, Atlanta, GA.

Infante Sedano, J.A., Garga, V.K, and Vanapalli, S.K. (2002). “Influence of volume chance behavior on the prediction of the shear strength of unsaturated soils.” Proceedings of the 55th Canadian Geotechnical and 3rd joint IAH-CNC, Niagara falls, Ontario, 1269-1276.

Infante Sedano, J.A., Vanapalli, S.K. and Garga, V.K. (2007). “Modified ring shear apparatus for unsaturated soils testing.” Geotechnical Testing Journal, 30(1), 39–47.

Jennings, J.E.B. and Burland, J.B. (1962). “Limitations to the use of effective stresses in partly saturated soils.” Géotechnique, 12(2), 125-144.

Khalili, N., Geiser, F., Blight, G. E. (2004). ‘‘Effective stress in unsaturated soils, a review with new evidence,’’ International Journal of Geomechanics, 4(2).

Leong, E. C., and Rahardjo, H. (1997). ‘‘Reviews of soil-water characteristic curve equations,’’ Journal of Geotechnical and Geoenvironmental Engineering, 123, 1106–1117.

Lu, N., and Likos, W.J. (2004). “Unsaturated soil mechanics” John Wiley & Sons, Inc.

Lupini, J.F., Skinner, A.E., and Vaughan, P.R. (1981). “The drained residual strength of cohesive soils.” Geotechnique, 31(2), 181-213.

Meehan, C.L., Brandon, T.L., and Duncan, J.M. (2007). “Measuring drained residual strength in the Bromhead ring shear.” Geotechnical Testing Journal, 30(6), 1-8.

Merchán, V., Vaunat, J., Romero, E., and Meca, T. (2008). “Experimental study of the influence of suction on the residual friction angle of clays.” Proceedings of the First European Conference on Unsaturated Soils, Durham, U.K., 423-428.

Najjar, S.S., Gilbert, R.B, Liedtke, E., McCarron, B., and Young, A.G. (2007) “Residual shear strength for interfaces between pipelines and clays at low effective normal stresses” Geotech. and Geoenvir. Eng. 133(6), 695-706.

Nuth, M., and Laloui, L. (2007). “Effective stress concept in unsaturated soils: Clarification and validation of a unified framework.” International Journal for Numerical and Analytical Methods in Geomechanics, 32, 771–801.

Padilla, J.M, Perera, Y.Y., Houston, W.N., Perez, N., and Fredlund, D.G. (2006). Quantification of air diffusion through high air-entry ceramics disks. Proc. 4st International Conference on Unsaturated Soils, Carefree, Arizona, 1, 1852-1863.

Pereira, A., Feuerharmel, C., Gehling, W.Y.Y., and Bica, A.V.D. (2006) “ A study on the shear strength envelope of an unsaturated colluviums soil”. Proc. 4st International Conference on Unsaturated Soils, Carefree, Arizona, 1, 1191-1199.

Petley, D.J. (1966) “The shear strength of soils at large strains” PhD Thesis, University of London.

Randolph, M.F., and Wroth, C.P. (1982). “Recent developments in Understanding the axial capacity of piles in clay” Ground Engineering, 15(7), 2517-2532.

Ridley, A.M., Dineen., K., Burland, J.B., and Vaughan, P.R. (2003). “Soil matrix suction: some examples of its measurement and application in geotechnical engineering.” Geotechnique, 53(2), 241–253

Röhm, S.A., and Vilar, O.M. (1995). “Shear strength of an unsaturated sandy soil.” Proc. 1st International Conference on Unsaturated Soils,1, 189-193.

Salman, T.H. (1995). “Triaxial behavior of partially saturated granular soils.” Ph.D. dissertation, University of Sheffield, U.K.

Sadrekarimi, A., and Olson, S. (2009). “A New Ring Shear Device to Measure the Large Displacement Shearing Behavior of Sands.” Geotechnical Testing Journal, 32(3), 1-12.

Sassa, K., Wang, G., and Fukuoka, Hiroshi. (2003). “Performing undrained shear tests on saturated sands in a new intelligent type of ring shear apparatus” Geotechnical testing Journal, 26(3). 1-9.

Seycek, J. (1978) “Residual shear strength of soils” Bull. Int. Ass. Eng. geol. 17, 73-75.

Skemptom, A.W. (1964). “Long-term stability of clays slopes.” Geotechnique., 14(2), 75-102.

Skemptom, A.W. (1985). “Residual strength of clays in landslides, folded strata, and the laboratory.” Geotechnique, 35(1), 3-18.

Stark, T.D., and Contreras, I.A., (1996). “Constant volume ring shear apparatus.” Geotechnical Testing Journal, 19(1), 3-11.

Stark, T.D., Choi, H., and McCone, S. (2005). “Drained shear strength parameters for analysis of landslides.” Journal of Geotechnical and Geoenvironmental Engineering, 131(5), 575–588.

Stark, T.D., and Eid, H.T., (1993). “Modified Bromhead ring shear apparatus.” Geotechnical Testing Journal., 6(1), 100-107.

Stark, T.D., and Eid, H.T., (1994). “Drained residual strength of cohesive soils." Journal of Geotechnical Engineering, 120(5), 856-871.

Stark, T.D., and Eid, H.T., (1997). “Slope stability analyses in stiff fissured clays." Journal of Geotechnical and Geoenviromental Engineering, 123(4), 335-343.

Stark, T.D., Hangseok, C., and McCone, S. (2005). “Drained shear strength parameters for analysis of landslides." Journal of Geotechnical and Geoenviromental Engineering, 131(5), 575-588.

Stark, T.D., and Vettel, J.J., (1992). “Bromhead ring shear test procedure.” Geotechnical Testing Journal, 15(1), 24-32.

Suescun, E.A. (2010). Development of a suction-controlled resonant column apparatus with self-contained bender elements. Ms. Thesis. University of Texas at Arlington

Terzaghi, K. (1936). “The shearing resistance of saturated soils and the angle between the planes of shear.” International Conference on Soil Mechanics and Foundations Engineering. Harvard University Press: Cambridge, MA, 54-56.

Tiwari, B., and Marui, H. (2004) “Objective oriented multistage ring shear test for shear strength of landslide soil.” Journal of Geotechnical and Geoenvironmental Engineering, ASCE, 130(2), 217-222.

Tiwari, B., Brandon, T.L., Mauri, H., and Tuladhar, G.R (2005) “Comparison of residual strength from back analysis and ring shear test on undisturbed and remolded specimens” Journal of Geotechnical and Geoenviromental Engineering., ASCE, 131(9), 1071-1079.

Van Genuchten, M. T. (1980). ‘‘A closed form equation for predicting the hydraulic conductivity of unsaturated soils,’’ Soil Science Society of America Journal, 44, 892–898.

Vanapalli, S. K., Pufahl, D. E., Fredlund, D. G., (1998). “The effect of stress on the soil-water characteristic behavior of a compacted sandy-clay till. 51st Canadian Geotechnical Conference, Edmonton, 81-86.

Vanapalli, S., Fredlund, D., Pufahl, D. (1999). “The influence of soil structure and stress history on the soil-water characteristics of a compacted till. Geotechnique, 49(2), 143-159.

Vanapalli, S.K., Fredlund, D.G., Pufahl, D.E. and Clifton, A.W. (1996). Model for the prediction of shear strength with respect to soil suction. Canadian Geotechnical Journal, 33(3), 379-392.

Vaunat, J., Amador, C., Romero, E., and Djeren-Maigre, I. (2006). “Residual strength of a low plasticity clay at high suctions.” Proceedings of the Fourth International Conference of Unsaturated Soils, 1, 1279-1289.

Vaunat, J., Merchan, V., Romero, E., and Pineda, J. (2007). “Residual strength of clays at high suctions.” Proceedings of the 2nd International Conference on Mechanics of Unsaturated Soils, Weimar, Germany, 2, 151–162.

Venkatarama, R.B., and Jagadish, K.S. (1993). The static compaction of soils. Géotechnique, 43(2): 337-341.

Wheeler, S.J., and Sivakumar, V. (1995). “An elasto-plastic critical state framework for unsaturated soils.” Géotechnique, 45(1), 35-53.

Zan, T.L.T., and Ng, C.W.W. (2006). “Shear strength characteristics of an unsaturated expansive clay.” Canadian Geotechnical Journal, 43, 751-763.

BIOGRAPHICAL INFORMATION

Claudia Liliana Velosa Gamboa was born in Bogota, Colombia on Febrary 21, 1979. She received her B.S degree in Civil Engineering from the “Escuela Colombiana de Ingenieria”, in Bogota, Colombia, in October, 2001. In 2002 she was admitted to the graduate program in the Geotechnical Area at the “Universidad Nacional de Colombia” in Bogota, Colombia, where she received a M.Sc. degree in Civil Engineering. In Summer 2007, she was admitted to the graduate program in Department of Civil Engineering at the University of Texas at Arlington, as a doctoral student. Mrs. Velosa has successfully completed all requirements for the Degree of Doctor of Philosophy in Civil Engineering on May, 2011 and she will receive the degree in Spring, 2011 Commencement ceremony.